

arXiv:hep-ex/0209039v1 18 Sep 2002

# On the application of “ $Z^0 + jet$ ” events for setting the absolute jet energy scale and determining the gluon distribution in a proton at the LHC

D.V. Bandurin, N.B. Skachkov

*Joint Institute for Nuclear Research, Dubna, Russia*

## Abstract

We study the effect of an application of a new set of cuts, proposed in our previous works, on the improvement of accuracy of the jet energy calibration with “ $pp \rightarrow Z^0 + jet + X$ ” process at LHC. Monte Carlo events produced by the PYTHIA 5.7 generator are used for this aim. The selection criteria for “ $Z + jet$ ” event samples that would provide a good balance of  $P_t^Z$  with  $P_t^{jet}$  and would allow to reduce the background are described. The distributions of these events over  $P_t^Z$  and  $\eta^{jet}$  intervals are presented. The features of “ $Z + jet$ ” events in the barrel region of the CMS detector ( $|\eta^{jet}| < 1.4$ ) are exposed. The efficiency of the cuts used for background suppression is demonstrated.

It is shown that the samples of “ $Z + jet$ ” events, gained with the cuts for the jet energy calibration, may have enough statistics for determining the gluon distribution inside a proton in the region of  $10^{-4} \leq x \leq 1$  with  $1.6 \cdot 10^3 \leq Q^2 \leq 2 \cdot 10^4 (GeV/c)^2$ .

<b>1. INTRODUCTION.</b>	<b>1</b>
<b>2. GENERALITIES OF THE “<math>Z + jet</math>” PROCESS.</b>	<b>2</b>
2.1 Leading order picture and sources of $P_t^Z$ and $P_t^{Jet}$ disbalance. . . . .	2
2.2 Definition of selection cuts. . . . .	4
2.3 Balance equation of $P_t^Z$ and $P_t^{Jet}$ . . . . .	5
<b>3. ESTIMATION OF A NON-DETECTABLE PART OF <math>P_t^{Jet}</math>.</b>	<b>6</b>
<b>4. EVENT RATES FOR DIFFERENT <math>P_t^Z</math> AND <math>\eta^Z</math> INTERVALS.</b>	<b>7</b>
4.1 Dependence of the distribution of the number of events on the ”back-to-back” angle $\phi_{(Z,jet)}$ and on $P_t^{ISR}$ . . . . .	7
4.2 $P_t^Z$ , $\eta^Z$ and $P_t^\mu$ dependence of rates. . . . .	10
4.3 Estimation of “ $Z + jet$ ” event rates for the HB, HE and HF regions. . . . .	11
<b>5. FEATURES OF “<math>Z + jet</math>” EVENTS IN THE HCAL BARREL REGION.</b>	<b>14</b>
5.1 Influence of the $P_{tcut}^{clust}$ parameter on the balance between $Z^0$ and jet transverse momenta and on the initial state radiation suppression. . . . .	14
5.2 $P_t$ distribution inside and outside of a jet. . . . .	17
<b>6. DEPENDENCE OF THE “<math>Z + jet</math>” SYSTEM <math>P_t</math> DISBALANCE ON <math>P_{tCUT}^{clust}</math> and <math>P_{tCUT}^{out}</math> PARAMETERS.</b>	<b>17</b>
<b>7. THE STUDY OF BACKGROUND SUPPRESSION.</b>	<b>29</b>
<b>8. ESTIMATION OF RATES AND BACKGROUND FOR GLUON DISTRIBUTION DETERMINATION AT THE LHC USING “<math>Z + jet</math>” EVENTS.</b>	<b>37</b>
<b>9. SUMMARY.</b>	<b>41</b>
<b>10. ACKNOWLEDGMENTS.</b>	<b>42</b>
<b>11. REFERENCES.</b>	<b>42</b>
<b>12. APPENDICES.</b>	<b>46</b>

## 1. INTRODUCTION.

Setting an absolute energy scale for a jet is an important task for all  $pp$  and  $p\bar{p}$  collider experiments (see e.g. [1, 2]). There is a number of publications, devoted to this subject in D0, CDF, CMS and ATLAS collaborations where application of different physical processes (like “ $Z^0/\gamma + jet$ ” and others) is considered ([3–10]).

“ $Z + jet$ ” events with one high- $P_t$  jet can provide a useful sample to perform *in situ* determination of a jet transverse momentum via a transverse momentum of  $Z^0$  boson reconstructed from the precisely measured leptonic  $Z^0$  decay ( $Z^0 \rightarrow \mu^+\mu^-, e^+e^-$ ).

In this paper we limit our consideration to  $Z^0 \rightarrow \mu^+\mu^-$  decay only. The amount of material in front and inside the muon detector system guarantees absorbing most hadronic background. Besides, by using the track segments matching between the muon system and the tracker one can reach a high enough reconstruction efficiency of muon track with a good momentum resolution (of order of 0.5–1%)<sup>1</sup>. A selection of “ $Z + jet$ ” events with the consequent decay  $Z^0 \rightarrow e^+e^-$  would require a supplementary introduction of isolation criteria for  $e^\pm$  tracks to perform a confident reconstruction of  $e^\pm$  signal in the cells of electromagnetic calorimeter (ECAL)<sup>2</sup>. Our study has shown that a background to “ $Z + jet$ ” events with electron channel of  $Z^0$  decay is about the same as one to “ $Z + jet$ ” events with muon channel of  $Z^0$  decay.

“ $Z + jet$ ” events is a useful tool to cross-check a setting an absolute jet energy scale with help of other processes like “ $\gamma + jet$ ” [19] (see also [18]) and “ $W \rightarrow 2 jets$ ” events [8], for example.

Here we present the results of our analysis of “ $Z + jet$ ” events generated by using PYTHIA 5.7 Monte-Carlo event simulation package [23].

Section 2 is an introduction into the problem. General features of “ $Z + jet$ ” processes at LHC energies as well as the reasons of the disbalance between transverse momenta of  $Z^0$  and jet are presented here. In Section 2.2 we list a set of the selection cuts used to identify signal “ $Z + jet$ ” events (implying subsequent  $Z^0$  decay to muon pair). New criteria (introduced for the first time in [12]) of  $P_t$  activity suppression beyond “ $Z + jet$ ” system and in some ring in the  $\eta - \phi$  space around a jet<sup>3</sup> are also described there. Vector and scalar forms of the balance equation of  $P_t^Z$  and  $P_t^{jet}$  are given in Section 2.3.

In Section 3 we briefly describe an estimation of non-detectable part of jet  $P_t$  without taking into account of the detector effects.

Section 4 is devoted to the study of the influence of  $P_{tCUT}^{clust}$  and  $P_{tCUT}^{out}$  as well as the angle between  $\vec{P}_t^Z$  and  $\vec{P}_t^{jet}$  on the initial state radiation (ISR) suppression. The rates of “ $Z + jet$ ” events with jet covering Barrel, Endcap and Forward parts of the calorimeter are also given in this section.

In Sections 5 and 6 we confine ourselves by consideration of “ $Z + jet$ ” events with the jet entirely contained in the Barrel region. The dependences of various physical variables on  $P_{tCUT}^{clust}$  and  $P_{tCUT}^{out}$  are analyzed there and shown in the tables of Appendices 2–5.

In Section 7 we calculate the background admixture to the signal events for different  $P_t^Z$  intervals. The values of the disbalance between  $P_t^Z$  and  $P_t^{jet}$  with an account of back-

<sup>1</sup>see [24]

<sup>2</sup>For instance, by requiring (1) a total transverse momentum  $E_t^{tot}$  around an electron with  $E_t^e$  in the cone with  $R = 0.3$  to be  $E_t^{tot} < 5 GeV$  and (2)  $E_t^{tot}/E_t^e < 0.1$  (these cuts are accepted in [22]) we additionally reduce a number of signal events by 2–4%.

<sup>3</sup>see points 6–8 of Section 2.2

ground contribution for three  $P_t^Z$  intervals and  $P_{tCUT}^{clust}$  and  $P_{tCUT}^{out}$  values are presented in Appendix 6 and described in Section 7.

In Section 8 we estimate a possibility of the gluon density determination in a proton by using “ $Z + jet$ ” event samples selected by the criteria from Section 2.2. The event rates and background contamination are calculated there for various  $x$  and  $Q^2$  intervals. It is shown that the kinematical region for the gluon density determination in the intervals:  $10^{-4} \leq x \leq 10^{-1}$  and  $1.6 \cdot 10^3 \leq Q^2 \leq 2 \cdot 10^4 (GeV/c)^2$  can be covered by studying the “ $Z + jet$ ” events.

## 2. GENERALITIES OF THE “ $Z + jet$ ” PROCESS.

### 2.1 Leading order picture and sources of $P_t^Z$ and $P_t^{Jet}$ disbalance.

In this section we observe briefly the main effects that lead to  $P_t^Z$  and  $P_t^{Jet}$  disbalance<sup>4</sup>.

At the parton level “ $Z + jet$ ” process is caused by two subprocesses:

Compton-like scattering

$$qg \rightarrow q + Z^0 \quad (1a)$$

and the annihilation process

$$q\bar{q} \rightarrow g + Z^0. \quad (1b)$$

The leading order Feynman diagrams of these processes are shown in Fig. 1.

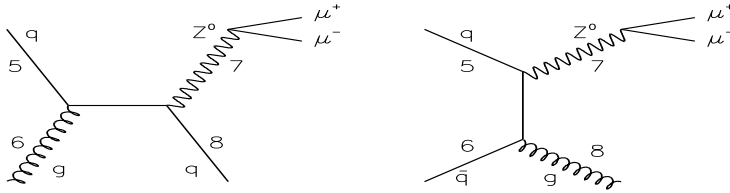


Fig. 1: Some of the leading order Feynman diagrams for  $Z^0$  production.

If the initial state radiation is absent, the total transverse momentum of the final state in the subprocesses (1a) or (1b) is equal to zero, i.e. the  $P_t$  balance equation for  $Z^0$  and final parton would look as

$$\vec{P}_t^{Z+part} = \vec{P}_t^Z + \vec{P}_t^{part} = 0. \quad (1)$$

Thus, having neglected hadronization effect we could expect that a jet transverse momentum  $P_t^{jet}$  is close enough to  $Z^0$  boson transverse momentum, i.e.  $\vec{P}_t^{jet} \approx -\vec{P}_t^Z$ .

A radiation of a gluon in the initial state with non-zero transverse momentum  $P_t^{gluon} \equiv P_t^{ISR} \neq 0$  can produce a disbalance between  $P_t^Z$  and  $P_t^{part}$  and, thus, between transverse momenta of  $Z^0$  boson and jet originating from this proton. The corresponding next-to-leading order diagram is shown in Fig. 2.

Following [12], we choose the sum of the modulus of the transverse momentum vectors  $\vec{P}_t^5$  and  $\vec{P}_t^6$  of the incoming (into  $2 \rightarrow 2$  fundamental QCD subprocesses  $5+6 \rightarrow 7+8$ ) partons (lines 5 and 6 in Fig. 2):

$$P_{t56} = |P_t^5| + |P_t^6| \quad (2)$$

<sup>4</sup>The more detailed consideration is given in our papers [18] and [19] devoted to the jet energy calibration by using “ $\gamma + jet$ ” events.

as a quantitative measure to estimate the  $P_t$  disbalance caused by ISR.

The numerical notations in the Feynman diagrams shown in Figs. 1 and 2 and in formula (2) are chosen to be in correspondence with those used in the PYTHIA event listing for description of the parton-parton subprocess displayed schematically in Fig. 3. The “ISR” block describes the initial state radiation process that can take place before the fundamental hard  $2 \rightarrow 2$  process.

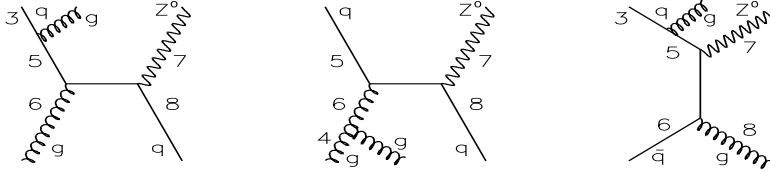


Fig. 2: Some of Feynman diagrams of  $Z^0$  production including gluon radiation in the initial state.

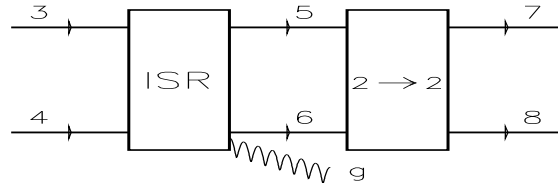


Fig. 3: PYTHIA “diagram” of a fundamental  $2 \rightarrow 2$  process ( $5+6 \rightarrow 7+8$ ) following the block ( $3+4 \rightarrow 5+6$ ) of initial state radiation (ISR).

Let us consider fundamental subprocesses in which there is no initial state radiation but instead final state radiation (FSR) takes place. The Feynman diagrams of the signal subprocesses with the FSR are shown in Fig. 4. An appearance of a gluon in the final state may also cause a disbalance between transverse momenta of  $Z^0$  and jet. But because it manifests itself as some extra jets or clusters, like in the case of ISR, the same selection criteria (see below) as for suppression of initial state radiation can be used.

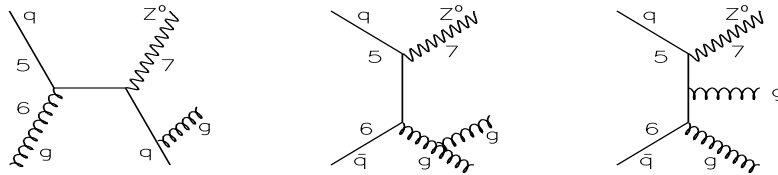


Fig. 4: Some of Feynman diagrams of  $Z^0$  production including gluon radiation in the final state.

A possible non-zero value of the intrinsic transverse momentum of a parton inside a colliding proton may be another source of the  $P_t^Z$  and  $P_t^{part}$  disbalance in the final state. Its reasonable value is supposed to lead to the value  $k_T \leq 1.0 \text{ GeV}/c$ . In what follows we shall keep the value of  $k_T$  to be fixed by the PYTHIA default value  $\langle k_T \rangle = 0.44 \text{ GeV}/c$ . The dependence of the disbalance between  $P_t^Z$  and  $P_t^{Jet}$  on possible variation of  $k_T$  is discussed in detail in [16]. The general conclusion is that the variation of  $k_T$  within reasonable boundaries does not produce a large effect when the initial state radiation is taken into account. The latter makes a dominant contribution.

Another non-perturbative effect that makes for the  $P_t^Z$  and  $P_t^{Jet}$  disbalance is an hadronization of the parton produced in the fundamental  $2 \rightarrow 2$  subprocess into a jet. The contribution of the hadronization to this disbalance is calculated within the Lund string fragmentation scheme used by default in PYTHIA. The mean values of the relative  $P_t^{Jet} - P_t^{part}$  disbalance are presented in the tables of Appendices 2 – 5 for three different jetfinders UA1, UA2 and LUCCELL as a function of the variable which limits a cluster activity beyond the “ $Z + jet$ ” system (see Section 2.2 and [14]).

## 2.2 Definition of selection cuts.

1. We shall select the events with one jet and  $Z^0$  boson <sup>5</sup> with

$$P_t^Z \geq 40 \text{ GeV}/c \quad \text{and} \quad P_t^{Jet} \geq 30 \text{ GeV}/c. \quad (3)$$

For most of our applications the jet is defined according to the PYTHIA jetfinding algorithm LUCCELL. The jet cone radius  $R$  in the  $\eta - \phi$  space counted from the jet initiator cell (ic) is taken to be  $R_{ic} = ((\Delta\eta)^2 + (\Delta\phi)^2)^{1/2} = 0.7$ . Comparison with the UA1 and UA2 jetfinding algorithms <sup>6</sup> is presented in Sections 5 and 6.

2. To guarantee a clear identification of muons from  $Z^0$  decay in muon stations and a high probability of muon track finding in the tracker we put the following restrictions on muons:

(a) on the  $P_t$  value of any considered muon:

$$P_t^\mu \geq 10 \text{ GeV}/c; \quad (4)$$

(b) on the  $P_t$  value of the most energetic muon in a pair:

$$P_{t_{max}}^\mu \geq P_{t_{CUT}}^\mu \quad (5)$$

( $P_{t_{CUT}}^\mu \geq 20 \text{ GeV}/c$  and depends on the energy scale).

(c) on the value of the scalar sum of  $P_t$  of charged particles surrounding a muon in the radius  $R = 0.3$ :

$$P_{t_{ch}}^\mu \leq 2 \text{ GeV}/c. \quad (6)$$

The isolated high- $P_t$  tracks can be reconstructed with a good efficiency (at least 98% over all pseudorapidity region  $|\eta| < 2.4$ ; see [24]) and with generation of a low number of fake and ghost tracks.

3. A muon is selected in the region of the muon system acceptance:

$$|\eta^\mu| < 2.4. \quad (7)$$

4. To select muon pairs only from the  $Z^0$  decay we limit the value of invariant mass of a muon pair  $M_{inv}^\mu$  by:

$$|M^Z - M_{inv}^\mu| \leq 5 \text{ GeV}/c^2. \quad (8)$$

5. We select the events with the vector  $\vec{P}_t^{Jet}$  being “back-to-back” to the vector  $\vec{P}_t^Z$  (in the plane transverse to the beam line) within  $\Delta\phi$  defined by the equation:

$$\phi_{(Z,jet)} = 180^\circ \pm \Delta\phi \quad (\Delta\phi = 15^\circ, 10^\circ, 5^\circ), \quad (9)$$

where  $\phi_{(Z,jet)}$  is the angle between the  $\vec{P}_t^Z$  and  $\vec{P}_t^{Jet}$  vectors:

$$\vec{P}_t^Z \vec{P}_t^{Jet} = P_t^Z P_t^{Jet} \cos(\phi_{(Z,jet)}), \quad \text{where} \quad P_t^Z = |\vec{P}_t^Z|, \quad P_t^{Jet} = |\vec{P}_t^{Jet}|.$$

6. The initial and final state radiations (ISR and FSR) manifest themselves most clearly as some final state mini-jets or clusters activity (see the previous section and [12]–[16], [19]). To suppress it, we impose a new cut condition that was not formulated in an evident form in previous experiments: we choose the “ $Z + jet$ ” events that do not have any other jet-like or cluster high  $P_t$  activity by taking values of  $P_t^{clust}$  (the cluster cone  $R_{clust}(\eta, \phi) = 0.7$ ), being smaller than some threshold  $P_{t_{CUT}}^{clust}$  value, i.e. we select the events with

<sup>5</sup>Here and below in the paper speaking about  $Z^0$  boson we imply reconstructed signal from the muon pair with muons selected by the criteria 2 – 4 of this section.

<sup>6</sup>(taken from the CMSJET program of fast simulation [22])

$$P_t^{clust} \leq P_{tCUT}^{clust}. \quad (10)$$

7. We limit the value of the modulus of the vector sum of  $\vec{P}_t$  of all particles that do not belong to the “ $Z + jet$ ” system but fit into the region  $|\eta| < 5$  covered by the calorimeter system, i.e., we limit the signal in the cells “beyond the jet and  $Z^0$ ” regions by the following cut:

$$\left| \sum_{i \notin Jet, Z^0} \vec{P}_t^i \right| \equiv P_t^{out} \leq P_{tCUT}^{out}, \quad |\eta| < 5. \quad (11)$$

The importance of  $P_{tCUT}^{out}$  and  $P_{tCUT}^{clust}$  for selection of events with a good balance of  $P_t^Z$  and  $P_t^{Jet}$  was already shown in [12] – [16] and in [18], [19]. Here it will be demonstrated once again for the case of “ $Z + jet$ ” events in Sections 5 and 6. The set of selection cuts 1 – 7 we call as “Selection 1”.

8. By analogy with [18], [19] and [12] – [16] we use a “jet isolation” requirement (introduced for the first time in [12]), i.e. the presence of a “clean enough” (in the sense of limited  $P_t$  activity) region inside the ring of  $\Delta R = 0.3$  (or of approximately a size of three HCAL towers) around the jet. Following this picture, we restrict the ratio of the scalar sum of transverse momenta of particles belonging to this ring, i.e.

$$P_t^{ring}/P_t^{jet} \equiv \epsilon^{jet}, \quad \text{where} \quad P_t^{ring} = \sum_{i \in 0.7 < R < 1} |\vec{P}_t^i| \quad (12)$$

with  $\epsilon^{jet} \leq 3 - 8\%$  (see Sections 6 and 7). The set of events that pass cuts 1 – 7 will be called “Selection 2”.

9. As in [18] and [19] in the following “Selection 3” we shall keep only those events in which one and the same jet (i.e. up to good accuracy having the same values of  $P_t^{jet}$ ,  $R^{jet}$  and  $\Delta\phi$ ) is found simultaneously by every of three jetfinders used here: UA1, UA2 and LUCCELL. For these jets (and also clusters) we require the following conditions:

$$P_t^{Jet} > 30 \text{ GeV}/c, \quad P_t^{clust} < P_{tCUT}^{clust}, \quad \Delta\phi < 15^\circ (10^\circ, 5^\circ), \quad \epsilon^{jet} \leq 5\%. \quad (13)$$

The exact values of the cut parameters  $P_{tCUT}^\mu$ ,  $\epsilon^{jet}$ ,  $P_{tCUT}^{clust}$ ,  $P_{tCUT}^{out}$  will be specified below, since they may be different, for instance, for various  $P_t^Z$  intervals.

10. As we shown in [18] and [19] one can expect reasonable results of the jet energy calibration procedure if one uses a set of selected events with small missing transverse momentum  $P_t^{miss}$ . So, we also use the following cut:

$$P_t^{miss} \leq P_{tCUT}^{miss}. \quad (14)$$

The aim of the event selection with small  $P_t^{miss}$  is quite obvious: we need a set of events with a reduced  $P_t^{Jet}$  uncertainty due to a possible presence of a non-detectable neutrino contribution to a jet, for example.

### 2.3 Balance equation of $P_t^Z$ and $P_t^{Jet}$ .

The conservation law for “ $Z + jet$ ” events as a whole can be written in the following vector form:

$$\vec{P}_t^Z + \vec{P}_t^{Jet} + \vec{P}_t^O + \vec{P}_t^{|\eta|>5} = 0. \quad (15)$$

Here  $\vec{P}_t^{|\eta|>5}$  is the total transverse momentum of non-observable particles  $i$  flying in the direction of the non-instrumented forward part of the CMS detector ( $|\eta| > 5$ ):

$$\sum_{i \in |\eta|>5} \vec{P}_t^i \equiv \vec{P}_t^{|\eta|>5}. \quad (16)$$

$\vec{P}_t^O$  is a total transverse momentum of all other ( $O$ ) particles besides “jet particles and muons from  $Z^0$  decay” (“ $Z + jet$ ” system) in the  $|\eta| < 5$  region and defined as:

$$\vec{P}_t^O = \vec{P}_t^{out} + \vec{P}_{t(\nu)}^O + \vec{P}_{t(\mu, |\eta^\mu|>2.4)}^O. \quad (17)$$

In its turn,  $\vec{P}_t^{out}$  is a sum of clusters  $P_t$  (with  $P_t^{clust}$  smaller than  $P_t^{Jet}$ ) and  $P_t$  of single hadrons ( $h$ ), photons ( $\gamma$ ) and electrons ( $e$ ) with  $|\eta| < 5$  and muons ( $\mu$ ) with  $|\eta^\mu| < 2.4$  that are out of the “ $Z + jet$ ” system:

$$\vec{P}_t^{out} = \vec{P}_t^{clust} + \vec{P}_{t(h)}^{sing} + \vec{P}_{t(\gamma)}^{nondir} + \vec{P}_{t(e)} + \vec{P}_{t(\mu, |\eta^\mu|<2.4)}^O, \quad |\eta| < 5. \quad (18)$$

The last two terms in equation (17) are the transverse momentum carried out by the neutrinos that do not belong to the jet but that are contained in the  $|\eta| < 5$  region ( $\vec{P}_{t(\nu)}^O$ ) and non-detectable muons flying with  $|\eta^\mu| > 2.4$  ( $\vec{P}_{t(\mu, |\eta^\mu|>2.4)}^O$ ).

To conclude this section, let us rewrite the basic  $P_t$ -balance equation obtained in [12] in the following scalar form, more suitable to present the final results:

$$\frac{P_t^Z - P_t^{Jet}}{P_t^Z} = (1 - \cos\Delta\phi) + P_t(O+\eta > 5)/P_t^Z, \quad (19)$$

where  $P_t(O+\eta > 5) \equiv (\vec{P}_t^O + \vec{P}_t^{|\eta|>5}) \cdot \vec{n}^{Jet}$  with  $\vec{n}^{Jet} = \vec{P}_t^{Jet}/P_t^{Jet}$  and  $\Delta\phi$  is the angle that enters equation (9).

As will be shown in Section 6, the first term on the right-hand side of equation (19) is negligibly small and tends to decrease fast with growing  $P_t^{Jet}$ . So, the main contribution to the  $P_t$  disbalance in the “ $Z + jet$ ” system is caused by the term  $P_t(O+\eta > 5)/P_t^Z$ .

### 3. ESTIMATION OF A NON-DETECTABLE PART OF $P_t^{Jet}$ .<sup>7</sup>

The main source of this part is non-detectable particles (like neutrinos and muons with  $|\eta| > 2.4$ ). But in a real experiment it can be also conditioned by energy leakage due to constructive features of the detector.

The missing transverse momentum  $P_t^{miss}$  and a  $P_t$  contribution to a jet from non-detectable particles are estimated here in the framework of simulation with PYTHIA<sup>8</sup>. The detailed information about the transverse momenta of non-detectable neutrinos  $P_{t(\nu)}^{Jet}$  averaged over all events (no cut on  $P_t^{miss}$  was used) as well as about mean  $P_t$  values of muons belonging to jets  $\langle P_{t(\mu)}^{Jet} \rangle$  is presented in Tables 1–12 of Appendix 1 for the sample of events with jets which are entirely contained in the barrel region of the HCAL ( $|\eta^{jet}| < 1.4$ , “HB-events”, see Section 4 and 5). In these tables the ratio of number of the events with non-zero  $P_{t(\nu)}^{Jet}$  to the total number of events is denoted by  $R_{event}^{\nu \in Jet}$  and the ratio of the number of events with non-zero  $P_{t(\mu)}^{Jet}$  to the total number of events is denoted by  $R_{event}^{\mu \in Jet}$ .

<sup>7</sup>This part was considered in detail in [19].

<sup>8</sup>We have considered the case of switched-off decays of  $\pi^\pm$  and  $K^\pm$  mesons (according to the PYTHIA default agreement,  $\pi^\pm$  and  $K^\pm$  mesons are stable).

A wide variation of  $P_{tCUT}^{miss}$  as well as the case of allowed  $K^\pm$  decays in the calorimeter volume were presented in detail in [12] and [19]. We choose here for the following analysis  $P_{tCUT}^{miss} = 10 \text{ GeV}/c$  found to be optimal in [12].

#### 4. EVENT RATES FOR DIFFERENT $P_t^Z$ AND $\eta^Z$ INTERVALS.

##### 4.1 Dependence of the distribution of the number of events on the "back-to-back" angle $\phi_{(Z,jet)}$ and on $P_t^{ISR}$ .

Here we study the spectrum of the variable  $P_{t56}$  for the sample of signal events<sup>9</sup>. For this aim four samples of " $Z + jet$ " events (each by  $5 \cdot 10^6$ ) were generated by using PYTHIA with 2 QCD subprocesses (1a) and (1b) for each of four  $P_t^Z$  intervals: 40–50, 70–85, 100–120, 150–200  $\text{GeV}/c$  with minimal  $P_t$  of hard  $2 \rightarrow 2$  scattering<sup>10</sup>  $\hat{p}_\perp^{min} = 20, 35, 50, 75 \text{ GeV}/c$  respectively. The obtained cross sections for these subprocesses are given in Table 1.

Table 1: The cross sections (in *microbarn*) of the  $qg \rightarrow q + Z^0$  and  $q\bar{q} \rightarrow g + Z^0$  subprocesses for four  $P_t^Z$  intervals.

Subprocess type	$P_t^Z$ interval ( $\text{GeV}/c$ )			
	40 – 50	70 – 85	100 – 120	150 – 200
$qg \rightarrow q + Z^0$	$3.83 \cdot 10^{-4}$	$1.71 \cdot 10^{-4}$	$9.14 \cdot 10^{-5}$	$3.80 \cdot 10^{-5}$
$q\bar{q} \rightarrow g + Z^0$	$1.20 \cdot 10^{-4}$	$0.42 \cdot 10^{-4}$	$1.93 \cdot 10^{-5}$	$0.69 \cdot 10^{-5}$
Total	$5.03 \cdot 10^{-4}$	$2.13 \cdot 10^{-4}$	$1.11 \cdot 10^{-4}$	$4.59 \cdot 10^{-5}$

\* It is meant in the table above that  $Z^0$  boson decays in the following to  $\mu^+ \mu_-$  pair.

For our analysis we used cuts (3) – (11) and the following cut parameters:

$$P_{tmin}^\mu > 10 \text{ GeV}/c, \quad P_{tmax}^\mu > 20 \text{ GeV}/c, \quad \Delta\phi < 15^\circ, \quad P_{tCUT}^{clust} = 30 \text{ GeV}/c. \quad (20)$$

In Tables 2, 3 and 5, 6 we study (as in [12])  $P_{t56}$  spectra for two most illustrative cases of  $P_t^Z$  intervals  $40 < P_t^Z < 50 \text{ GeV}/c$  (Tables 2 and 5) and  $100 < P_t^Z < 120 \text{ GeV}/c$  (Tables 3 and 6). The distributions of the number of events for the integrated luminosity  $L_{int} = 10 \text{ fb}^{-1}$  in different  $P_{t56}$  intervals and for different "back-to-back" angle intervals  $\phi_{(Z,jet)} = 180^\circ \pm \Delta\phi$  ( $\Delta\phi = 15^\circ, 10^\circ$  and  $5^\circ$  as well as without any restriction on  $\Delta\phi$ , i.e. for the whole  $\phi$  interval  $\Delta\phi = 180^\circ$ ) are given there. The LUCCELL jetfinder was used to find jets and clusters. Tables 2 and 3 correspond to cuts  $P_t^{clust} < 30 \text{ GeV}/c$  without any limit on  $P_t^{out}$  value, while Tables 5 and 6 correspond to more restrictive selection cuts  $P_t^{clust} < 10 \text{ GeV}/c$  and  $P_t^{out} < 10 \text{ GeV}/c$ .

First, from the last summary lines of Tables 2, 3 and 5, 6 we can make a general conclusion about the  $\Delta\phi$  dependence of the event spectrum. In the case when no restriction is used we can see that for the  $40 \leq P_t^Z \leq 50 \text{ GeV}/c$  (Table 2) interval about 65% of events are concentrated in the  $\Delta\phi < 15^\circ$  range, while 30% of events are in the  $\Delta\phi < 5^\circ$  range. At the same time the analogous summary line of Table 3 shows us that for  $100 \leq P_t^Z \leq 120 \text{ GeV}/c$  the event spectrum moves noticeably to the small  $\Delta\phi$  region: more than 94% of events have  $\Delta\phi < 15^\circ$  and 56% of them have  $\Delta\phi < 5^\circ$ .

We observe a tendency of the distributions of the number of signal " $Z + jet$ " events to be concentrated in a rather narrow back-to-back angle interval  $\Delta\phi < 15^\circ$  with  $P_t^Z$  growing. It becomes more distinct with a more restrictive cuts  $P_{tCUT}^{out} = 10 \text{ GeV}/c$  and  $P_{tCUT}^{out} = 10 \text{ GeV}/c$

<sup>9</sup> $P_{t56}$  is approximately proportional to  $P_t^{ISR}$  up to the value of intrinsic parton transverse momentum  $k_T$  inside a proton ( $\langle k_T \rangle$ ) was taken to be fixed at the PYTHIA default value, i.e.  $\langle k_T \rangle = 0.44 \text{ GeV}/c$ .

<sup>10</sup>CKIN(3) parameter in PYTHIA

Table 2: Number of events dependence on  $P_t^{56}$  and  $\Delta\phi$  for  $40 \leq P_t^Z \leq 50 \text{ GeV}/c$  and  $P_t^{clust} = 30 \text{ GeV}/c$  for  $L_{int}=10 \text{ fb}^{-1}$ .

$P_t^{56}$ ( $\text{GeV}/c$ )	$\Delta\phi_{max}$			
	$180^\circ$	$15^\circ$	$10^\circ$	$5^\circ$
0 – 5	18525	16965	15880	12708
5 – 10	29094	26671	23419	13579
10 – 15	24192	19935	14042	7033
15 – 20	18168	10910	7088	3481
20 – 25	13424	5833	3924	1968
25 – 30	10169	3604	2380	1172
30 – 40	14070	4114	2677	1311
40 – 50	7544	1833	1184	618
50 – 100	5904	1727	1097	550
100 – 300	8	3	2	0
300 – 500	0	0	0	0
30 – 500	141095	91594	71694	42423

Table 3: Number of events dependence on  $P_t^{56}$  and  $\Delta\phi$  for  $100 \leq P_t^Z \leq 120 \text{ GeV}/c$  and  $P_t^{clust} = 30 \text{ GeV}/c$  for  $L_{int}=10 \text{ fb}^{-1}$ .

$P_t^{56}$ ( $\text{GeV}/c$ )	$\Delta\phi_{max}$			
	$180^\circ$	$15^\circ$	$10^\circ$	$5^\circ$
0 – 5	1849	1837	1790	1616
5 – 10	3798	3770	3667	3247
10 – 15	3635	3600	3477	2542
15 – 20	3065	3025	2847	1592
20 – 25	2491	2424	1976	986
25 – 30	2115	2000	1418	709
30 – 40	2507	2039	1398	721
40 – 50	1061	744	527	289
50 – 100	1105	768	582	325
100 – 300	194	147	107	63
300 – 500	2	2	1	0
0 – 500	21826	20356	17797	12094

Table 4: Number of events dependence on  $\Delta\phi$  and on  $P_t^Z$  for  $L_{int} = 10 \text{ fb}^{-1}$ .  
 $P_t^{clust} = 30 \text{ GeV}/c$  (summary).

$P_t^Z$ ( $\text{GeV}/c$ )	$\Delta\phi_{max}$			
	$180^\circ$	$15^\circ$	$10^\circ$	$5^\circ$
40 – 50	141095	91591	71694	42423
70 – 80	40032	32551	26710	16794
100 – 120	2182	20356	17797	12094
150 – 200	8649	8558	8134	6182

Table 5: Number of events dependence on  $P_{t56}$  and  $\Delta\phi$  for  $40 \leq P_t^Z \leq 50 \text{ GeV}/c$  and  $P_{tCUT}^{clust} = 10 \text{ GeV}/c$  and  $P_{tCUT}^{out} = 10 \text{ GeV}/c$  for  $L_{int}=10 \text{ fb}^{-1}$ .

$P_{t56}$ ( $\text{GeV}/c$ )	$\Delta\phi_{max}$			
	$180^\circ$	$15^\circ$	$10^\circ$	$5^\circ$
0 – 5	11619	11603	11409	9603
5 – 10	15329	15258	14288	8767
10 – 15	6787	6479	5156	2768
15 – 20	1810	1533	1204	645
20 – 25	677	527	432	253
25 – 30	305	238	195	119
30 – 40	277	222	193	111
40 – 50	127	111	91	44
50 – 100	36	32	24	12
100 – 300	0	0	0	0
300 – 500	0	0	0	0
0 – 500	36967	35996	32987	22315

Table 6: Number of events dependence on  $P_{t56}$  and  $\Delta\phi$  for  $100 \leq P_t^Z \leq 120 \text{ GeV}/c$  and  $P_{tCUT}^{clust} = 10 \text{ GeV}/c$  and  $P_{tCUT}^{out} = 10 \text{ GeV}/c$  for  $L_{int}=10 \text{ fb}^{-1}$ .

$P_{t56}$ ( $\text{GeV}/c$ )	$\Delta\phi_{max}$			
	$180^\circ$	$15^\circ$	$10^\circ$	$5^\circ$
0 – 5	1133	1133	1133	1121
5 – 10	1932	1932	1932	1877
10 – 15	1002	1002	1002	867
15 – 20	309	309	309	234
20 – 25	95	95	91	63
25 – 30	49	49	45	33
30 – 40	48	44	40	32
40 – 50	27	25	25	25
50 – 100	44	44	44	40
100 – 300	5	5	5	5
300 – 500	0	0	0	0
0 – 500	4641	4637	4621	4293

Table 7: Number of events dependence on  $\Delta\phi$  and on  $P_t^Z$  for  $L_{int} = 10 \text{ fb}^{-1}$ .  
 $P_{tCUT}^{clust} = 10 \text{ GeV}/c$  and  $P_{tCUT}^{out} = 10 \text{ GeV}/c$  (summary).

$P_t^Z$ ( $\text{GeV}/c$ )	$\Delta\phi_{max}$			
	$180^\circ$	$15^\circ$	$10^\circ$	$5^\circ$
40 – 50	36967	35996	32987	22315
70 – 80	8688	8657	8542	7033
100 – 120	4641	4637	4621	4293
150 – 200	1746	1746	1742	1719

(Tables 5 and 6). From the last summary line of Table 5 we see for these cuts that in the case of  $40 \leq P_t^Z \leq 50 \text{ GeV}/c$  more than 96% of the events have  $\Delta\phi < 15^\circ$ , while 60% of them are in the  $\Delta\phi < 5^\circ$  range. For  $100 \leq P_t^Z \leq 120 \text{ GeV}/c$  (see Table 6) more than 92% of the events, subject to these cuts, have  $\Delta\phi < 5^\circ$ . It means that while suppressing  $P_t$  activity beyond the “ $Z + jet$ ” system by imposing  $P_{tCUT}^{clust} = 10 \text{ GeV}/c$  and  $P_{tCUT}^{out} = 10 \text{ GeV}/c$  we can select the sample of events with a clean back-to-back ( $\Delta\phi < 15^\circ$ ) topology of  $\vec{P}_t^Z$  and  $\vec{P}_t^{jet}$  orientation <sup>11</sup>.

The other lines of Tables 2, 3 and 5, 6 contain the information about the  $P_t56$  spectrum (or, up to  $k_T$  effect,  $P_t^{ISR}$  spectrum).

From the comparison of Table 2 with Table 5 (as well as from Tables 3 and 6) one can conclude that the width of the most populated part of the  $P_t56$  (or  $P_t^{ISR}$ ) spectrum reduces about twofold with restricting  $P_{tCUT}^{clust}$  and  $P_{tCUT}^{out}$ . So, for  $\Delta\phi_{max} = 15^\circ$  we see that its width reduces from  $P_t56 < 30 \text{ GeV}/c$  for  $P_{tCUT}^{clust} = 30 \text{ GeV}/c$  to a narrower interval of  $P_t56 < 15 \text{ GeV}/c$  for  $P_{tCUT}^{clust} = 10 \text{ GeV}/c$  and  $P_{tCUT}^{out} = 10 \text{ GeV}/c$ . But the tails of  $P_t^{ISR}$  spectra remain to be long enough.

We supply Tables 2, 3 and 5, 6 with summarising Tables 4 and 7 containing an illustrative information on  $\Delta\phi$  dependence of the total number of events. They include more  $P_t^Z$  intervals and contain analogous numbers of events that can be collected in different  $\Delta\phi$  intervals for  $P_{tCUT}^{clust}$ ,  $P_{tCUT}^{out}$  and other cuts, defined by (20), at  $L_{int} = 10 \text{ fb}^{-1}$ .

We can conclude from Tables 2–7 that restriction on the  $P_{tCUT}^{clust}$  and  $P_{tCUT}^{out}$  variables are good tools to reduce ISR while by limiting  $\Delta\phi$  angle the ISR remains, in fact, without a change. Meanwhile, in spite of about twofold spectra reduction of the ISR (or  $P_t56$ ), it continues to be noticeable at the LHC energies <sup>12</sup>.

## 4.2 $P_t^Z$ , $\eta^Z$ and $P_t^\mu$ dependence of rates.

In Table 8 we present the number of events calculated after passing selection cuts (3)–(11) for different  $P_t^Z$  and  $\eta^Z$  intervals (lines and columns of the table, respectively). The last column of this table contains the total number of events (at  $L_{int} = 10 \text{ fb}^{-1}$ ) at  $|\eta^Z| < 5.0$  for a given  $P_t^Z$  interval. We see that the number of events decreases fast with growing  $P_t^Z$  (but it decreases much slower as compared with decrease in  $P_t^\gamma$  spectrum in the case of “ $\gamma + jet$ ” events, see [19]). It also drops with growing  $|\eta^Z|$  starting from  $|\eta^Z| \approx 2.0$  and has weak dependence on  $\eta^Z$  in the interval  $|\eta^Z| < 2.0$ . The analogous information is illustrated by Fig. 5 for three  $P_t^Z$  intervals <sup>13</sup>.

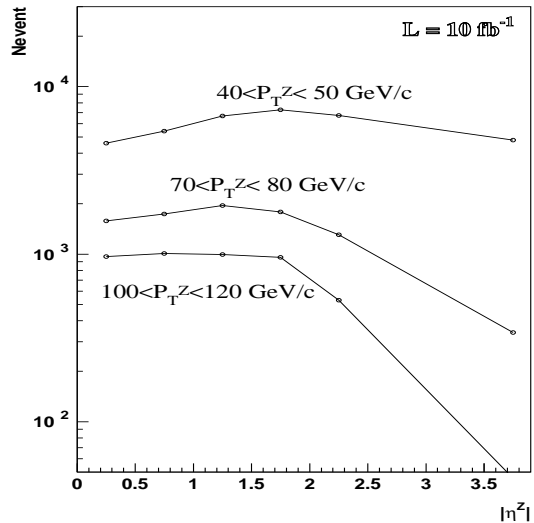


Fig. 5:  $\eta$ -dependence of rates for different  $P_t^Z$  intervals.

<sup>11</sup>An increase in  $P_t^Z$  produces the same effect, as is seen from Tables 3 and 5, and will be demonstrated in more detail in Section 6 and Appendices 2–5.

<sup>12</sup>The analogous conclusion was done by studying “ $\gamma + jet$ ” events in [19].

<sup>13</sup>We have limited  $Z^0$  pseudorapidity spectrum from above in Fig. 5 and Table 8 only to give understanding about its behaviour inside this  $\eta^Z$  interval and, certainly, have not used those limits as cuts anywhere in this paper.

Table 8: Rates for  $L_{int} = 10 \text{ fb}^{-1}$  for different intervals of  $P_t^Z$  and  $\eta^Z$  ( $P_{tCUT}^{clust} = 10 \text{ GeV}/c$ ,  $P_{tCUT}^{out} = 10 \text{ GeV}/c$  and  $\Delta\phi \leq 15^\circ$ ).

$P_t^Z$ (GeV/c)	$ \Delta\eta^Z $ intervals						all $ \eta^Z $ 0.0-5.0
	0.0-0.5	0.5-1.0	1.0-1.5	1.5-2.0	2.0-2.5	2.5-5.0	
40 – 50	4594	5425	6673	7267	6732	4796	35486
50 – 60	3128	3509	4297	4570	3976	2000	21471
60 – 70	2253	2443	2855	2934	2229	851	13567
70 – 80	1580	1734	1948	1786	1307	341	8692
80 – 90	1152	1148	1267	1236	824	170	5790
90 – 100	741	859	812	808	523	59	3802
100 – 110	582	590	594	546	305	36	2657
110 – 120	384	428	451	412	226	8	1905
120 – 140	523	582	562	531	293	12	2503
140 – 170	392	380	368	341	190	4	1675
170 – 200	170	186	162	170	63	2	756
200 – 240	111	103	99	91	40	0	444
240 – 300	71	51	44	48	20	0	238

In Fig. 6 we have plotted a normalized distributions of the number of events over  $P_t$  of muons from  $Z^0$  decay for two  $P_t^Z$  intervals:  $40 < P_t^Z < 50$  and  $100 < P_t^Z < 120 \text{ GeV}/c$ . The muon spectra are cut by the condition (4)  $P_t^\mu > 10 \text{ GeV}/c$ . We also see that the spectra with muons with maximal  $P_t$  in the pair starts at  $20 \text{ GeV}/c$  for  $40 < P_t^Z < 50$  and at  $50 \text{ GeV}/c$  for  $100 < P_t^Z < 120 \text{ GeV}/c$ . It explains our choice in (5) for  $P_{t_{max}}^\mu$  restriction.

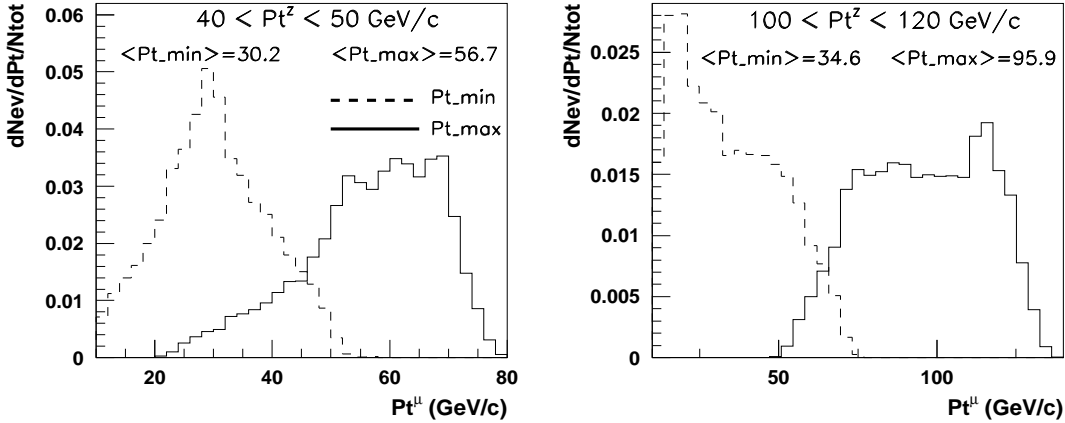


Fig. 6: A normalized distributions of the number of events over  $P_t$  of muons from  $Z^0$  decay: for a muon with maximal  $P_t$  (full line) and for a muon with minimal  $P_t$  (dashed line) in the pair.

### 4.3 Estimation of “ $Z + jet$ ” event rates for the HB, HE and HF regions.

Since a jet is a wide-spread object, we present the  $\eta^{jet}$  dependence of rates (for different  $P_t^Z$  intervals) in a different way. Namely, Tables 9–12 include the rates of events (at  $L_{int} = 10 \text{ fb}^{-1}$ ) for different  $\eta^{jet}$  intervals, covered by the Barrel, Endcap and Forward (HB, HE and HF) parts

of the HCAL. The events are selected after the cuts (3) – (11) (Selection 1) with the following values of the cut parameters:

$$\Delta\phi < 15^\circ, \quad P_{tCUT}^{clust} = 10 \text{ GeV}/c, \quad P_{tCUT}^{out} = 10 \text{ GeV}/c. \quad (21)$$

The first columns of these tables give the number of events with jets (found by the LUCCELL jetfinding algorithm of PYTHIA), all particles of which are comprised entirely (100%) in the Barrel part (HB) and there is a 0% sharing ( $\Delta P_t^{jet} = 0$ ) of  $P_t^{jet}$  between the HB and the neighbouring HE part of the HCAL. The second columns of the tables contain the number of

Table 9: Selection 1.  $\Delta P_t^{jet}/P_t^{jet} = 0.00$  ( $L_{int}=10 \text{ fb}^{-1}$ ).

$P_t^Z$	HB	HB+HE	HE	HE+HF	HF
40 – 50	15072	11179	5417	3045	729
50 – 60	9076	7037	3231	1734	376
60 – 70	5813	4447	2055	1030	218
70 – 80	3726	2903	1275	669	123
80 – 90	2542	1901	847	432	67
90 – 100	1711	1243	558	246	44
100 – 110	1263	879	352	150	12
110 – 120	836	681	289	107	20
120 – 140	1085	836	400	154	8
140 – 170	752	626	218	71	8
170 – 200	348	261	103	44	0
200 – 240	206	139	75	20	0
240 – 300	111	95	28	4	0
40 – 300	44554	34076	15789	8510	2020

Table 10: Selection 1.  $\Delta P_t^{jet}/P_t^{jet} \leq 0.10$  ( $L_{int}=10 \text{ fb}^{-1}$ ).

$P_t^Z$	HB	HB+HE	HE	HE+HF	HF
40 – 50	19610	3251	10328	887	1366
50 – 60	12161	1667	6439	420	768
60 – 70	7797	950	4166	202	444
70 – 80	5077	570	2633	162	253
80 – 90	3453	372	1734	83	147
90 – 100	2261	242	1152	48	95
100 – 110	1683	170	729	32	40
110 – 120	1176	87	582	16	45
120 – 140	1465	139	816	36	43
140 – 170	1026	115	511	12	12
170 – 200	475	48	222	5	8
200 – 240	273	17	147	3	4
240 – 300	158	15	59	0	0
40 – 300	59392	8169	31395	2127	3861

events in which  $P_t$  of the jet is shared between the HB and HE regions. The same sequence of restriction conditions takes place in the next columns. Thus, the HE and HF columns include the number of events with jets entirely contained in these regions, while the HE+HF column gives the number of events where the jet covers both the HE and HF regions. From these tables we can see what number of events can, in principle, be suitable for the most precise jet energy calibration procedure, carried out separately for the HB, HE and HF parts of the HCAL in different  $P_t^Z (\approx P_t^{jet})$  intervals.

Less restrictive conditions, when up to 10% of the jet  $P_t$  are allowed to be shared between the HB, HE and HF parts of the HCAL, are given in Tables 10 and 12. Tables 9 and 10

Table 11: Selection 2.  $\Delta P_t^{jet}/P_t^{jet} = 0.00$  ( $L_{int}=10 fb^{-1}$ ).

$P_t^Z$	HB	HB+HE	HE	HE+HF	HF
40 – 50	6039	4221	2364	1152	352
50 – 60	4578	3398	1810	847	182
60 – 70	3461	2637	1319	645	154
70 – 80	2542	2020	915	447	91
80 – 90	1936	1382	681	329	55
90 – 100	1390	962	475	190	36
100 – 110	1093	717	305	123	13
110 – 120	744	614	273	79	15
120 – 140	990	760	376	158	9
140 – 170	713	602	210	71	7
170 – 200	341	257	103	45	1
200 – 240	206	131	75	19	0
240 – 300	111	95	28	4	0
40 – 300	24912	18489	9393	4499	1169

Table 12: Selection 2.  $\Delta P_t^{jet}/P_t^{jet} \leq 0.10$  ( $L_{int}=10 fb^{-1}$ ).

$P_t^Z$	HB	HB+HE	HE	HE+HF	HF
40 – 50	7770	1148	4297	309	602
50 – 60	6083	729	3425	190	384
60 – 70	4629	554	2602	119	305
70 – 80	3465	388	1885	99	178
80 – 90	2610	249	1350	59	115
90 – 100	1806	190	950	37	79
100 – 110	1434	139	610	23	36
110 – 120	1057	85	635	31	40
120 – 140	1338	117	656	21	37
140 – 170	974	111	491	12	11
170 – 200	467	48	218	4	9
200 – 240	273	18	143	4	3
240 – 300	158	14	59	0	0
40 – 300	33117	3952	18224	990	2174

correspond to the case of Selection 1. Tables 11 and 12 contain the number of events collected with the added Selection 2 restriction (with  $\epsilon^{jet} < 5\%$ ), i.e. they include only the events with “isolated jets” (defined in Section 2.2). The reduction factor of about 2 for the number of events can be found by comparing Tables 9 and 10 with Tables 11 and 12.

From the last summarising line of Table 9 we see that for the whole interval  $45 < Pt^Z < 300 \text{ GeV}/c$  PYTHIA predicts about 45 000 events for HB and 16 000 events for HE while for HF the expected value is about 2 000 events.

An additional information on the numbers of “ $Z + jet$ ” events with jets produced by  $c$  and  $b$  quarks (see also [12] and [45]), given for the integrated luminosity  $L_{int} = 10 \text{ fb}^{-1}$  for different  $P_t^Z (\approx P_t^{Jet})$  intervals 45–55, 70–85, 100–120 and 150–200  $\text{GeV}/c$  is contained in Tables 1–12 of Appendix 1 (they denoted as  $Nevent_{(c)}$  and  $Nevent_{(b)}$  there). They also show the ratio of the number of events caused by gluonic Compton-like subprocess (1a) to the number of events due to the sum of subprocesses (1a) and (1b) ( $30_{sub/all}$ ) and averaged jet radii  $\langle R_{gc}^{jet} \rangle$ .

## 5. FEATURES OF “ $Z + jet$ ” EVENTS IN THE HCAL BARREL REGION.

### 5.1 Influence of the $P_{tcut}^{clust}$ parameter on the balance between $Z^0$ and jet transverse momenta and on the initial state radiation suppression.

Here we shall study transverse momenta correlation of a cluster  $P_t^{clust}$  with  $P_t^{ISR}$ . The samples of 1-jet “ $Z + jet$ ” events, gained from the PYTHIA simulation of  $5 \cdot 10^6$  signal “ $Z + jet$ ” events in two  $P_t^Z$  intervals 45 – 55 and 100 – 120  $\text{GeV}/c$ , will be used here. The observables defined in Section 2 will be restricted here by Selection 1 cuts (3) – (11) of Section 2.2 with  $P_{tCUT}^{clust} = 30 \text{ GeV}/c$ .  $P_{tCUT}^{out}$  is not limited here.

The influence of the  $P_{tCUT}^{clust}$  variation on the distribution of some important physical variables is shown in Fig. 7 for  $45 < P_t^Z < 55 \text{ GeV}/c$  and in Fig. 8 for  $100 < P_t^Z < 120 \text{ GeV}/c$ . Besides of distributions for three auxiliary variables  $P_{t56}$ ,  $P_t^{\eta>5}$ ,  $P_t^{out}$  (defined by (2), (16), (18)) we present distributions for  $P_t(O+\eta > 5)$  and  $(1 - \cos\Delta\phi)$  which define the right-hand side of equation (19). The distribution of the back-to-back  $\Delta\phi$  angle (9), defining the second variable  $(1 - \cos\Delta\phi)$ , is also presented in Figs. 7, 8.

The  $P_{t56}$  variable and both components defining  $P_t^Z$  and  $P_t^{Jet}$  disbalance,  $(1 - \cos\Delta\phi)$  and  $P_t(O+\eta > 5)$  (see (19)), as well as two others variables,  $P_t^{out}$  and  $\Delta\phi$ , show a tendency to become smaller (as the mean values as the widths of distributions) by restricting an upper limit on the  $P_t^{clust}$  value (see Figs. 7 and 8). It means that the calibration precision may increase with decreasing  $P_{tCUT}^{clust}$ . The origin of this improvement becomes clear from the  $P_{t56}$  density plot which demonstrates ISR suppression (or  $P_t^{ISR}$ ) as a more restrictive cut is imposed on  $P_t^{clust}$ .

Comparison of Fig. 7 (for  $45 < P_t^Z < 55 \text{ GeV}/c$ ) and Fig. 8 (for  $100 < P_t^Z < 120 \text{ GeV}/c$ ) shows that  $\Delta\phi$  as a degree of back-to-backness of  $Z^0$  boson and jet  $P_t$  vectors in the  $\phi$ -plane decreases with increasing  $P_t^Z$ . At the same time  $P_t^{ISR}$  distribution becomes wider, while the  $P_t^{\eta>5}$  and  $P_t^{out}$  distributions practically do not depend on  $P_t^Z$  (see for details Appendices 2–5).

It should be mentioned that the results presented in Figs. 7 and 8 were obtained with the LUCCELL jetfinder of PYTHIA <sup>14</sup>.

<sup>14</sup>The results obtained with all jetfinders and  $P_t^Z$  and  $P_t^{Jet}$  balance will be discussed in Sections 7 in more detail.

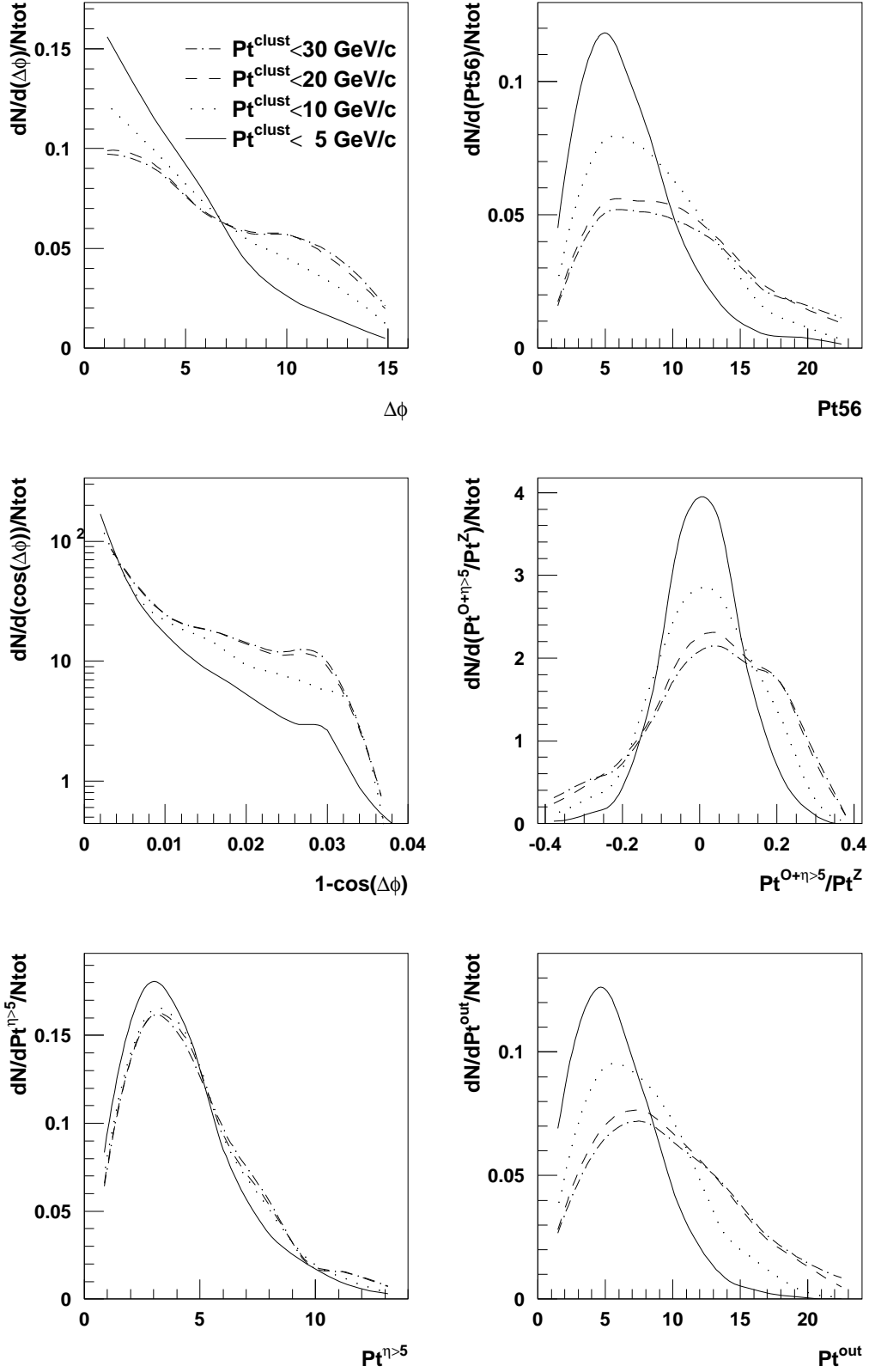


Fig. 7: LUCCELL algorithm,  $\Delta\phi < 15^\circ$ ,  $45 < P_t^Z < 55 \text{ GeV}/c$ . Selection 1.

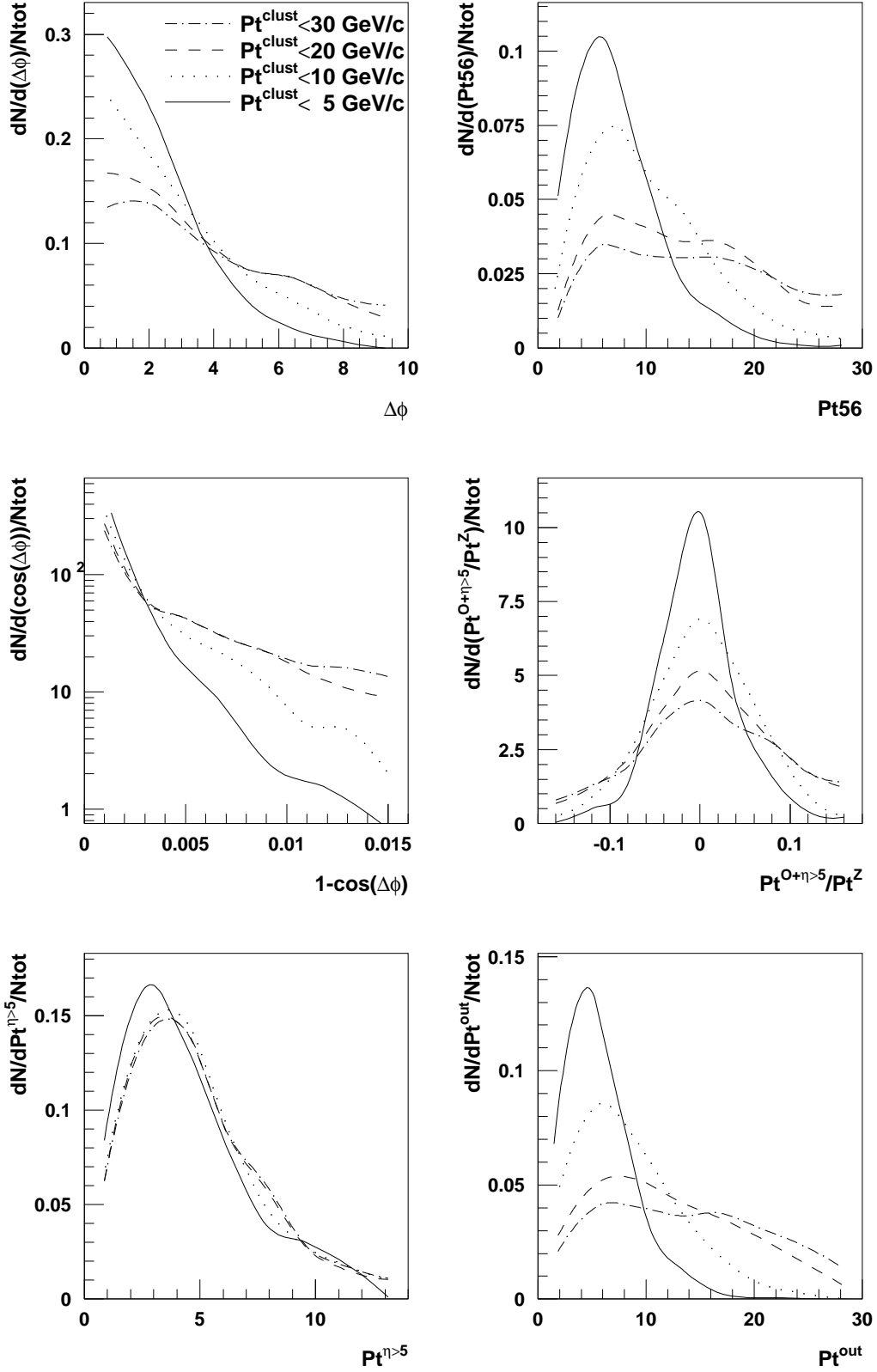


Fig. 8: LUCCELL algorithm,  $\Delta\phi < 15^\circ$ ,  $100 < P_t^Z < 120 \text{ GeV}/c$ . Selection 1.

## 5.2 $P_t$ distribution inside and outside of a jet.

Now let us see how the space outside the jet may be populated by  $P_t$  in the “ $Z + jet$ ” HB events. For this purpose we calculate a vector sum  $\vec{P}_t^{sum}$  of individual transverse momenta of the calorimeter cells included by a jetfinder into a jet and of cells in a larger volume that surrounds a jet. In the latter case this procedure can be viewed as straightforward enlarging of the jet radius in the  $\eta - \phi$  space.

The plots that present the ratio  $P_t^{sum}/P_t^Z$  as a function of the distance  $R(\eta, \phi)$  counted from a jet gravity center towards its boundary and further into the space outside a jet are shown in the left-hand columns of Figs. 9 and 10 for two  $P_t^Z$  intervals ( $45 < P_t^Z < 55 \text{ GeV}/c$  and  $100 < P_t^Z < 120 \text{ GeV}/c$ ) and three jetfinding algorithms (UA1, UA2 and LUCCELL).

From these figures we see that the space surrounding the jet is in general far from being empty. We also see that the average value of  $P_t^{sum}$  increases with increasing volume around a jet and it exceeds  $P_t^Z$  at  $R = 0.7 - 0.8$  (see Figs. 9 and 10).

From the right-hand columns of Figs. 11 and 12 we see that the vector disbalance measure

$$P_t^{Z+sum} = \left| \vec{P}_t^Z + \vec{P}_t^{sum} \right| \quad (22)$$

achieves its minimum again at  $R \approx 0.7 - 0.8$  for all jetfinding algorithms. (The minimum of the vector sum  $\vec{P}_t^{Z+sum}$  can serve as an illustration of the  $P_t^Z - P_t^{jet}$  disbalance minimum.)

The value of  $P_t^{Z+sum}$  (as well as  $P_t^{sum}/P_t^Z$ ) continues to grow rapidly for  $40 < P_t^Z < 50 \text{ GeV}/c$  and more slowly for  $100 < P_t^Z < 120 \text{ GeV}/c$  with increasing  $R$  after the point  $R = 0.7 - 0.8$  (see Figs. 9 and 10). This means that at higher  $P_t^Z$  (or  $P_t^{jet}$ ) the topology of “ $Z + jet$ ” events becomes more distinct and we get a clearer picture of an “isolated” jet. This feature clarifies the motivation of introducing the “Selection 2” criteria in Section 2.2 (see point (12)) for selection of events with isolated jets.

## 6. DEPENDENCE OF THE “ $Z + jet$ ” SYSTEM $P_t$ DISBALANCE ON $P_{tCUT}^{clust}$ AND $P_{tCUT}^{out}$ PARAMETERS.

Here we shall study in detail a dependence of the  $P_t$  disbalance in the “ $Z + jet$ ” system on the values of  $P_{tCUT}^{clust}$  and  $P_{tCUT}^{out}$ . For this aim four samples (each by  $5 \cdot 10^6$  “ $Z + jet$ ” events) generated by using PYTHIA with 2 QCD subprocesses (1a) and (1b) were used. To collect the data samples for analysis of four  $P_t^Z$  intervals (45–55, 70–85, 100–120, 150–200  $\text{GeV}/c$ ) these generations were done with the values of the minimal  $P_t$  of the hard subprocess <sup>15</sup>  $2 \rightarrow 2 \hat{p}_\perp^{min}$  equal to 20, 35, 50, 75  $\text{GeV}/c$  respectively. For our consideration we have selected events after cuts (3) – (11) with

$$\Delta\phi < 15^\circ, \quad P_{tCUT}^{clust} = 30 \text{ GeV}/c. \quad (23)$$

$P_{tCUT}^{out}$  is unlimited.

The main results of our analysis are given in the tables of Appendices 2–5. They show mean values of the most important variables that reflect the main features of “ $Z + jet$ ” events and the other values that characterise  $P_t^Z$  and  $P_t^{jet}$  balance in the abovementioned  $P_t^Z$  intervals.

Appendix 2 contains the tables for events inside  $45 < P_t^Z < 55 \text{ GeV}/c$  interval. In these tables we present the values of interest found with UA1, UA2 and LUCCELL jetfinders for three different Selections mentioned in Section 2.2. Each page corresponds to a definite value of  $\Delta\phi$

---

<sup>15</sup>( $\equiv$  CKIN(3) of PYTHIA)

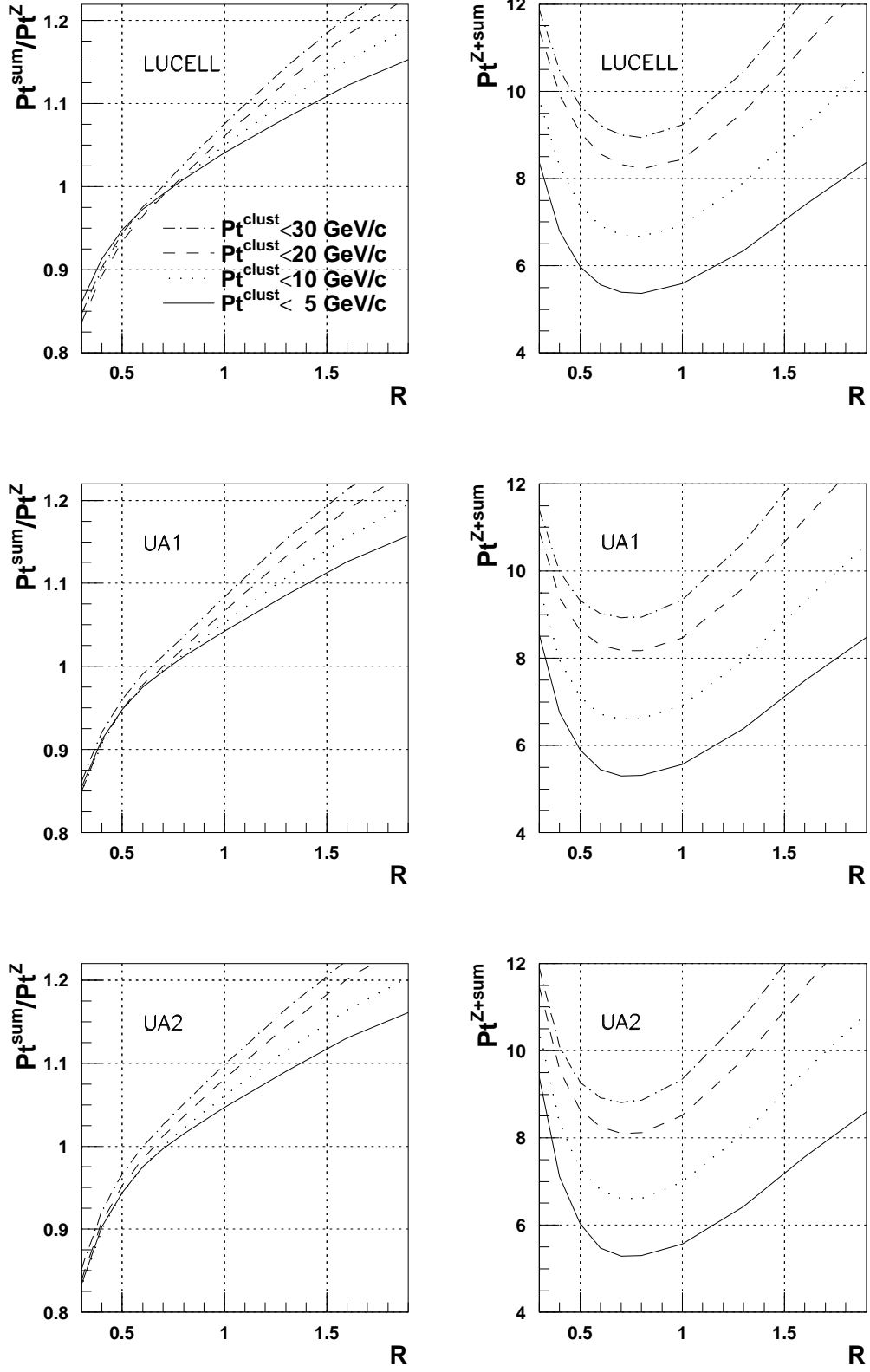


Fig. 9: LUCCELL, UA1 and UA2 algorithms,  $\Delta\phi < 15^\circ$ ,  $45 < P_t^Z < 55 \text{ GeV}/c$ .

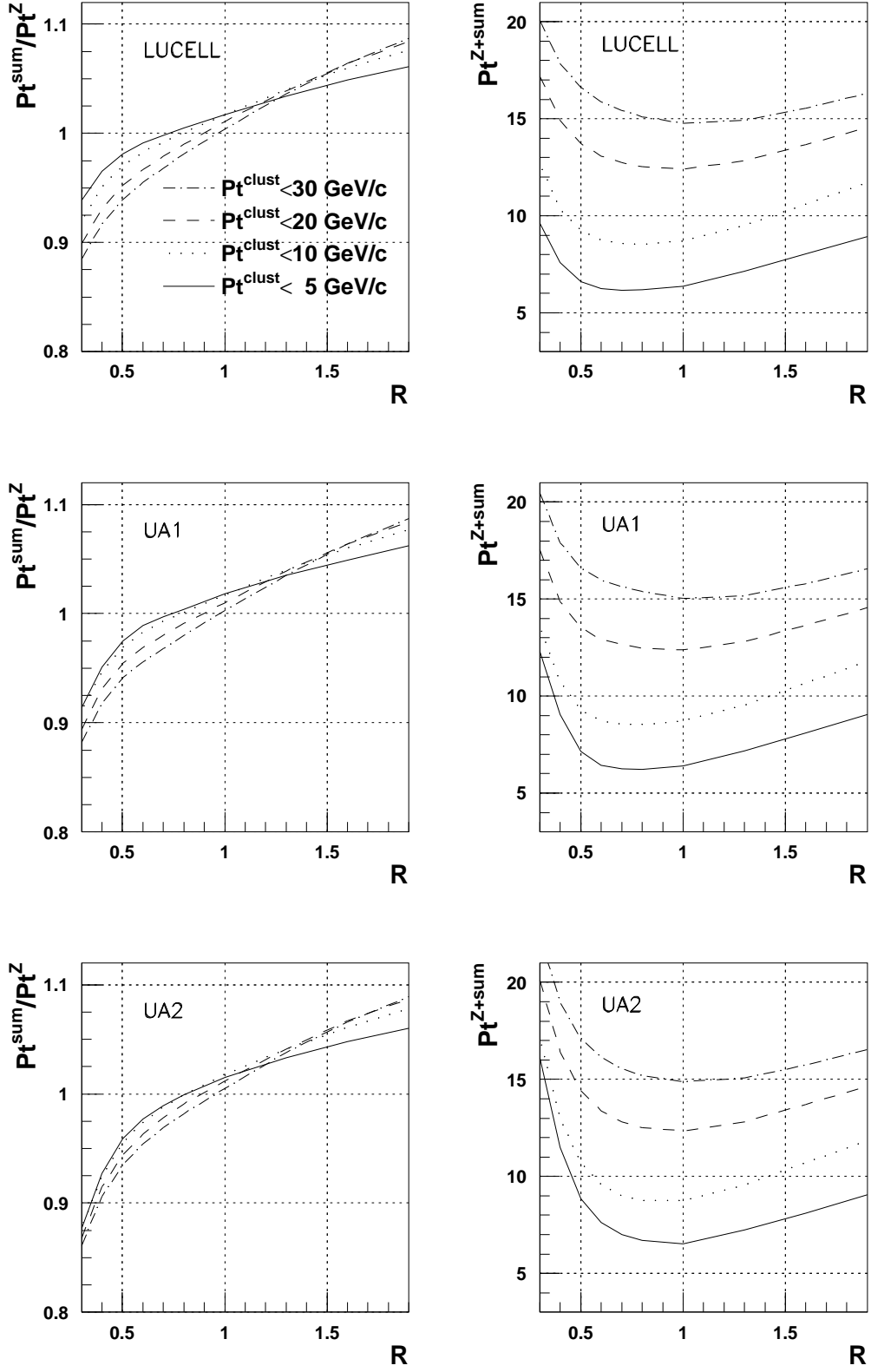


Fig. 10: LUCCELL, UA1 and UA2 algorithms,  $\Delta\phi < 15^\circ$ ,  $100 < P_t^Z < 120 \text{ GeV}/c$ .

as a measure of deviation from the absolute back-to-back orientation of  $\vec{P}_t^Z$  and  $\vec{P}_t^{Jet}$  vectors. The first four pages of each Appendix contain the information about variables that characterise the  $P_t^Z - P_t^{Jet}$  balance for events passed the cuts (3)–(11) (Selection 1).

On the fifth page of each of Appendices 2–5 we present Tables 13 – 15 (for the cut  $\Delta\phi < 15^\circ$ ) that correspond to Selection 2 described in Section 2.2. We have limited  $\epsilon^{jet} \leq 9\%$  for  $45 < P_t^Z < 55$  with a gradual change to  $\epsilon^{jet} \leq 3\%$  for  $P_t^Z \geq 100 \text{ GeV}/c$ . The best result for UA2 in the case of  $45 < P_t^Z < 55$  is obtained with  $\epsilon^{jet} \leq 6\%$  instead of the cut  $\epsilon^{jet} \leq 9\%$  chosen for UA1 and LUCCELL algorithms <sup>16</sup>. The results obtained with Selection 3 <sup>17</sup> are given on the sixth page of Appendices 2–5. Appendix 2 ( $45 < P_t^Z < 55 \text{ GeV}/c$ ) is supplemented on the seventh page by a variant of Selection 3 where we collect only events with jets found simultaneously by UA1 and LUCCELL jetfinders only.

The columns in Tables 1 – 18 correspond to five different values of  $P_{tCUT}^{clust} = 30, 20, 15, 10$  and  $5 \text{ GeV}/c$ . The upper lines of these tables contain the expected numbers  $N_{event}$  of “HB events”, i.e. those “ $Z + jet$ ” events in which the jet is entirely fitted into the barrel region of the HCAL (see Section 5), for the integrated luminosity  $L_{int} = 10 \text{ fb}^{-1}$ .

In the next four lines of the tables we put the values of  $P_t56, \Delta\phi, P_t^{out}, P_t^{\eta>5}$  defined by formulae (2), (9), (18) and (16), respectively, and averaged over the events selected with a chosen  $P_{tCUT}^{clust}$  value.

From the tables we see that the values of  $P_t56, \Delta\phi, P_t^{out}$  decrease fast with decreasing  $P_{tCUT}^{clust}$ , while the averaged values of  $P_t^{\eta>5}$  show very weak dependence on it (practically constant) <sup>18</sup>, what is in complete agreement with behaviour of these variables in the case of the “ $\gamma + jet$ ” events [14].

The following three lines (from 6-th to 8-th) show the average values of the variables  $(P_t^Z - P_t^{part})/P_t^Z, (P_t^J - P_t^{part})/P_t^J, (P_t^Z - P_t^J)/P_t^Z$  (here  $J \equiv \text{Jet}$ ). These lines correspond to the relative  $P_t$  balance at the  $Z^0$ -parton level (final state of the fundamental subprocess  $2 \rightarrow 2$ ), the difference of a parton  $P_t$  and a jet  $P_t$  (parton hadronization effect) and the relative  $P_t$  balance of the “ $Z^0 + \text{complete jet}$ ” system.

The next 9-th and 10-th lines include the averaged values of  $P_t(O + \eta > 5)/P_t^Z$  and  $(1 - \cos(\Delta\phi))$  that appear on the right-hand side of the balance equation (19).

As a rule, the value of  $\langle 1 - \cos(\Delta\phi) \rangle$  is smaller than the value of  $\langle P_t(O + \eta > 5)/P_t^Z \rangle$  for the cut  $\Delta\phi < 15^\circ$  and tends to decrease more with growing energy. So, we can conclude that the main source of the  $P_t$  disbalance in the “ $Z + jet$ ” system is defined by the term  $\langle P_t(O + \eta > 5)/P_t^Z \rangle$ .

The following line contains the averaged values of the standard deviations of  $(P_t^Z - P_t^J)/P_t^Z (\equiv Db[Z, J])$ . The values of this variable drop approximately by a factor of two (and even more for all intervals with  $P_t^Z > 100 \text{ GeV}/c$ ) while moving from  $P_{tCUT}^{clust} = 30 \text{ GeV}/c$  to  $P_{tCUT}^{clust} = 5 \text{ GeV}/c$  for all jetfinding algorithms.

The last lines of the tables present the number of generated events, i.e. entries left after cuts.

We see from the tables that more restrictive cuts on the observable  $P_t^{clust}$  lead to a de-

<sup>16</sup>In [12] – [16] the Selection 2 criterion was considered with a more severe cut  $\epsilon^{jet} \leq 2\%$ .

<sup>17</sup>Selection 3 (see Section 2.2, point 9) leaves only those events in which jets are found simultaneously by UA1, UA2 and LUCCELL jetfinders i.e. events with jets having up to a good accuracy equal coordinates of the center of gravity,  $P_t^{jet}$  and  $\phi_{(Z,jet)}$ .

<sup>18</sup>Compare with Figs. 9 and 10.

crease in  $P_t^{56}$  variable (non-observable one) that serves, according to (2), as measure of the initial state radiation transverse momentum  $P_t^{ISR}$ , i.e. of the main source of the  $P_t$  disbalance in the fundamental  $2 \rightarrow 2$  subprocesses (1a) and (1b). So, variation of  $P_{tCUT}^{clust}$  from 30 to 10  $GeV/c$  for  $\Delta\phi < 15^\circ$  leads to suppression of the  $P_t^{56}$  value (or  $P_t^{ISR}$ ) approximately by  $\approx 40 - 45\%$  for all  $P_t^Z$ .

A decrease in  $P_{tCUT}^{clust}$  leads to a decrease in the  $(P_t^Z - P_t^J)/P_t^Z$  ratio (mean values as well as standard deviations), i.e. we select the events that can be used to improve the jet energy calibration accuracy. For instance, in the case of  $70 < P_t^Z < 85 GeV/c$  the mean value of  $(P_t^Z - P_t^J)/P_t^Z$  drops from 4.5–4.9% to 0.9–1.5% (see Tables 4, 6 of Appendix 3) and in the case of  $100 < P_t^Z < 120 GeV/c$  the mean value of this variable drops from 3.4 – 3.7% to less than 0.6 – 1.0% for UA1 and LUCCELL jetfinders (Tables 4, 6 of Appendix 4). A worse situation is seen for the  $45 < P_t^Z < 55 GeV/c$  interval, where the disbalance changes, e.g. for LUCCELL algorithm, as 2.1  $\rightarrow$  1.8%. Meantime, RMS values with the same variations of  $P_{tCUT}^{clust}$  (from 30 to 10  $GeV/c$ ) decrease by 40 – 50%.

After imposing the jet isolation requirement (see Tables 13 – 15 of Appendices 2–5) we observe that for  $P_t^Z \geq 100 GeV/c$  the mean values of  $P_t^Z$  and  $P_t^{Jet}$  disbalance, i.e.  $(P_t^Z - P_t^J)/P_t^Z$ , are contained inside the 1% window for any  $P_{tCUT}^{clust}$ . For  $45 < P_t^Z < 55 GeV/c$  we see that  $P_{tCUT}^{clust}$  works more effectively than in the case of Selection 1. Thus,  $P_{tCUT}^{clust} = 15 GeV/c$  allows to reduce  $(P_t^Z - P_t^J)/P_t^Z$  to less than 1% level for all algorithms. The Selection 2 criterion leaves quite a sufficient number of events: about 10 000 – 18 000 (the lower value corresponds to UA2 algorithm for which stricter jet isolation cut was used) for  $45 < P_t^Z < 55 GeV/c$  with  $P_{tCUT}^{clust} = 15 GeV/c$  and about 4 500 for  $100 < P_t^Z < 120 GeV/c$  with  $P_{tCUT}^{clust} = 20 GeV/c$  (see Tables 13 – 15 of Appendices 2, 3) at  $L_{int} = 10 fb^{-1}$ .

The analogous results for Selection 3 are presented in Tables 16–18 of Appendices 2–5. Let us consider first the most difficult interval  $45 < P_t^Z < 55 GeV/c$ . From the tables of Appendix 2 one can see that this selection leads to approximately 20% reduction of the number of selected events as compared with the case of Selection 2. A combined usage of all three jetfinders (Tables 16–18) worsen the balance values. A requirement of simultaneous jet finding by only UA1 and LUCCELL algorithms practically does not change values of the  $P_t^Z$  and  $P_t^{Jet}$  balance and other variables, presented in Tables 19, 20, as compared with the case of Selection 2 and gives a better result (from point of view of the  $P_t^Z$  and  $P_t^{Jet}$  balance values as well as from point of view of the number of selected events) as compared with the case of combined usage of all three jetfinders for this aim (see plots A and B in Fig. 16). This fact stresses a good compatibility of UA1 and LUCCELL jetfinders. For other considered  $P_t^Z$  intervals UA1, UA2 and LUCCELL algorithms give more or less close results and a passage to Selection 3 does not worsen a situation.

In addition we can note that Selections 2 and 3, besides improving the  $P_t^Z$  and  $P_t^{Jet}$  balance value, also important for selecting events with a clean jet topology and rising the confidence level of a jet determination.

Figs. 11 – 19 can be considered as an illustration and a complement to the tables of Appendices 2–5 for the cut  $\Delta\phi < 15^\circ$ . In Fig. 11 we show dependence of the ratio  $(P_t^Z - P_t^J)/P_t^Z$  on  $P_{tCUT}^{clust}$  for Selection 1 and three jetfinders LUCCELL, UA1 and UA2 for two  $P_t^Z$  intervals:  $45 < P_t^Z < 55 GeV/c$  and  $100 < P_t^Z < 120 GeV/c$ .

Up to now we have been studying the influence of the  $P_{tCUT}^{clust}$  parameter on the  $P_t^Z - P_t^{Jet}$

disbalance. Let us see in analogy with Fig. 11 what effect is produced by  $P_{tCUT}^{out}$  variation<sup>19</sup>. If we constrain this variable to 5 GeV/c, keeping  $P_t^{clust}$  practically unbound by  $P_{tCUT}^{clust} = 30$  GeV/c then the mean and RMS values of  $(P_t^Z - P_t^J)/P_t^Z$  in the case of LUCCELL algorithm for  $45 < P_t^Z < 55$  GeV/c decrease from 3.8% to 0.7% and from 19.2% to 9.5%, respectively (see Fig. 18). For  $100 < P_t^Z < 120$  GeV/c practically all events, starting from the cut  $P_{tCUT}^{out} = 10$  GeV/c, have the mean and RMS values of  $(P_t^Z - P_t^J)/P_t^Z$  less than 1% and 6%, respectively. From these plots we also conclude that variation of  $P_{tCUT}^{out}$  improves the disbalance, in fact, in the same way as a variation of  $P_{tCUT}^{clust}$ . It is not surprising since the cluster  $P_t$  activity is a part of the  $P_t^{out}$  activity.

The influence of the  $P_{tCUT}^{out}$  variation (with the fixed value  $P_{tCUT}^{clust} = 10$  GeV/c) on the distribution of  $(P_t^Z - P_t^J)/P_t^Z$  is shown in Fig. 19 for Selection 1. By changing  $P_{tCUT}^{out}$  from 30 to 5 GeV/c the mean value of  $(P_t^Z - P_t^J)/P_t^Z$  drops from 2.2% to 0.2% for LUCCELL and from 3.5% to 1.1% for UA2 algorithms for the  $45 < P_t^Z < 55$  GeV/c interval. At the same time RMS values change from 13% to 9% for all algorithms.

Thus, we may conclude that the new cuts  $P_{tCUT}^{clust}$  and  $P_{tCUT}^{out}$  introduced in Section 2 as well as introduction of a new object of the “isolated jet” are found to be very efficient tools to improve the jet energy calibration accuracy. Their combined usage for this aim with an account of background events is studied in Section 7.

---

<sup>19</sup>The variable  $P_t^{out}$  enters into the expression  $P_t(O+\eta > 5)/P_t^Z$ , which makes a dominant contribution to the right-hand side of the  $P_t$  balance equation (19), as we mentioned above in connection with Figs. 9 and 10.

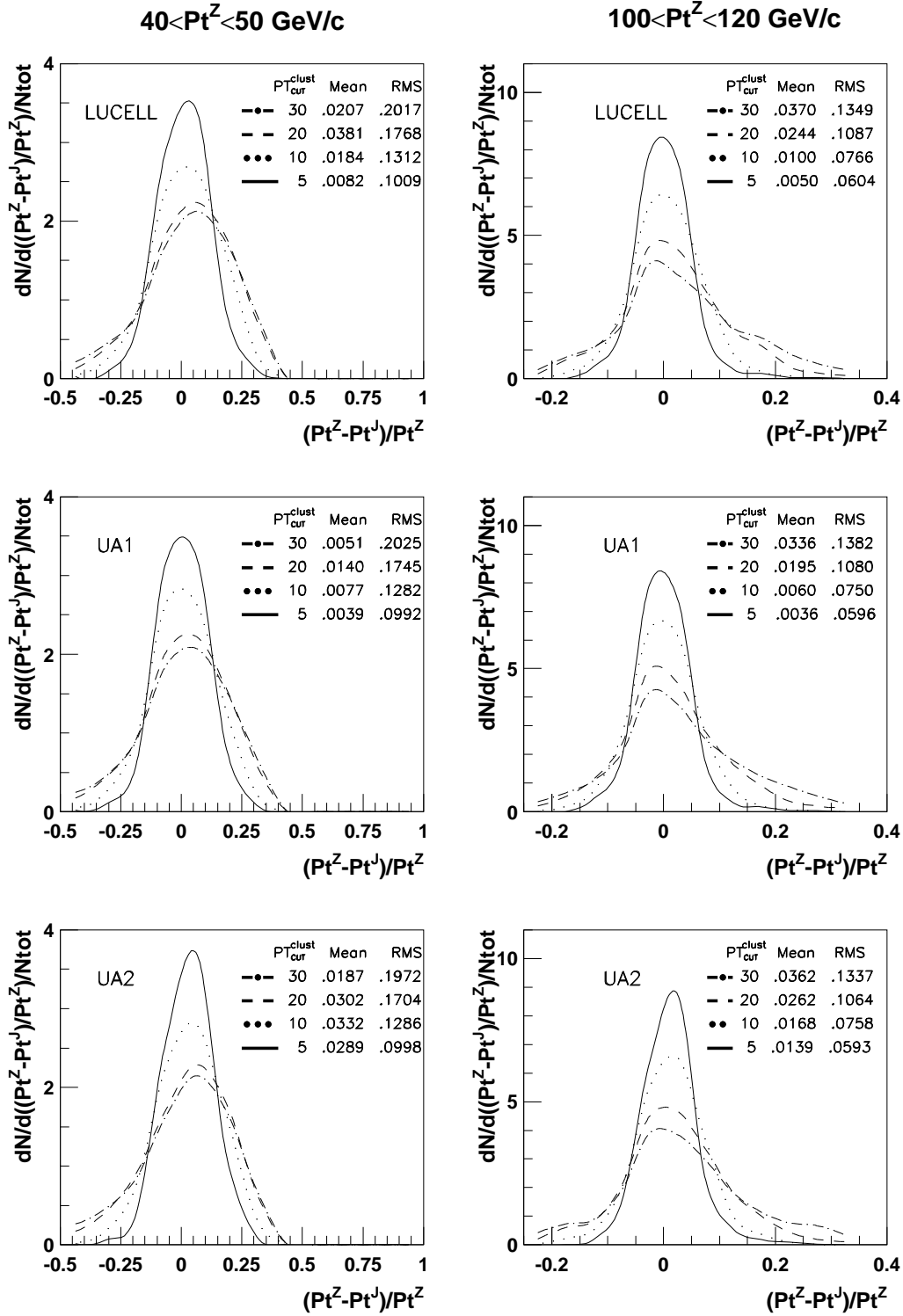
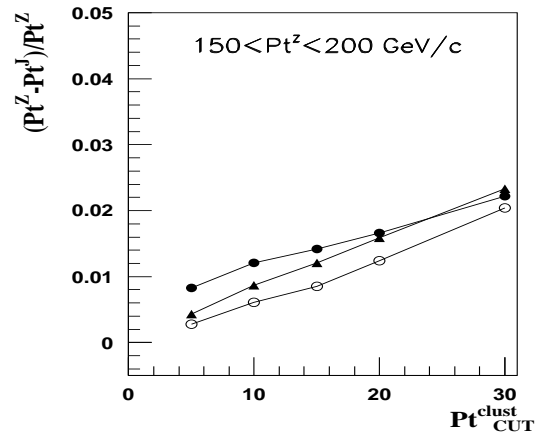
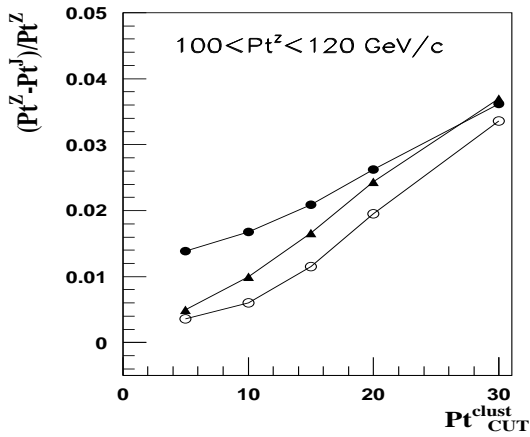
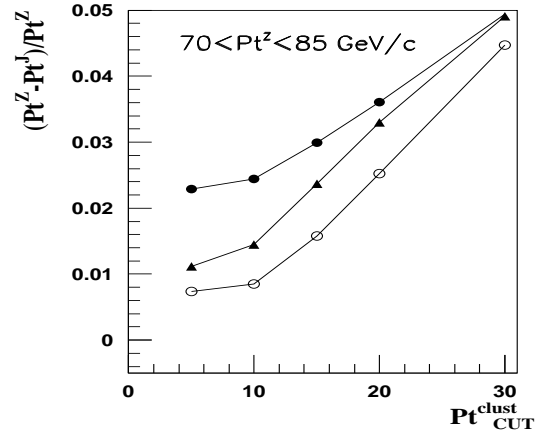
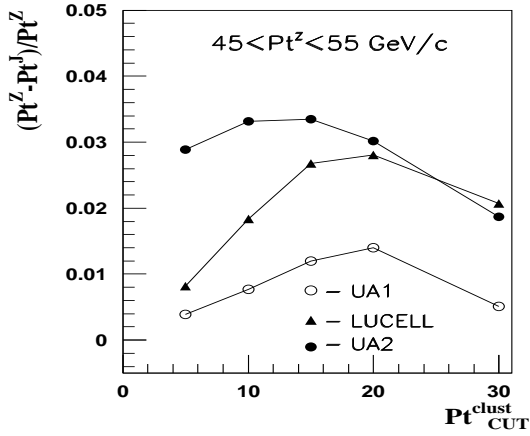
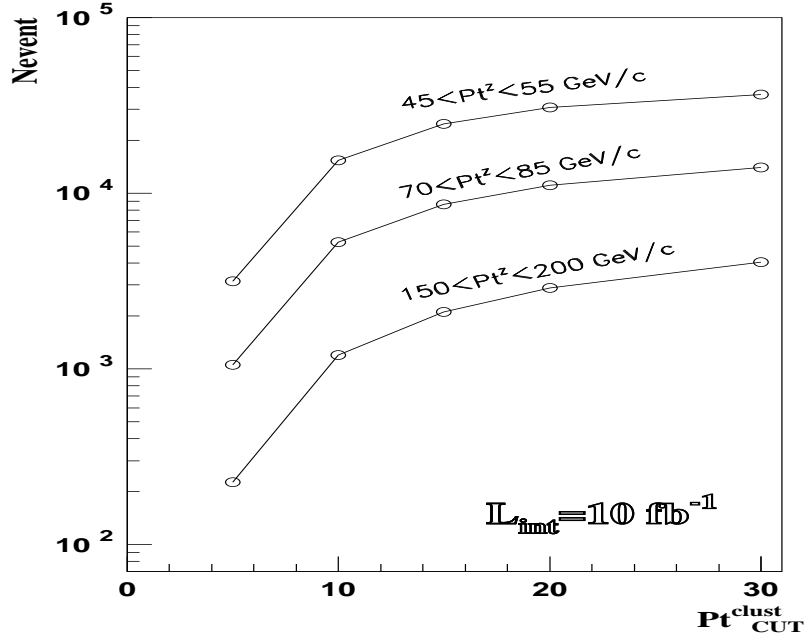
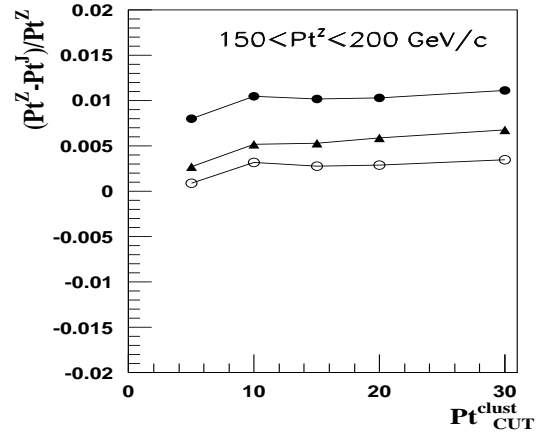
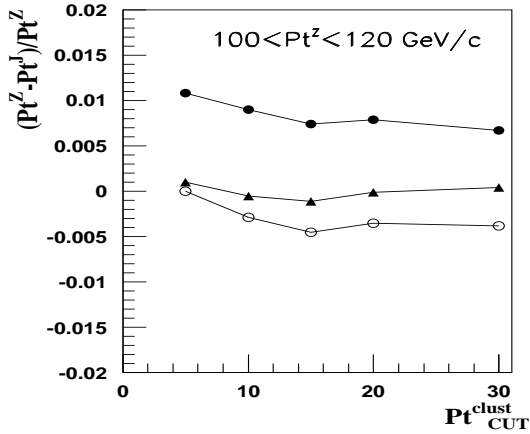
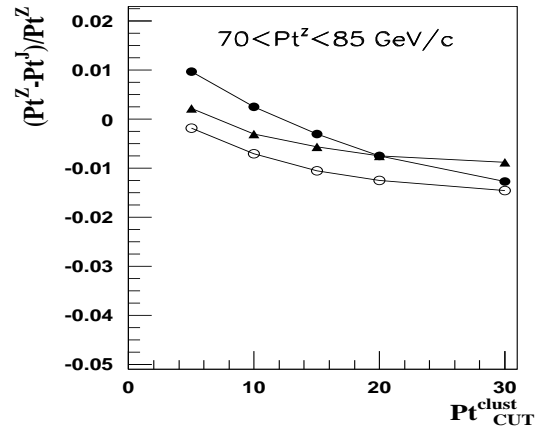
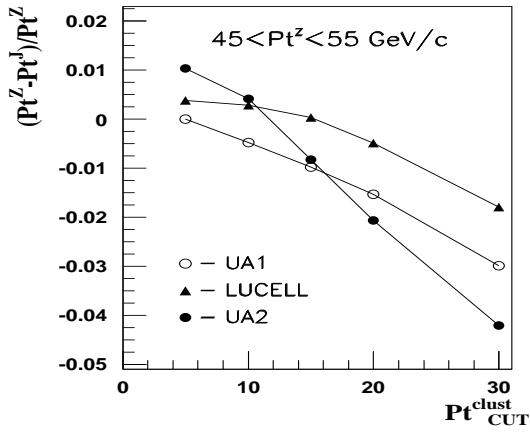
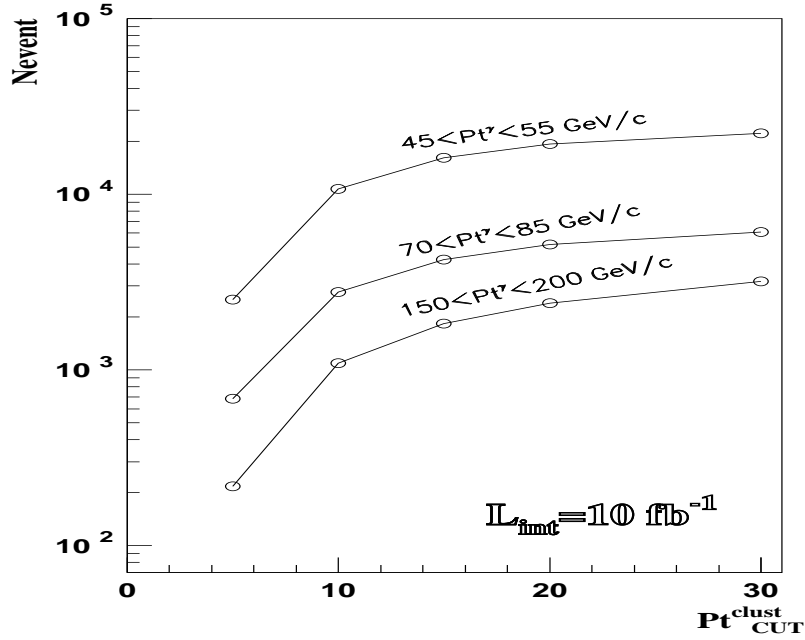


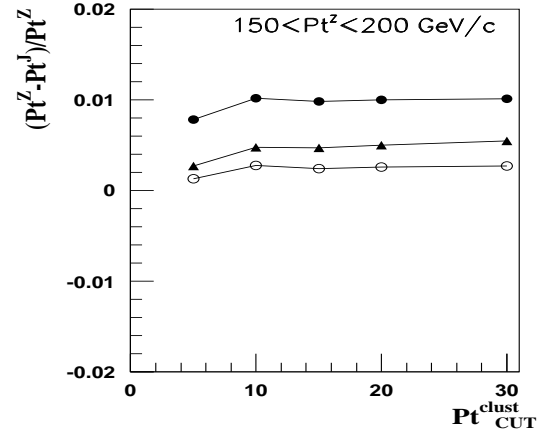
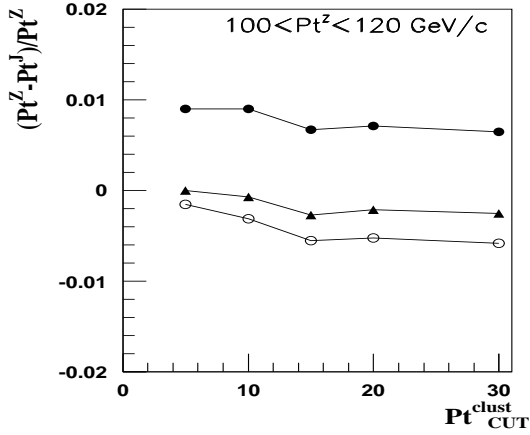
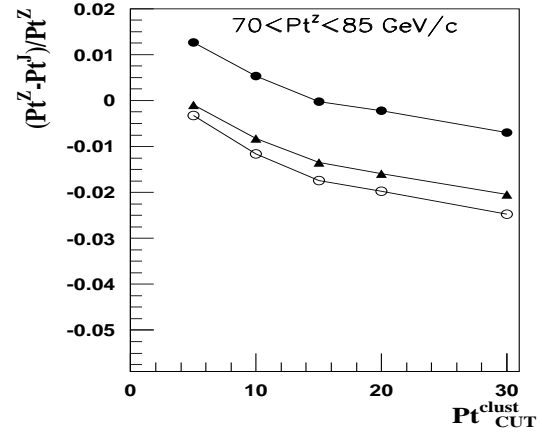
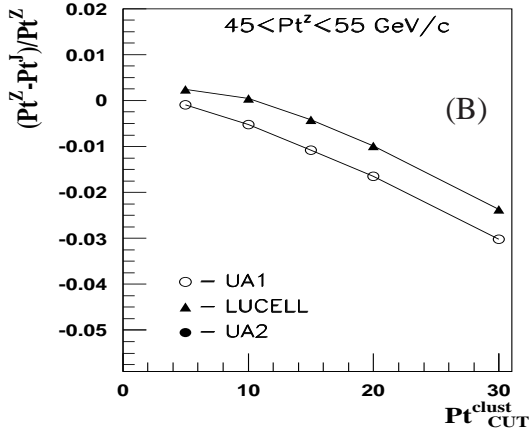
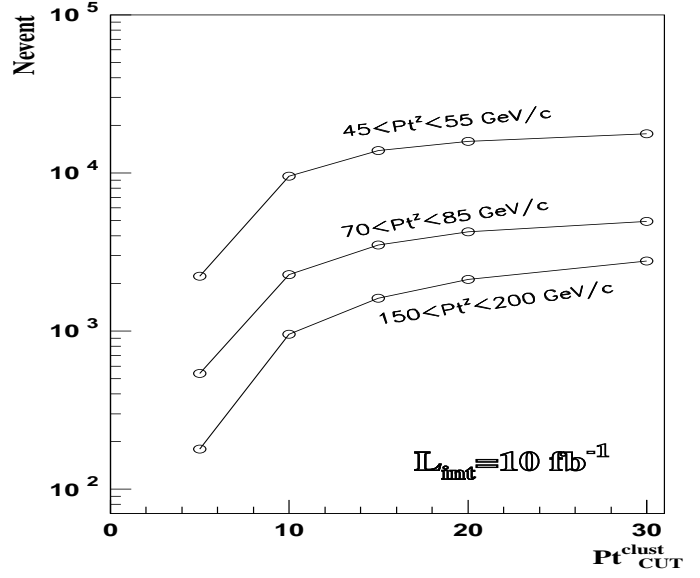
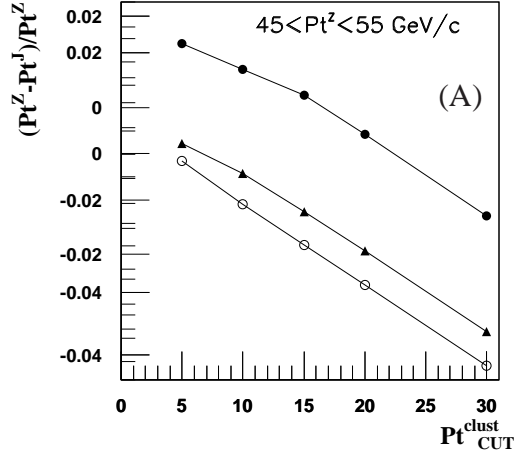
Fig. 11: A dependence of  $(P_t^Z - P_t^J)/P_t^Z$  on  $P_t^{clust}$  for LUCCELL, UA1 and UA2 jetfinding algorithms and two intervals of  $P_t^Z$ . The mean and RMS values of the distributions are displayed on the figures.  $P_t^{out}$  is not limited. Selection 1.



Selection 1. Dependence of the number of events for  $L_{int} = 10 \text{ fb}^{-1}$  (Fig. 12, top) and  $(P_t^Z - P_t^J)/P_t^Z$  (Fig. 13, four bottom plots) on  $Pt_{CUT}^{clust}$  in cases of LUCELL, UA1 and UA2 jetfinding algorithms.  $\Delta\phi = 15^\circ$ .  $P_t^{out}$  is not limited.



Selection 2. Dependence of the number of events for  $L_{int} = 10 fb^{-1}$  (Fig. 14, top) and  $(P_t^Z - P_t^J)/P_t^Z$  (Fig. 15, four bottom plots) on  $P_t^{clust CUT}$  in cases of LUCCELL, UA1 and UA2 jetfinding algorithms.  $\Delta\phi = 15^\circ$ .  $P_t^{out}$  is not limited.  $\epsilon^{jet} < 6 - 9\%$  ( $45 < P_t^Z < 55$ ),  $< 5\%$  ( $70 < P_t^Z < 85$ ),  $< 4\%$  ( $100 < P_t^Z < 120$ ),  $< 3\%$  ( $150 < P_t^Z < 200$ ).



Selection 3. Dependence of the number of events for  $L_{int} = 10 fb^{-1}$  (Fig. 16, top) and  $(P_t^Z - P_t^J)/P_t^Z$  (Fig. 17, one left-hand top and four bottom plots) on  $P_{tCUT}^{clust}$  in cases of LUCCELL, UA1 and UA2 jetfinding algorithms.  $\Delta\phi = 15^\circ$ .  $P_t^{out}$  is not limited.  $\epsilon^{jet} < 9\%$  ( $45 < P_t^Z < 55$ ),  $< 5\%$  ( $70 < P_t^Z < 85$ ),  $< 4\%$  ( $100 < P_t^Z < 120$ ),  $< 3\%$  ( $150 < P_t^Z < 200$ ).

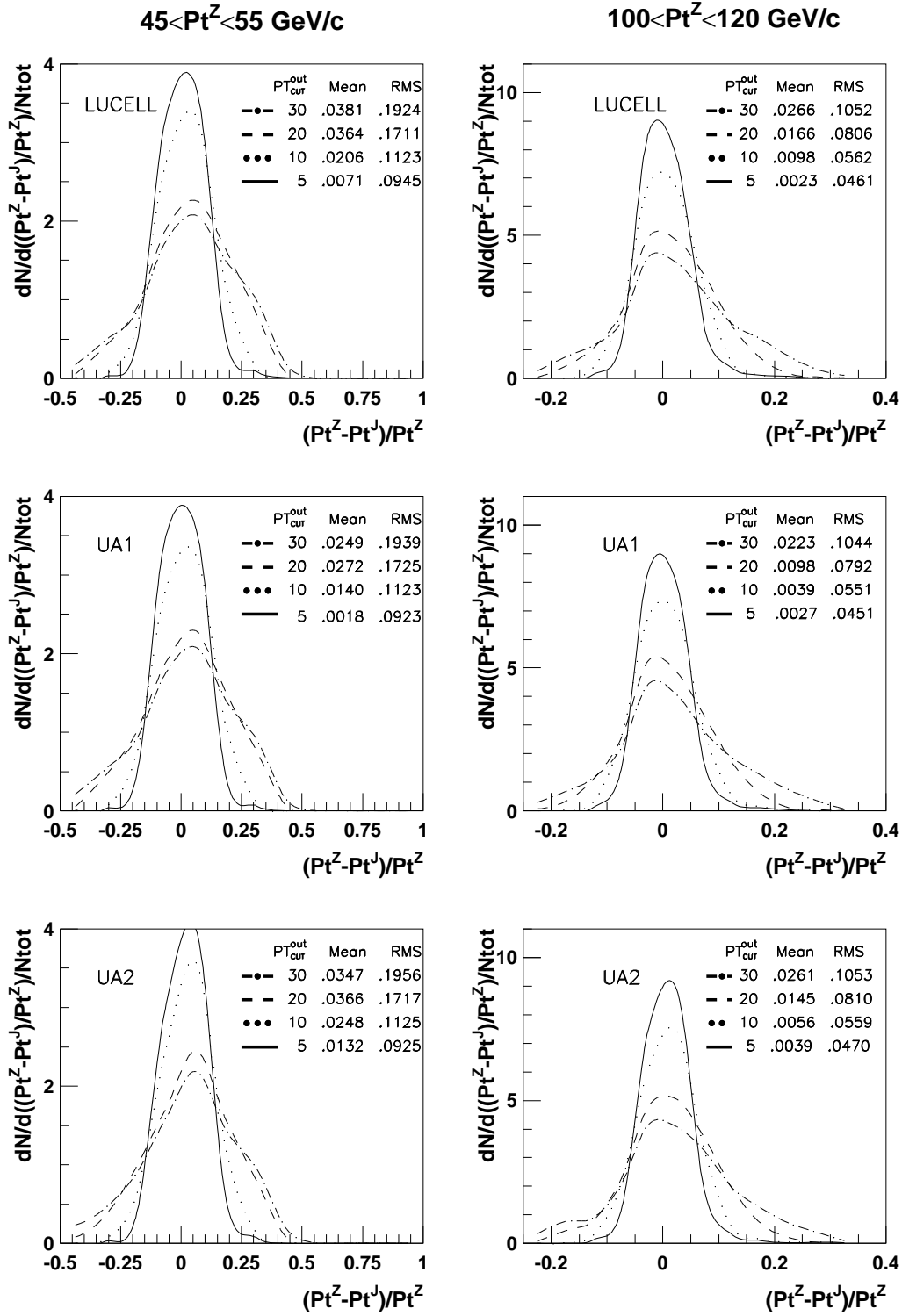


Fig. 18: A dependence of  $(P_t^Z - P_t^J)/P_t^Z$  on  $P_t^{out}_{CUT}$  for LUCCELL, UA1 and UA2 jetfinding algorithms and two intervals of  $P_t^Z$ . The mean and RMS values of the distributions are displayed on the figures.  $P_t^{clust} < 30 GeV/c$ . Selection 1.

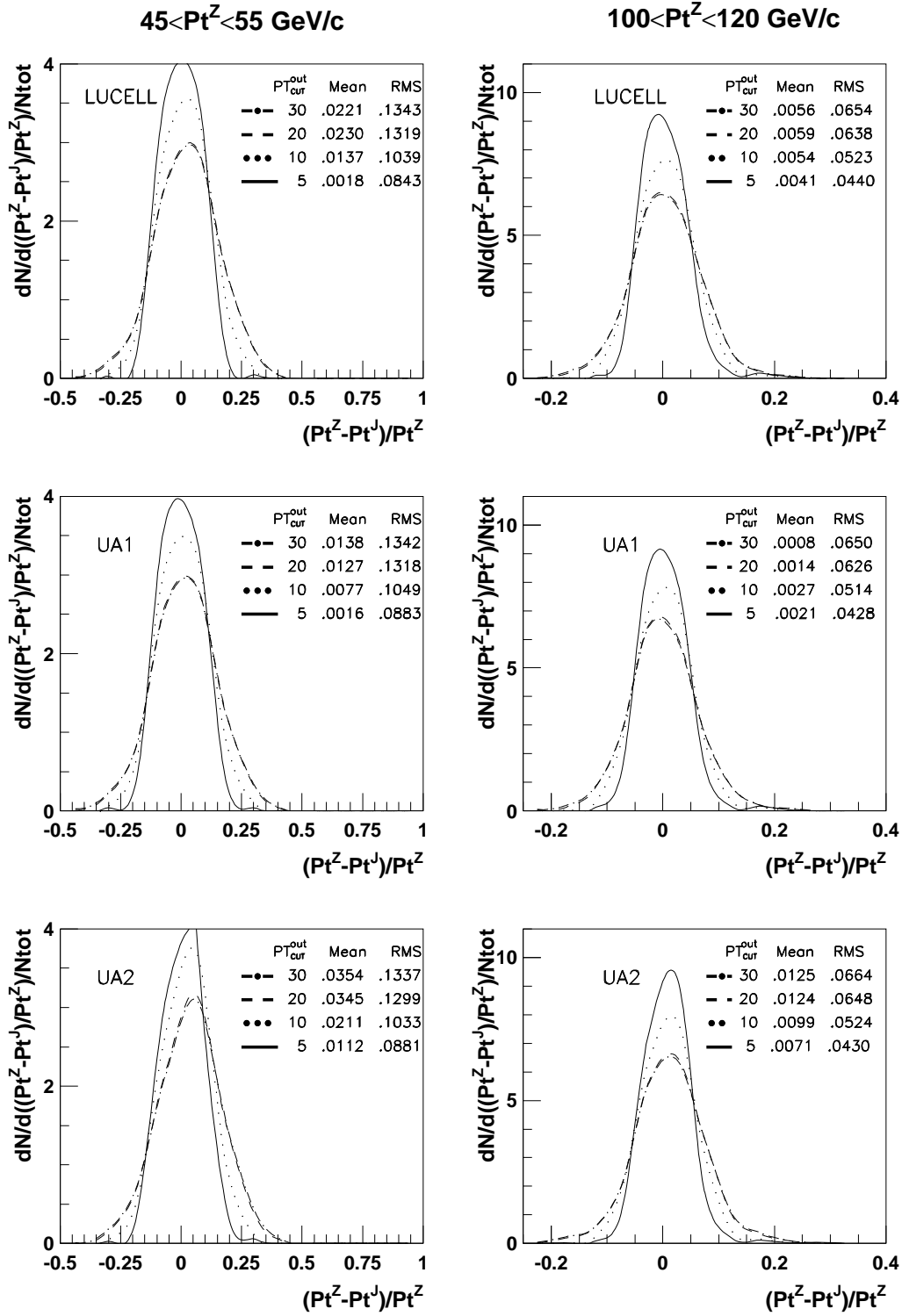


Fig. 19: A dependence of  $(P_t^Z - P_t^J)/P_t^Z$  on  $P_t^{out}_{CUT}$  for LUCCELL, UA1 and UA2 jetfinding algorithms and two intervals of  $P_t^Z$ . The mean and RMS values of the distributions are displayed on the figures.  $P_t^{clust} < 10 GeV/c$ . Selection 1.

## 7. THE STUDY OF BACKGROUND SUPPRESSION.

The main source of the background to our signal “ $Z + jet$ ” events, based on the subprocesses (1a) and (1b), is the Drell-Yan (DY) subprocess  $q\bar{q} \rightarrow \mu^+\mu^-$  with a hard gluon radiation in the initial state. The next-to-leading order (NLO) Feynman diagrams of this process are shown in Fig. 20. The radiated gluon fragments to a jet which has a transverse momentum directed in the opposite side (in  $\phi$ ) with respect to a transverse momentum of  $Z^0$  boson (if we neglect  $k_T$  and gluon-jet hadronization effects).

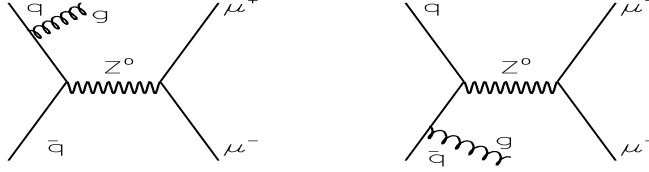


Fig. 20: NLO Feynman diagrams of Drell-Yan process with radiation of a gluon in the initial state.

The second source of the background theoretically can be produced in the events which are based on the QCD subprocesses (like  $qq \rightarrow qq$  or  $qg \rightarrow qg$ ) having much larger cross sections than our signal subprocesses (1a) and (1b). Both background contributions are considered here.

To estimate the background from the DY subprocess, we carried out simulation<sup>20</sup> with a mixture of our main signal subprocesses (1a) and (1b) (ISUB=15 and 30 in PYTHIA) and DY subprocess (ISUB=1 in PYTHIA) with allowed only one decay mode of  $Z^0$  boson to the muon pair. Three generations with the abovementioned set of subprocesses were performed, each with different minimal values of  $P_t$  of the hard  $2 \rightarrow 2$  subprocess<sup>21</sup>  $\hat{p}_\perp^{min}$ . These values were  $\hat{p}_\perp^{min} = 20, 35$  and  $50 \text{ GeV}/c$ . By 2–3 million events were generated for every  $\hat{p}_\perp^{min}$  value.

We selected “ $Z^0 + 1 \text{ Jet}$ ” events according to the criteria from Section 2.2 in which  $Z^0$  boson is reconstructed from high-energetic isolated muons<sup>22</sup>.

Table 13: List of the applied cuts used in Tables 14, 15.

---

<b>0.</b> Total number of $\mu^+\mu^-$ pairs (No selection);
<b>1.</b> (a) $P_t^\mu > 10 \text{ GeV}/c$ ; (b) $ \eta^\mu  < 2.4$ ; (c) $P_{t_{ch}}^\mu < 2 \text{ GeV}/c$ ; (d) $ M_Z - M_{inv}^\mu  < 5 \text{ GeV}/c^2$ ; (e) $P_t^Z > P_{t_{min}}^Z (= 40, 70, 100 \text{ GeV}/c)$ ; (f) 1 jet events selected;
<b>2.</b> $\Delta\phi < 15^\circ$ ;
<b>3.</b> $P_{t_{max}}^\mu > P_{t_{CUT}}^\mu (= 40, 50, 60 \text{ GeV}/c)$ .
<b>4.</b> $P_t^{clust} < 15 \text{ GeV}/c$ ;
<b>5.</b> $P_t^{clust} < 10 \text{ GeV}/c$ ;
<b>6.</b> $\Delta P_t^{Jet}(\Delta R = 0.3)/P_t^{Jet} \leq 0.10$ .
<b>7.</b> $\Delta P_t^{Jet}(\Delta R = 0.3)/P_t^{Jet} \leq 0.05$ .

---

Points 1(e) means that in the first generation we selected the events with  $P_t^Z > 40 \text{ GeV}/c$ , in the second with  $P_t^Z > 70 \text{ GeV}/c$  and in the third with  $P_t^Z > 100 \text{ GeV}/c$ .

<sup>20</sup>PYTHIA 5.7 version with default CTEQ2L parameterisation of structure functions is used here.

<sup>21</sup>i.e  $CKIN(3)$  parameter in PYTHIA

<sup>22</sup>Everywhere throughout the paper speaking about  $Z^0$  boson we imply the muon pair with the characteristics of muons listed in Section 2.2 and Table 13.

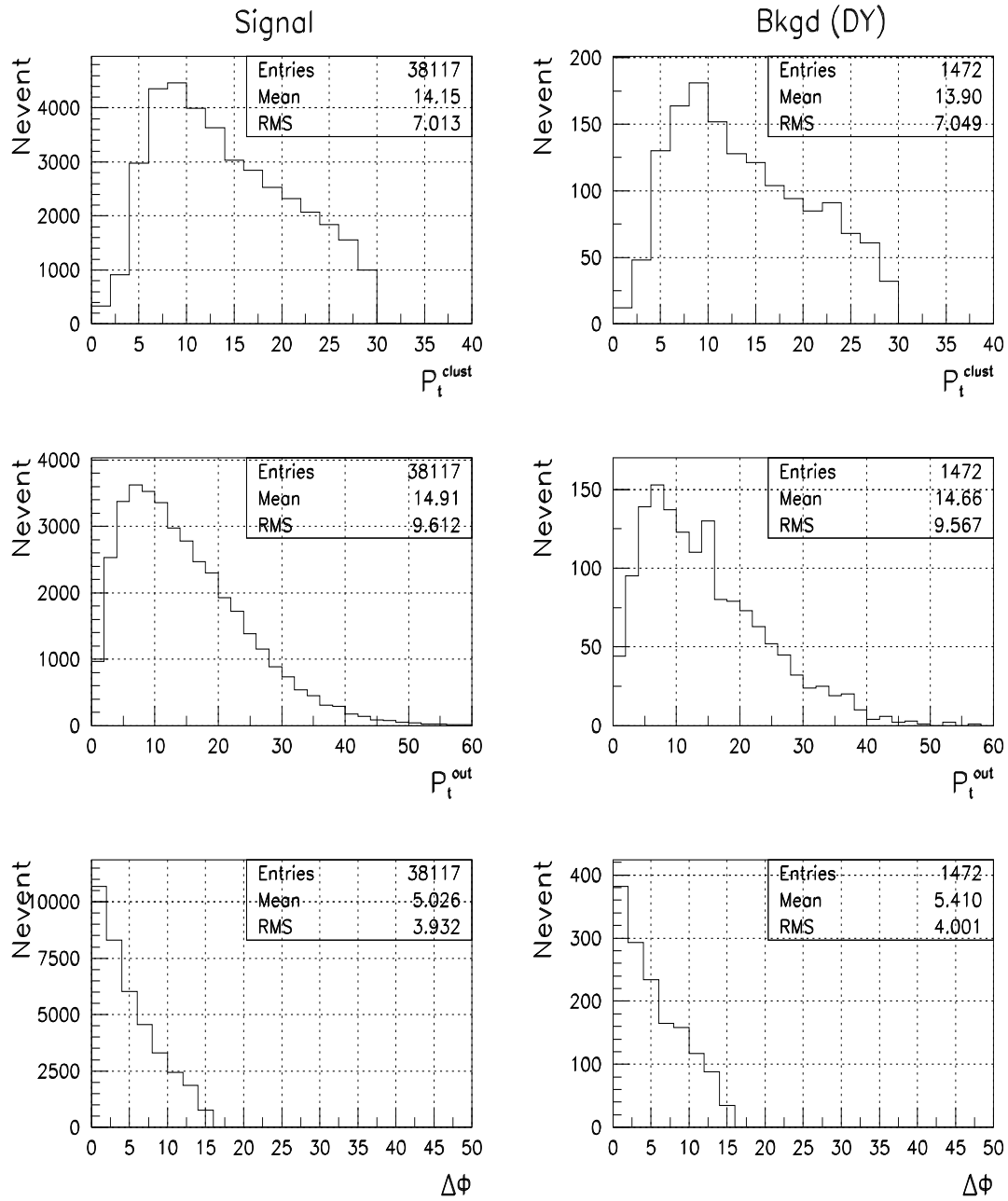


Fig. 21: Signal/Background: Number of events distribution over  $P_t^{clust}$ ,  $P_t^{out}$ ,  $\Delta\phi$  ( $P_t^Z \geq 70 \text{ GeV}/c$ ).

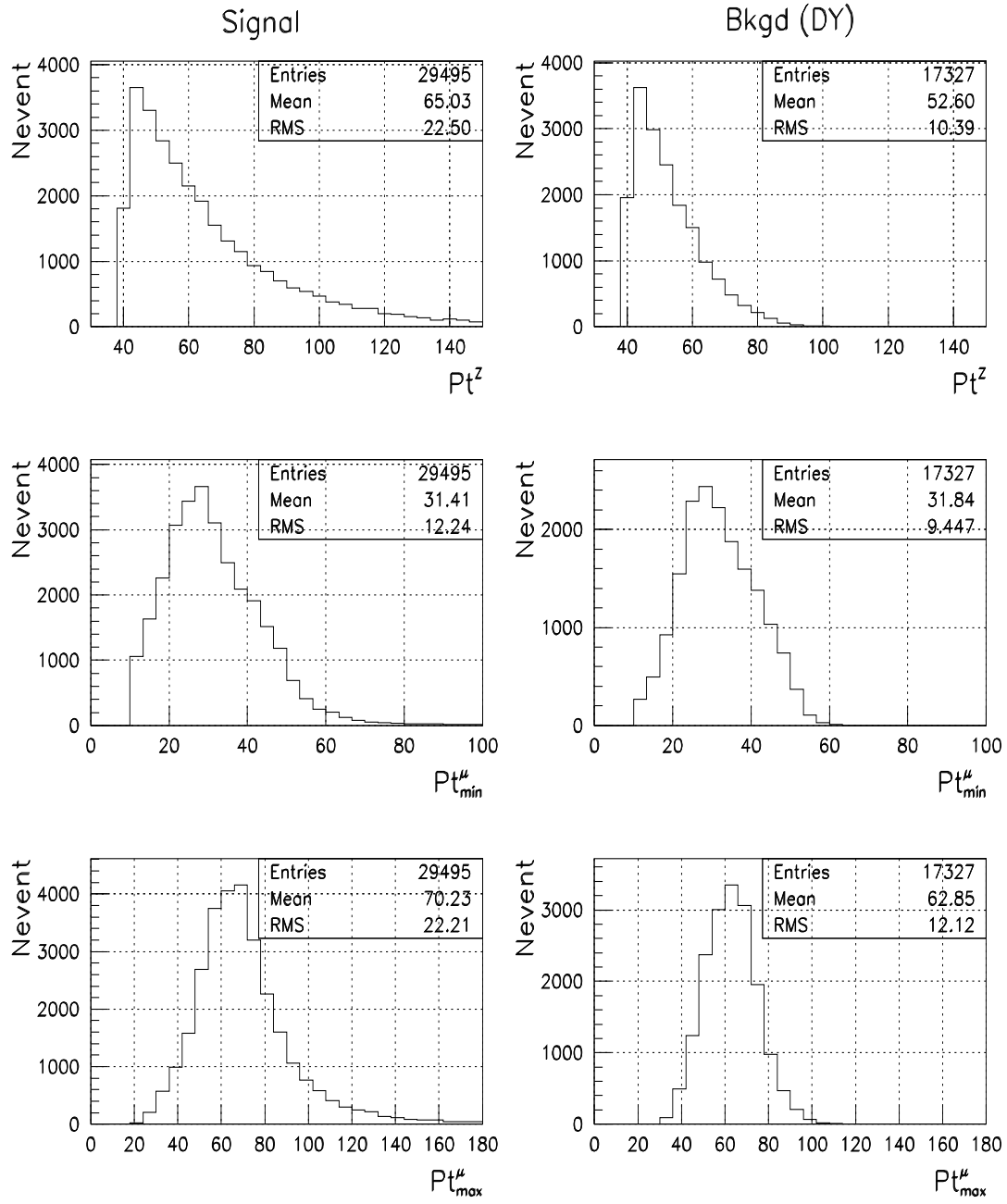


Fig. 22: Signal/Background: Number of events distribution over  $P_t^Z$ ,  $P_t^\mu_{min}$ ,  $P_t^\mu_{max}$  ( $P_t^Z \geq 40 \text{ GeV}/c$ ).

It turned out that the signal and background (DY) events have very similar distributions over variables  $P_t^{clust}$ ,  $P_t^{out}$  and  $\Delta\phi$  (angle between the transverse momenta vectors of  $Z^0$  boson and jet; see (9)). As an example, we have shown them in Fig. 21 for the case of  $P_t^Z \geq 70 \text{ GeV}/c$ . The events used in these distributions were preselected after the cut 1 of Table 13 above.

In Fig. 22 we have plotted the distributions over reconstructed  $P_t$  of  $Z^0$  boson ( $P_t^Z$ ), minimal and maximal  $P_t$  of muons in the pair ( $P_{tmin}^\mu$  and  $P_{tmax}^\mu$ ). We can see from the pictures that  $P_t^Z$  distribution in signal events is much wider than one for background (DY) events (compare RMS values of the corresponding plots) and has, on the average, greater mean value of  $P_t^Z$ . The same is true with respect to the distributions over  $P_{tmax}^\mu$ .

To demonstrate the way we have come to the final results, we shall apply the cuts from Table 13 on the observable physical variables one after another. The influence of these cuts on the signal to background (DY) ratio  $S/B$  is presented in Table 14 for a case of  $P_t^Z \geq 70 \text{ GeV}/c$ . The numbers in left-hand column of this table (“Selection”) coincide with the numbers of cuts listed in Table 13. The second and the third columns contain the numbers of  $\mu^+\mu^-$  pairs in signal (“Signal”) and background (“Bkgd”) events, respectively, left after application of each cut. The other columns of Table 14 include efficiencies  $Eff_{S(B)}$  (with their errors) defined as a ratio of the number of signal (background) events that passed under a cut (1–7) to the total number of muon pairs in events (zeroth cut in Tables 13, 14). They are followed by the column containing the values of  $S/B$ .

Table 14: Values of efficiencies and signal-to-background ratios for  $P_t^Z = 70 \text{ GeV}/c$  (main background).

Selection	Signal	Bkgd	$Eff_S(\%)$	$Eff_B(\%)$	$S/B$
0	1627466	3537480	100.00±0.00	100.00±0.00	0.46
1	115422	4470	7.092 0.022	0.1264 0.0019	25.8
2	103147	3678	6.338± 0.020	0.104± 0.002	28.0
3	81086	2718	4.982± 0.018	0.077± 0.002	29.8
4	46846	1572	2.878± 0.013	0.044± 0.001	29.8
5	26963	918	1.657± 0.010	0.026± 0.001	29.3
6	26165	888	1.608± 0.010	0.025± 0.001	29.5
7	21503	630	1.321± 0.009	0.018± 0.001	34.1

Total number collected  $\mu^+\mu^-$  pairs is presented in the first line of this table. We see that initially to every muon pair in the signal events sample corresponds, on the average, two pairs from the background (DY) sample ( $S/B = 0.46$ ). After the set of cuts 1(a) – 1(f) of Table 13 we obtain  $S/B = 25.8$ . Criteria 2 ( $\Delta\phi < 15^\circ$ ) and 3 ( $P_{tmax}^\mu > 50 \text{ GeV}/c$ ) improve the ratio up to  $S/B = 29.8$ , while the cluster suppressions cuts 4 and 5 remain it, in fact, without a change. The selection of events with well-isolated jet ( $\Delta P_t^{Jet}/P_t^{Jet} \leq 0.05$ ), i.e. suppression  $P_t$  activity in the ring of  $\Delta R = 0.3$  around a jet to the level less than 5%, allows to increase the  $S/B$  ratio to 34.1<sup>23</sup>. The summary of Table 14 is presented in the middle section ( $P_{tmin}^Z = 70 \text{ GeV}/c$ ) of Table 15 where lines “Total (no selection)” corresponds to point 0 of Table 13 and correspondingly to the line with 0th selection of Table 14. The lines

<sup>23</sup>One can suppose that a reason of such an improvement is that in the background (DY) events a jet originates from a gluon, i.e. of the gluon type, while in the signal sample a jet is mainly of a quark type. As it is known, a jet of the first type is a little broader than a jet of the last type.

“Main (1–5)” of Table 15 corresponds to the line with 5th selection of Table 14 and lines “jet isol. (6, 7)” corresponds to selections 6 and 7 of Table 14. The first and last section of Table 15 present the results of generations with selection of events with  $P_t^Z \geq 70 \text{ GeV}/c$  and  $P_t^Z \geq 100 \text{ GeV}/c$  respectively. In the case of  $P_t^Z \geq 100 \text{ GeV}/c$  we see that there is no background events at all after cuts 1–5 of Table 13.

Table 15: Values of efficiencies and signal-to-background ratios  
(main background).

$P_t^Z$	Selections	Signal	Bkgd	$Eff_S(\%)$	$Eff_B(\%)$	$S/B$
40 ( $\text{GeV}/c$ )	Total (no selection)	1465190	3786758	100.00±0.00	100.00±0.00	0.39
	Main (1 – 5)	23796	11880	1.624 ± 0.011	0.314 ± 0.003	2.0
	jet isol. (6, 7)	15006	5532	1.024 ± 0.008	0.146 ± 0.002	2.7
70 ( $\text{GeV}/c$ )	Total (no selection)	1627466	3537480	100.00±0.00	100.00±0.00	0.46
	Main (1 – 5)	26963	918	1.657± 0.010	0.026± 0.001	29.3
	jet isol. (6, 7)	21503	630	1.321± 0.009	0.018± 0.001	34.1
100 ( $\text{GeV}/c$ )	Total (no selection)	4880652	704632	100.00±0.00	100.00±0.00	6.9
	Main (1 – 5)	139046	0	2.849±0.008	0.000	—
	jet isol. (6, 7)	117483	0	2.407±0.007	0.000	—

The Signal/Background ratios as a function of  $P_t^Z$  for events generated with  $\hat{p}_\perp^{min} = 20 \text{ GeV}/c$  and selected after cuts 1 – 3 of Table 13 are shown in Fig. 23.

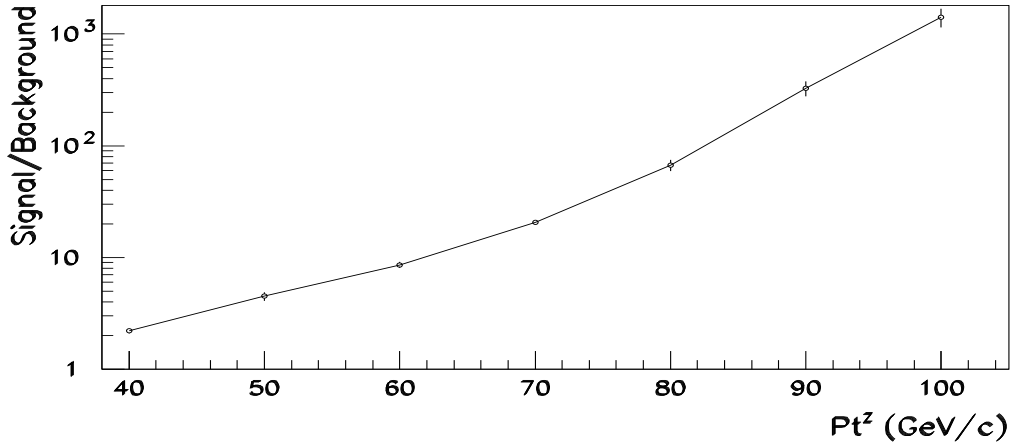


Fig. 23: Signal/Background ratio as a function of  $P_t^Z$  after the set of cuts 1 – 3 from Table 13 (Errors are about 5%, 10% and 20% at  $P_t^Z = 40, 80$  and  $100 \text{ GeV}/c$  respectively).

In principle, there is a probability, that some combination of muons in the events, based on the QCD subprocesses with much larger cross sections than ones in our signal subprocesses, can be registered as the  $Z^0$  signal. This type of background we call as “combinatorial background”. To study a rejection possibility of such type of events by about 40 million events with a mixture of all QCD and SM subprocesses with large cross sections existing in PYTHIA<sup>24</sup> which can lead to a background for the signal subprocesses (1a) and (1b) were generated. Each generation was performed with different  $\hat{p}_\perp^{min}$ . These values were  $\hat{p}_\perp^{min} = 40, 70$  and  $100 \text{ GeV}/c$ . It is

<sup>24</sup>(namely, ISUB=11–20, 28–31, 53, 68)

worth mentioning that total cross section of background processes exceeds the cross section of signal processes by about 5 orders of magnitude at all considered energies. That is why we carried out the simulation of such a big number of events.

Table 16 contains the set of applied cuts, that is more detailed as compared with the set in Table 13. These criteria have the same meaning as in Table 13.

Table 16: List of the applied cuts used in Tables 17, 18.

---

<b>0.</b> Total number of $\mu^+\mu^-$ pairs (No selection);
1. $P_t^\mu > 10 \text{ GeV}/c,  \eta^\mu  < 2.4$ ;
2. $ M_Z - M_{inv}^{\mu\mu}  < 20 \text{ GeV}/c^2$ ;
3. 1 jet events selected;
4. $P_{tch}^\mu < 2 \text{ GeV}/c$ ;
5. $ M_Z - M_{inv}^{\mu\mu}  < 5 \text{ GeV}/c^2$ ;
6. $\Delta\phi < 15^\circ$ .

---

Again, to follow the effect of their application let us consider first the case of one (intermediate) energy, i.e. the generation with  $\hat{p}_\perp^{min}=70 \text{ GeV}/c$ . The total number of  $\mu^+\mu^-$  pairs corresponds to the 0th selection in Table 17. A weak restriction in the 1st selection increase  $S/B$  by about 2 order (as  $5e-4 \rightarrow 2e-2$ ). The invariant mass criterion and one-jet events selection makes  $S/B = 18.0$  and the last criterion ( $\Delta\phi < 15^\circ$ ) suppresses the background events completely.

The information on other intervals is presented in Table 18. Line ‘‘Preselected’’ corresponds to the first cuts in Table 16 ( $P_t^\mu > 10 \text{ GeV}/c, |\eta^\mu| < 2.4$ ) while line ‘‘1–5’’ corresponds to results of application of criteria from 1 to 5 of Table 16. After the last criterion ( $\Delta\phi < 15^\circ$ ) we have observed no background events with 20 – 30% reduction of the signal events <sup>25</sup>.

Table 17: Values of efficiencies and signal-to-background ratios for  $\hat{p}_\perp^{min}=70 \text{ GeV}/c$  (combinatorial background).

Selection	Signal	Bkgd	$Eff_S(\%)$	$Eff_B(\%)$	$S/B$
0	401	850821			5e-4
1	245	15842	100.00±0.00	100.00±0.000	0.02
2	226	467	92.24±8.51	2.948±0.138	0.5
3	99	12	40.41±4.81	0.076±0.022	8.3
4	81	10	33.00±4.24	0.063±0.020	8.1
5	72	4	29.39±3.94	0.025±0.013	18.0
6	62	0	25.31±3.60	0.000±0.000	–

In the previous section we have seen that introduced in Section 2.2 (and earlier in [12] and [19])  $P_{tCUT}^{clust}$  and  $P_{tCUT}^{out}$  allow to select ‘‘Z + jet’’ events with a good  $P_t^Z$  and  $P_t^{Jet}$  balance. The influence of a wide variation of these two cuts on  
(a) the number of selected events (for  $L_{int} = 10 \text{ fb}^{-1}$ );

<sup>25</sup>not shown in Table 18

Table 18: Values of efficiencies and signal-to-background ratios  
(combinatorial background).

$\hat{p}_\perp^{min}$	Selections	Signal	Bkgd	$Eff_S(\%)$	$Eff_B(\%)$	$S/B$
40 (GeV/c)	Preselected (1)	89	1090	100.00±0.00	100.00±0.00	0.08
	1 – 5	30	0	33.71±7.12	0.00±0.00	–
70 (GeV/c)	Preselected (1)	245	15842	100.00±0.00	100.00±0.00	0.02
	1 – 5	72	4	29.39±3.94	0.025±0.013	18.0
100 (GeV/c)	Preselected (1)	497	37118	100.00±0.00	100.00±0.00	0.01
	1 – 5	127	4	25.55±2.54	0.011±0.005	31.8

(b) the signal-to-background ratio  $S/B$ ;

(c) the mean value of  $(P_t^Z - P_t^{jet})/P_t^Z$  and its standard deviation value  $\sigma(F)$

is presented in Tables 1–12 of Appendix 6. The set of cuts (1) – (4) of Table 13 were applied to select “ $Z + jet$ ” events (signal+background (DY)) for the tables of Appendix 6. The jets in these events as well as clusters were found by only one jetfinder LUCCELL (for the whole  $\eta$  region  $|\eta^{jet}| < 5.0$ ).

Tables 1–4 of Appendix 6 correspond to the “ $Z + jet$ ” events selection with  $P_t^Z > 40$  GeV/c (and simulation with  $\hat{p}_\perp^{min} = 20$  GeV/c), Tables 5–8 to that with  $P_t^Z > 70$  GeV/c (and simulation with  $\hat{p}_\perp^{min} = 35$  GeV/c) and Tables 9–12 to that with  $P_t^Z > 100$  GeV/c (and simulation with  $\hat{p}_\perp^{min} = 50$  GeV/c).

The rows and columns of Tables 1–12 illustrate the influence of  $P_{tCUT}^{clust}$  and  $P_{tCUT}^{out}$  on the quantities mentioned in the points (a), (b) and (c) above.

First of all, we see from Tables 2 and 6 of Appendix 6 that the signal-to-background ratios  $S/B$  practically do not depend on the values of  $P_{tCUT}^{clust}$  and  $P_{tCUT}^{out}$ . This fact can be easily understood if one looks at the upper two rows of plots in Fig. 21 with distributions over  $P_t^{clust}$  and  $P_t^{out}$  in signal and background (DY) events. Because of the statistics shortage for the background events in the case of  $P_t^Z > 100$  GeV/c (Table 10) the errors to  $S/B$  values in many  $P_t^{clust}$  and  $P_t^{out}$  intervals are big enough and in some cells the error reaches 100% (they marked by “—”).

Secondly, we can see that the restriction of  $P_{tCUT}^{clust}$  and  $P_{tCUT}^{out}$  improves the calibration accuracy. Tables 3 (for  $P_t^Z > 40$  GeV/c) and 11 (for  $P_t^Z > 100$  GeV/c) of Appendix 6 show that the mean values of the fraction  $F \equiv (P_t^Z - P_t^{jet})/P_t^Z$  decreases with variation of the two cuts from  $P_{tCUT}^{clust} = 30$  GeV/c and  $P_{tCUT}^{out} = 1000$  GeV/c (i.e. without limits) to  $P_{tCUT}^{clust} = 10$  GeV/c and  $P_{tCUT}^{out} = 10$  GeV/c as 0.050 to 0.014 and as 0.028 to 0.007, respectively. At the same time this restriction noticeably decreases the width of the gaussian  $\sigma(F)$  (see Tables 4, 8 and 12 of Appendix 6). So, it drops from 0.175 to 0.095 for  $P_t^Z > 40$  GeV/c and from 0.105 to 0.049 for  $P_t^Z > 100$  GeV/c (i.e. about a factor of two) for the same variation of  $P_{tCUT}^{clust}$  and  $P_{tCUT}^{out}$ .

The explanation is the following. Disbalance equation (19) contains 2 terms on the right-hand side,  $(1 - \cos\Delta\phi)$  and  $P_t(O+\eta > 5)/P_t^Z$ . The first one is negligibly small as compared with the second term and tends to decrease with growing  $P_t^Z$  (see tables in Appendices 2–5). So, we see that the main source of the disbalance in equation (19) is defined by the term  $P_t(O+\eta > 5)/P_t^Z$ . This term can be decreased by decreasing  $P_t$  activity in the space beyond the “ $Z + jet$ ” system.

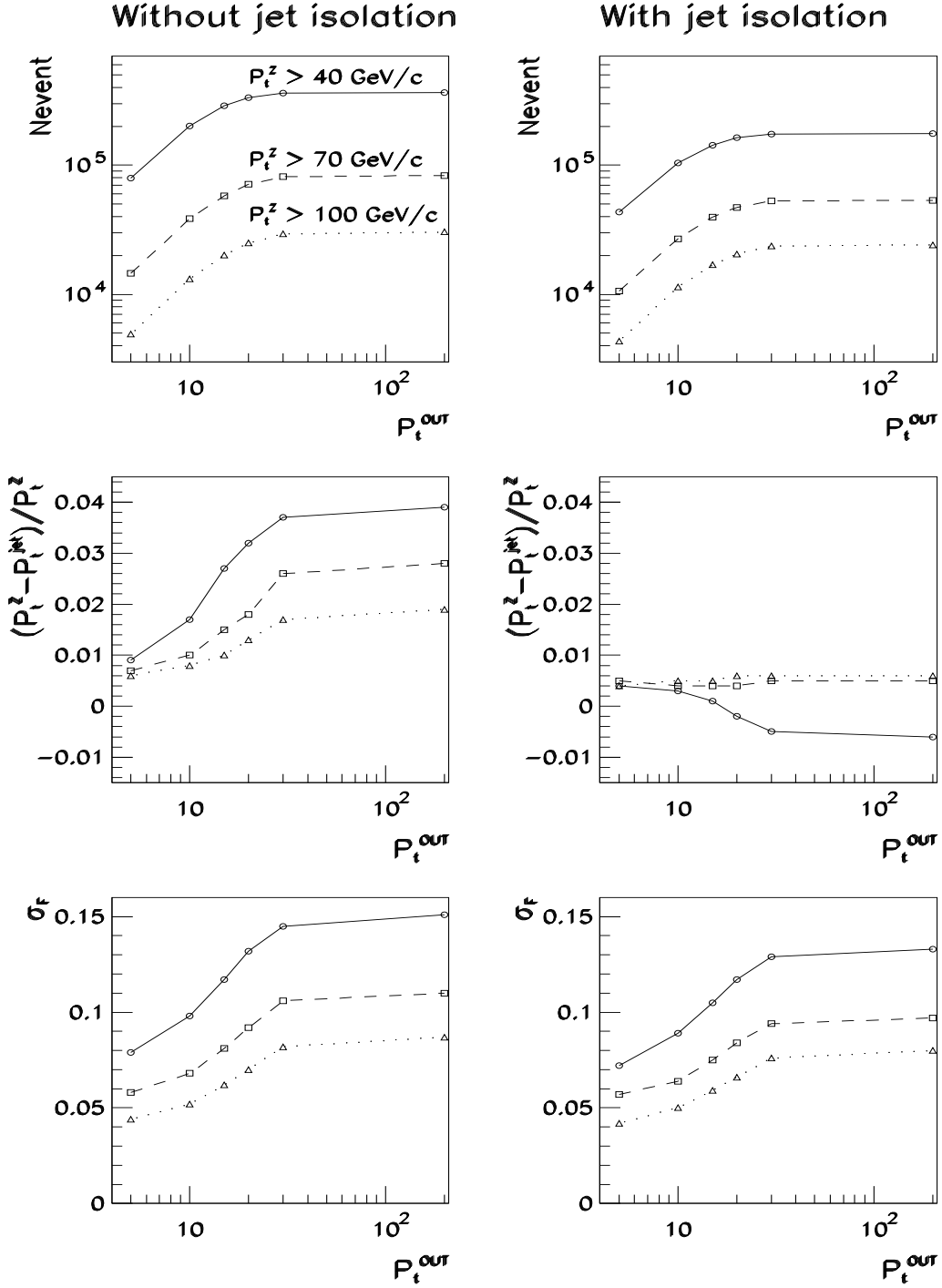


Fig. 24: Number of events per  $L = 10 \text{ fb}^{-1}$ , mean value  $(P_t^Z - P_t^{jet})/P_t^Z (\equiv F)$ , its standard deviation  $\sigma_F$  as a function of  $P_t^{out}$  value.  $P_t^{CUT}$  value is limited by  $20 \text{ GeV}/c$ .

The behaviour of number of the selected events for  $L_{int} = 10 fb^{-1}$ , the mean values of  $(P_t^Z - P_t^{jet})/P_t^Z$  and its standard deviation  $\sigma(F)$  are also displayed in Fig. 24 for non-isolated (left-hand column) and isolated jets with  $\epsilon^{jet} = 5\%$  (right-hand column).

The numbers of events at the integrated luminosity  $L_{int} = 10 fb^{-1}$  for different  $P_{tCUT}^{clust}$  and  $P_{tCUT}^{out}$  are given in Tables 1, 5 and 9 of Appendix 6. One can see that even with such strict  $P_{tCUT}^{clust}$  and  $P_{tCUT}^{out}$  values as  $10 GeV/c$  for both, for example, we would have a sufficient number of events (about 140 000, 27 000 and 9 000 for  $P_t^Z \geq 40 GeV/c$ ,  $P_t^Z \geq 70 GeV/c$  and  $P_t^Z \geq 100 GeV/c$  respectively) with an acceptable accuracy of the absolute jet energy scale setting.

Thus, we can conclude that application of two criteria introduced in Section 2.2, i.e.  $P_{tCUT}^{clust}$  and  $P_{tCUT}^{out}$ , results in the important consequence for our final “signal+background” event samples: essential improvement of the calibration accuracy. From Tables 1, 5 and 9 of Appendix 6 one can also see at what cost (from the statistics point of view) various  $(P_t^Z - P_t^{jet})/P_t^Z$  balance values can be obtained.

## 8. ESTIMATION OF RATES AND BACKGROUND FOR GLUON DISTRIBUTION DETERMINATION AT THE LHC USING “ $Z + jet$ ” EVENTS.

Many theoretical predictions for production of new particles (Higgs, SUSY) at the LHC are based on model estimations of the gluon density behavior at low  $x$  and high  $Q^2$ . Thus, determining the proton gluon density for this kinematic region directly in LHC experiments would be obviously very useful.

One of the channels for this measurement is a high  $P_t$  direct photon production  $pp \rightarrow \gamma^{dir} + X$  (see [25]). The region of high  $P_t$ , reached by UA1 [26], UA2 [27], CDF [28] and D0 [29] extends up to  $P_t \approx 60 GeV/c$  and recently up to  $P_t = 105 GeV/c$  [30]. These data together with the later ones (see references in [31]–[40]) and recent E706 [41] and UA6 [42] results give an opportunity for tuning the form of gluon distribution (see [34], [37], [43]). The rates and estimated cross sections of inclusive direct photon production at the LHC are given in [25] (see also [44]).

Another process that can be used for the same aim

$$pp \rightarrow \gamma^{dir} + 1 Jet + X \quad (24)$$

defined in the leading order by two QCD subprocesses  $qg \rightarrow q + \gamma$  and  $q\bar{q} \rightarrow g + \gamma$  was considered in [17] (see also [19], [45] and for experimental results see [46], [47]).

Here to estimate a possibility of extraction of information on the gluon density in a proton we shall consider the analogous to (24) process:

$$pp \rightarrow Z^0 + 1 Jet + X \quad (25)$$

where  $Z^0$  boson decays in the following to muon pair, the signal from which can be perfectly measured in the detector.

In the case of  $pp \rightarrow Z^0/\gamma^{dir} + 1 Jet + X$  for  $P_t^{jet} \geq 30 GeV/c$  (i.e. in the region where  $k_T$  smearing effects are not important, see [38]) the cross section is expressed directly in terms of parton distribution functions  $f_a(x_a, Q^2)$  (see, for example, [35]):

$$\frac{d\sigma}{d\eta_1 d\eta_2 dP_t^2} = \sum_{a,b} x_a f_a(x_a, Q^2) x_b f_b(x_b, Q^2) \frac{d\sigma}{dt}(ab \rightarrow 34) \quad (26)$$

where  $x_{a,b}$  are defined by

$$x_{a,b} = P_t/\sqrt{s} \cdot (\exp(\pm\eta_1) + \exp(\pm\eta_2)). \quad (27)$$

We also used the following designations above:  $\eta_1 = \eta^Z$ ,  $\eta_2 = \eta^{jet}$ ;  $P_t = P_t^Z$ ;  $a, b = q, \bar{q}, g$ ;  $3, 4 = q, \bar{q}, g, \gamma$ . Formula (26) and the knowledge of the results of independent measurements of  $q, \bar{q}$  distributions [45] allow the gluon distribution  $f_g(x, Q^2)$  to be determined with an account of selection efficiencies of “ $Z + jet$ ” events and the contribution of background, left after the used selection cuts (3) – (10) (see Section 2.2).

Table 19 shows the percentage of Compton-like subprocess (1a) (amounting to 100% together with (1b)) in the samples of events selected by the cuts (3) – (10) for  $P_{tCUT}^{clust} = 10 \text{ GeV}/c$  for different  $P_t^Z$  and  $\eta^{jet}$  intervals: Barrel (HB) part ( $|\eta^{jet}| < 1.4$ ) and Endcap+Forward (HE+HF) part ( $1.4 < |\eta^{jet}| < 5.0$ )<sup>26</sup>.

Table 19: The percentage of the process  $qg \rightarrow Z^0 + q$  ( $P_{tCUT}^{clust} = 10 \text{ GeV}/c$ ).

Calorimeter part	$P_t^{jet}$ interval ( $\text{GeV}/c$ )			
	40–50	70–80	100–120	150–200
Barrel	72	78	82	83
Endcap	71	76	78	79

We have found that to the same selection criteria (3) – (10) satisfy the events based on the annihilation subprocess  $q\bar{q} \rightarrow g + Z^0$  (see Fig. 1) and a part of events based on the Drell-Yan subprocess  $q\bar{q} \rightarrow \mu^+\mu^-$  with a hard gluon radiation in the initial state (see Fig. 19). Their contribution to the total background as a function of  $P_t^Z$  is shown in Fig. 25.

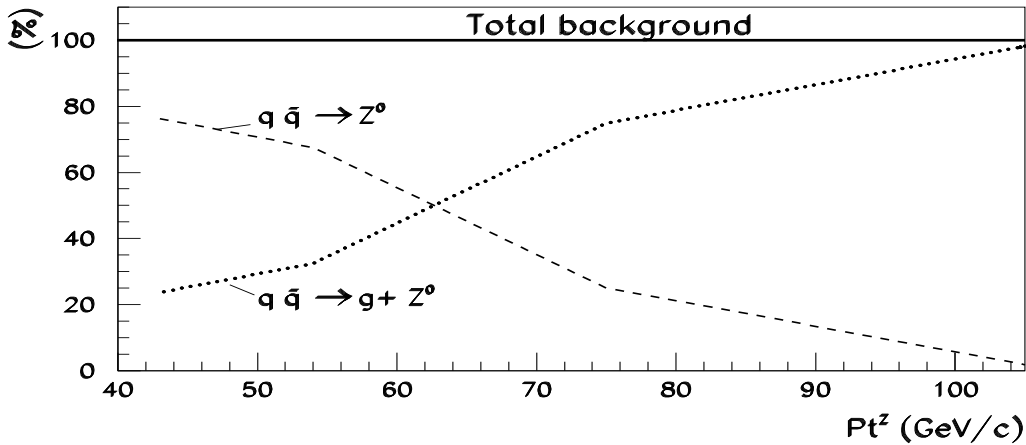


Fig. 25: The percentage of different background sources as a function of  $P_t^Z$ .

In Table 20 we present the  $Q^2 (\equiv (P_t^Z)^2)$  and  $x$  distribution (with  $x$  defined according to (27)) of the number of events that are caused by all events (signal, i.e. based on subprocess (1a) and background, i.e. based on the DY  $q\bar{q} \rightarrow \mu^+\mu^-$  and (1b) subprocesses) which have passed cuts (3) – (10) of Section 2.2 with the following parameter values ( $P_t^{out}$  was not limited):

$$|\eta^{jet}| < 5.0, \quad P_{tmax}^\mu \geq 20 \text{ GeV}/c, \quad \Delta\phi < 15^\circ, \quad P_{tCUT}^{clust} = 10 \text{ GeV}/c.$$

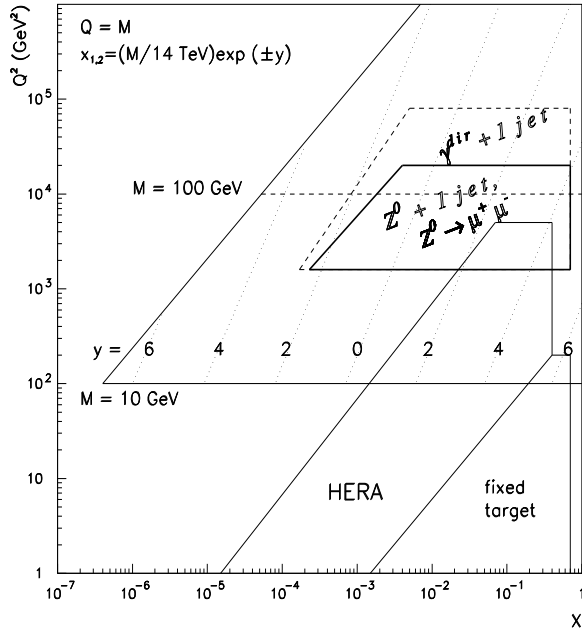
<sup>26</sup>see also tables of Appendix 1

The admixture of the background events (as  $S/B$  ratios) is presented in Table 21 for various  $x$  and  $Q^2$  intervals.

We know that in the one-jet background events of both types a jet is always originated from a gluon and in the signal events it is always originated from a quark. Thus, one can apply here the quark/gluon jet separation efficiencies found earlier in [20] for the case of direct photon production using the fact of a similarity of the fundamental QCD subprocesses and selection criteria of “ $\gamma^{dir} + jet$ ” and “ $Z + jet$ ” events.

Taking, as an example, the quark jet selection efficiency  $\epsilon_{jet}^q = 60\%$  one can reject about 81 – 86% (it depends on the  $P_t$  scale) of the background events containing a gluon jet. These efficiencies, applied to the events passed selection cuts (3) – (10), were used in calculating the number of events and signal-to-background ratios in Tables 22 and 23. By comparing Tables 21 and 23 one can notice that after taking into account of the abovementioned efficiencies  $S/B$  ratios increased in 3.0 – 3.4 times.

The area that can be covered by studying the process  $qg \rightarrow Z^0 + q$  with the subsequent decay  $Z^0 \rightarrow \mu^+\mu^-$  is shown in Fig. 25. The number of events in this area is given in Tables 20 and 22 for two values of the quark jet selection efficiencies  $\epsilon_{jet}^q$  (and, thus, different  $S/B$  ratios).



From this figure (and Tables 20, 22) it is seen that during first two years of LHC running at low luminosity ( $L = 10^{33} \text{ cm}^2 \text{ s}^{-1}$ ) it would be possible to extract an information for the gluon distribution determination  $f_g(x, Q^2)$  in a proton in the region of  $1.6 \cdot 10^3 \leq Q^2 \leq 2 \cdot 10^4 \text{ (GeV/c)}^2$  with as small  $x$  values as accessible at HERA. It is also worth emphasising that the sample of the “ $Z + jet$ ” events selected for this aim can be used to perform a cross-check of  $f_g(x, Q^2)$  determination with help of “ $\gamma + jet$ ” events to which were devoted two last our works [17] and [21] (The area covered with “ $\gamma + jet$ ” events is also shown in Fig. 25 by dashed lines).

Figure 25: LHC ( $x, Q^2$ ) kinematic region for the  $pp \rightarrow Z^0 + jet$  ( $Z^0 \rightarrow \mu^+\mu^-$ ) process.

Table 20: Number of  $gq \rightarrow Z^0 + q$  ( $Z^0 \rightarrow \mu^+\mu^-$ ) events at different  $Q^2$  and  $x$  intervals for  $L_{int} = 20 fb^{-1}$ .  
 $P_{tCUT}^{clust} = 10 GeV/c$ ,  $\epsilon_{jet}^q = 100\%$ .

$Q^2$ (GeV/c) <sup>2</sup>	$x$ values of a parton				All $x$	$P_t^Z$ (GeV/c)
	$10^{-4}$ - $10^{-3}$	$10^{-3}$ - $10^{-2}$	$10^{-2}$ - $10^{-1}$	$10^{-1}$ - $10^0$	$10^{-4}$ - $10^0$	
1600-2500	12204	42796	49464	4216	108681	40-50
2500-5000	7373	46424	55700	5653	115150	50-71
5000-10000	616	14831	20215	2384	38046	71-100
10000-20000	8	5498	9683	1691	16880	100-141
20000-40000	2	1362	3529	947	5840	141-200

Table 21: Signal/Background ratios for  $gq \rightarrow Z^0 + q$  ( $Z^0 \rightarrow \mu^+\mu^-$ ) events at different  $Q^2$  and  $x$  intervals.  
 $P_{tCUT}^{clust} = 10 GeV/c$ ,  $\epsilon_{jet}^q = 100\%$ .

$Q^2$ (GeV/c) <sup>2</sup>	$x$ values of a parton				$\langle S/B \rangle$	$P_t^\gamma$ (GeV/c)
	$10^{-4}$ - $10^{-3}$	$10^{-3}$ - $10^{-2}$	$10^{-2}$ - $10^{-1}$	$10^{-1}$ - $10^0$	$10^{-4}$ - $10^0$	
1600-2500	0.4± 0.0	0.6± 0.0	0.6± 0.0	0.4± 0.0	0.5	40-50
2500-5000	0.7± 0.1	1.1± 0.0	1.0± 0.0	0.6± 0.0	0.9	50-71
5000-10000	2.2± 0.3	3.3± 0.1	3.4± 0.1	2.5± 0.2	3.1	71-100
10000-20000	3.8± 2.5	3.7± 0.2	4.2± 0.1	3.2± 0.2	3.8	100-141
20000-40000	—	3.7± 0.2	4.3± 0.2	3.7± 0.3	4.1	141-200

Table 22: Number of  $gq \rightarrow Z^0 + q$  ( $Z^0 \rightarrow \mu^+\mu^-$ ) events at different  $Q^2$  and  $x$  intervals for  $L_{int} = 20 fb^{-1}$ .  
 $P_{tCUT}^{clust} = 10 GeV/c$ ,  $\epsilon_{jet}^q = 60\%$ .

$Q^2$ (GeV/c) <sup>2</sup>	$x$ values of a parton				All $x$	$P_t^Z$ (GeV/c)
	$10^{-4}$ - $10^{-3}$	$10^{-3}$ - $10^{-2}$	$10^{-2}$ - $10^{-1}$	$10^{-1}$ - $10^0$	$10^{-4}$ - $10^0$	
1600-2500	3516	13862	15890	1141	34409	40-50
2500-5000	2458	17702	20919	1754	42833	50-71
5000-10000	283	7331	10083	1124	18820	71-100
10000-20000	4	2782	4931	833	8549	100-141
20000-40000	0	687	1820	476	2984	141-200

Table 23: Signal/Background ratios for  $gq \rightarrow Z^0 + q$  ( $Z^0 \rightarrow \mu^+\mu^-$ ) events at different  $Q^2$  and  $x$  intervals.  
 $P_{tCUT}^{clust} = 10 GeV/c$ ,  $\epsilon_{jet}^q = 60\%$ .

$Q^2$ (GeV/c) <sup>2</sup>	$x$ values of a parton				$\langle S/B \rangle$	$P_t^\gamma$ (GeV/c)
	$10^{-4}$ - $10^{-3}$	$10^{-3}$ - $10^{-2}$	$10^{-2}$ - $10^{-1}$	$10^{-1}$ - $10^0$	$10^{-4}$ - $10^0$	
1600-2500	1.4± 0.2	2.0± 0.1	1.9± 0.1	1.1± 0.2	1.7	40-50
2500-5000	2.2± 0.3	3.3± 0.2	3.2± 0.2	1.7± 0.3	2.7	50-71
5000-10000	7.1± 1.8	10.3± 0.6	10.9± 0.5	7.9± 1.1	9.7	71-100
10000-20000	—	11.4± 0.7	12.6± 0.6	9.4± 1.0	11.5	100-141
20000-40000	—	12.3± 1.5	14.4± 1.2	12.1± 1.8	13.1	141-200

## 9. SUMMARY.

A possibility of the absolute jet energy scale setting with help of “ $Z + jet$ ” events based on the  $q\bar{q} \rightarrow g + Z^0$  and  $qg \rightarrow q + Z^0$  with subsequent  $Z^0$  decay to the muon pair is studied. The PYTHIA event generator is applied here to find the selection criteria of the “ $Z + jet$ ” events that would provide a good  $P_t^Z - P_t^{Jet}$  balance.

It is shown here (by analogy with [12]–[16]) that the limitation of the clusters  $P_t$  that may be found in an event in addition to the main jet as well as the limitation of  $P_t$  activity of all particles beyond the “ $Z + jet$ ” system (see Section 2) leads to an improvement of the  $P_t^Z$  and  $P_t^{Jet}$  balance value. The further improvement of  $P_t^Z$  and  $P_t^{Jet}$  balance can be reached by selection of events having the isolated jets only. Besides, this criterion (as well as the simultaneous jet finding by two or three algorithms; see Selection 3 in Section 2.2) is also important for selecting events with a clean jet topology and rising the confidence level of a jet determination.

The possibility of the background event suppression based on the Drell-Yan subprocess is also studied. Using the introduced selection criteria, the background suppression factors, signal and background event selection efficiencies and the number of events that can be collected at the LHC with low luminosity  $L = 10^{33} \text{ cm}^2 \text{ s}^{-1}$  during one year are determined. The main results of the jet calibration studying are given in Tables 1 – 12 of Appendix 6 and Fig. 24.

We want to underline that the number of events presented here were not our main goal as they may depend on the used event generator and the particular choice of a long set of its parameters. The most important result of our work is finding out the set of new selection criteria that may be useful for the jet energy scale determination in future experiments.

It is also shown that the selected sample of the “ $Z + jet$ ” events, most suitable for the absolute jet energy scale setting at the LHC energy, can provide useful information for the gluon density determination inside a proton in the kinematic region with  $x$  values as small as accessible at HERA [57], [58], but at much higher  $Q^2$  values (by about 2 orders of magnitude):  $10^{-4} \leq x \leq 10^{-1}$  with  $1.6 \cdot 10^3 \leq Q^2 \leq 2 \cdot 10^4 (\text{GeV}/c)^2$ . This sample of “ $Z + jet$ ” events can be used to perform a cross-check of the  $f_g(x, Q^2)$  determination with help of “ $\gamma + jet$ ” events (see [17] and [21]). The  $x - Q^2$  kinematic area covered with the “ $Z + jet$ ” events (as well as with the “ $\gamma + jet$ ” events) is shown in Fig. 25.

## 10. ACKNOWLEDGMENTS.

We are greatly thankful to D. Denegri for having offered this theme to study, fruitful discussions and permanent support and encouragement. It is a pleasure for us to express our recognition for helpful discussions to P. Aurenche, M. Dittmar, M. Fontannaz, J.Ph. Guillet, M.L. Mangano, E. Pilon, H. Rohringer, S. Tapprogge and especially to J. Womersley for supplying us with the preliminary version of paper [1].

## References

- [1] D0 Collaboration, F. Abachi *et al.*, NIM **A424** (1999)352.
- [2] CDF Collaboration. F. Abe *et al.*, Phys.Rev. **D50** (1994)2966; F. Abe *et al.*, Phys.Rev.Lett. **73** (1994)225.
- [3] D. Denegri, R. Kinnunen, A. Nikitenko, CMS Note 1997/039 “Study of calorimeter calibration with  $\tau$ ’s in CMS”.
- [4] R. Kinnunen, A. Nikitenko, CMS Note 1997/097 “Study of calorimeter calibration with pions from jets in CMS”.
- [5] J. Womersley, A talk at CMS physics group meeting at CMS Week, Aachen, 1996. See also <http://cmsdoc.cern.ch/doc/gen/agendas/960908-1>.
- [6] J. Freeman, W. Wu, **draft** “In situ calibration of CMS HCAL calorimeter”.
- [7] R. Mehdiyev, I. Vichou, ATLAS Note ATL-COM-PHYS-99-054 (1999) “Hadronic jet energy scale calibration using Z+jet events”.
- [8] P. Savard, ATLAS Note CAL-NO-092 (1997), “The  $W \rightarrow jet - jet$  and top mass reconstructions with the ATLAS detector”.
- [9] ATLAS Detector and Physics Performance, Technical Design Report, Volumes **1, 2**, 1999. CERN/LHCC 99-14.
- [10] N.B. Skachkov, V.F. Konoplyanikov, D.V. Bandourin, “Photon – jet events for calibration of HCAL”. Second Annual RDMS CMS Collaboration Meeting. CMS-Document, 1996–213. CERN, December 16-17, 1996, p.7-23.
- [11] N.B. Skachkov, V.F. Konoplyanikov, D.V. Bandourin, “ $\gamma$ -direct + 1 jet events for HCAL calibration”. Third Annual RDMS CMS Collaboration Meeting. CMS-Document, 1997–168. CERN, December 16-17, 1997, p.139-153.
- [12] D.V. Bandourin, V.F. Konoplyanikov, N.B. Skachkov. “Jet energy scale setting with “ $\gamma + jet$ ” events at LHC energies. Generalities, selection rules.” JINR Preprint E2-2000-251, JINR, Dubna, hep-ex/0011012.
- [13] D.V. Bandourin, V.F. Konoplyanikov, N.B. Skachkov. “Jet energy scale setting with “ $\gamma + jet$ ” events at LHC energies. Event rates,  $P_t$  structure of jet.” JINR Preprint E2-2000-252, JINR, Dubna, hep-ex/0011013.

- [14] D.V. Bandourin, V.F. Konoplyanikov, N.B. Skachkov. “Jet energy scale setting with “ $\gamma + jet$ ” events at LHC energies. Minijets and cluster suppression and  $P_t^\gamma - P_t^{Jet}$  disbalance.” JINR Preprint E2-2000-253, JINR, Dubna, hep-ex/0011084.
- [15] D.V. Bandourin, V.F. Konoplyanikov, N.B. Skachkov. “Jet energy scale setting with “ $\gamma + jet$ ” events at LHC energies. Selection of events with a clean “ $\gamma + jet$ ” topology and  $P_t^\gamma - P_t^{Jet}$  disbalance.” JINR Preprint E2-2000-254, JINR, Dubna, hep-ex/0011014.
- [16] D.V. Bandourin, V.F. Konoplyanikov, N.B. Skachkov. “Jet energy scale setting with “ $\gamma + jet$ ” events at LHC energies. Detailed study of the background suppression.” JINR Preprint E2-2000-255, JINR, Dubna, hep-ex/0011017.
- [17] D.V. Bandourin, V.F. Konoplyanikov, N.B. Skachkov, “ “ $\gamma + jet$ ” events rate estimation for gluon distribution determination at LHC”, Part.Nucl.Lett.103:34-43,2000, hep-ex/0011015.
- [18] D.V. Bandourin, N.B. Skachkov. “ “ $\gamma + jet$ ” process application for setting the absolute scale of jet energy and determining the gluon distribution at the Tevatron Run II.” D0 Note 3948, 2002.
- [19] D.V. Bandourin, V.F. Konoplyanikov, N.B. Skachkov. “On the application of “ $\gamma + jet$ ” events for setting the absolute jet energy scale at the LHC and determining the gluon distribution”. CMS Note in preparation.
- [20] D.V. Bandourin, N.B. Skachkov, “Separation of quark and gluon jets in the direct photon production processes at the LHC using the neural network approach”, JINR Communication E2-2001-260, hep-ex/0109001.
- [21] D.V. Bandourin, N.B. Skachkov, “On estimating and reducing the background to a determination of the gluon density in a proton using the direct photon production processes at the LHC”, In preparation.
- [22] S. Abdullin, A. Khanov, N. Stepanov, CMS Note CMS TN/94–180 “CMSJET”.
- [23] T. Sjostrand, Comp.Phys.Comm. **82** (1994)74.
- [24] CMS Muon Project, Technical Design Report, CERN/LHCC 97–32, CMS TDR 3, CERN, 1997.
- [25] P. Aurenche *et al.* Proc. of “ECFA LHC Workshop”, Aachen, Germany, 4-9 Oktob. 1990, edited by G. Jarlskog and D. Rein (CERN-Report No 90-10; Geneva, Switzerland 1990), Vol. **II**.
- [26] UA1 Collaboration, C. Albajar *et al.*, Phys.Lett, **209B** (1998)385.
- [27] UA2 Collaboration, R. Ansari *et al.*, Phys.Lett. **176B** (1986)239.
- [28] CDF Collaboration. F. Abe *et al.*, Phys.Rev.Lett. **68** (1992)2734; F. Abe *et al.*, Phys.Rev. **D48** (1993)2998; F. Abe *et al.*, Phys.Rev.Lett., **73** (1994)2662.
- [29] D0 Collaboration, F. Abachi *et al.*, Phys.Rev.Lett, **77** (1996)5011.

- [30] D0 Collaboration, B. Abbott *et al.*, Phys.Rev.Lett. **84** 2786-2791,2000.
- [31] T. Ferbel and W.R. Molzon, Rev.Mod.Phys. **56** (1984)181.
- [32] P. Aurenche, *et al.* Phys.Lett. **169B**441 (1986).
- [33] E.N. Argyres, A.P. Contogouris, N. Mebarki, add S. D.P. Vlassopoulos, Phys.Rev.D 35, 1584-1589 (1987).
- [34] P. Aurenche, *et al.* Phys.Rev. **D39** (1989)3275.
- [35] J.F. Owens, Rev.Mod.Phys. **59** (1987)465.
- [36] J. Huston *et al.*, Phys.Rev. **D51** (1995)6139.
- [37] W. Vogelsang and A. Vogt, Nucl.Phys. **B453** (1995)334.
- [38] J. Huston ATLAS Note ATL-Phys-99-008, CERN,1999.
- [39] W. Vogelsang and M. Whally, J.Phys. **G23** (1997)A1.
- [40] S. Frixione and W. Vogelsang, CERN-TH/99-247 hep-ph/9908387.
- [41] E706 Collaboration, L. Apanasevich *et al.*, Phys.Rev.Lett., **81** (1997)2642.
- [42] UA6 Collaboration, G. Ballochi *et al.*, Phys.Lett.,**B436** (1998)222.
- [43] A.D. Martin *et al.*, Eur.Phys.J. **C4** (1998)463.
- [44] P. Aurenche, M. Fontannaz, S. Frixione Proc. of “CERN Workshop on Standard Model Physics (and more) at the LHC”, QCD, Section 6.1 “General features of photon production”, Yellow Report CERN-2000-004, 9 May 2000, CERN, Geneva.
- [45] M. Dittmar, F. Pauss, D. Zurcher, Phys.Rev.D56:7284-7290,1997.
- [46] ISR–AFS Collaboration, T.Akesson *et al.*, Zeit.Phys. **C34** (1987)293.
- [47] CDF Collaboration, F. Abe *et al.*,Phys.Rev. **D57** (1998)1359 (see also p.67).
- [48] G.P. Skoro, M.V. Tokarev, “Asymmetry of jet production in polarized  $pp$  collisions and sign of  $\Delta G$ ”, Proc. of the XIV International Seminar on High Energy Physics Problems “Relativistic Nuclear Physics and QCD”, Vol.II, p.120., hep-ph/0009028.
- [49] G.P. Skoro, M.V. Tokarev, “Asymmetry of jet production in polarized  $pp$  collisions at RHIC and sign of  $\Delta G$ ”, Nuov. Cim. **A111** (1998) 353.
- [50] G.P. Skoro, M. Zupan, M.V. Tokarev, ”Asymmetry of Prompt Photon Production in  $\vec{p} - \vec{p}$  Collisions at RHIC” Nuov. Cim. **A112** (1999) 809.
- [51] P. Chiapetta, G.J. Gounaris, J. Layssac and F.M. Renard, “Glue constraining asymmetries in  $W, \gamma$  or  $Z$  production at CERN LHC”, hep-ph/9807563.

- [52] See for example the presentations of M. Dittmar and K. Mazumdar at <http://cmsdoc.cern.ch/doc/ph/agendas/990518-1> “gamma+c-jets” and <http://cmsdoc.cern.ch/doc/ph/agendas/000607-1> “Constraining structure functions of s,c,b quarks at LHC”.
- [53] M. Dittmar, K.Mazumdar, “Measuring the parton distribution functions of charm, beauty and strange quark and antiquarks at the LHC”, CMS Note 2001/002.
- [54] M. Dittmar, K.Mazumdar, N. Skachkov, Proc. of “CERN Workshop on Standard Model Physics (and more) at the LHC”, QCD, Section 2.7 “Measuring parton luminosities ...”, Yellow Report CERN-2000-004, 9 May 2000, CERN, Geneva.
- [55] J. Huston *et al.*, “Study of the uncertainty of the gluon distribution”, hep-ph/9801444.
- [56] R. Ball, M. Dittmar, W.J. Stirling, Proc. of “CERN Workshop on Standard Model Physics (and more) at the LHC”, QCD, Section 2 “Parton distribution functions”, Yellow Report CERN-2000-004, 9 May 2000, CERN, Geneva.
- [57] H1 Collaboration, S. Aid *et al.*, Nucl.Phys. **B470** (1996)3; C. Adloff *et al.* Nucl.Phys. **B497** (1997)3.
- [58] ZEUS Collaboration, M. Derrick *et al.*, Zeit.Phys. **C69** (1996)607; M. Derrick *et al.*, Zeit.Phys. **C72** (1996)399.
- [59] Particle Data Group, D.E. Groom *et al.*, The European Physical Journal C15 (2000) 1.

## Appendix 1

$$45 < P_t^Z < 55 \text{ GeV}/c$$

Table 1: Selection 1.  $\Delta\phi_{(Z,jet)} = 180^\circ \pm 15^\circ$ . UA1 algorithm.

$P_{tCUT}^{clust}$	30	20	15	10	5
$P_t^{jet}$	48.145	47.600	47.417	47.334	47.323
$P_t^{Jet} - P_t^{jet}$	0.140	0.129	0.122	0.106	0.084
$P_{t(\nu)}^{Jet}$	0.141	0.130	0.123	0.107	0.085
$R_{event}^{\nu \in Jet}$	0.027	0.026	0.025	0.023	0.022
$P_{t(\mu)}^{Jet}$	0.046	0.042	0.043	0.038	0.029
$R_{event}^{\mu \in Jet}$	0.011	0.011	0.010	0.009	0.010
$P_t^{miss}$	5.009	4.897	4.777	4.577	4.239
$P_{t\nu \in Jet}^{miss}$	9.016	8.843	8.517	7.653	6.880
$Nevent_{(c)}$	2774	2300	1763	1027	201
$Nevent_{(b)}$	2129	1677	1257	626	80
30sub/all	0.71	0.70	0.69	0.68	0.65
$R_{qc}^{jet}$	0.65	0.65	0.65	0.65	0.64
Entries	33240	29704	25482	17162	3842

Table 2: Selection 1.  $\Delta\phi_{(Z,jet)} = 180^\circ \pm 15^\circ$ . UA2 algorithm.

$P_{tCUT}^{clust}$	30	20	15	10	5
$P_t^{jet}$	47.520	46.883	46.520	46.296	46.254
$P_t^{Jet} - P_t^{jet}$	0.129	0.116	0.106	0.096	0.085
$P_{t(\nu)}^{Jet}$	0.131	0.117	0.107	0.097	0.086
$R_{event}^{\nu \in Jet}$	0.026	0.025	0.023	0.022	0.021
$P_{t(\mu)}^{Jet}$	0.048	0.045	0.044	0.042	0.038
$R_{event}^{\mu \in Jet}$	0.010	0.010	0.009	0.009	0.010
$P_t^{miss}$	5.012	4.890	4.765	4.571	4.221
$P_{t\nu \in Jet}^{miss}$	8.635	8.336	8.008	7.290	6.366
$Nevent_{(c)}$	2793	2322	1792	1057	187
$Nevent_{(b)}$	2354	1856	1386	693	91
30sub/all	0.69	0.68	0.66	0.64	0.61
$R_{qc}^{jet}$	0.56	0.56	0.55	0.55	0.56
Entries	32326	29057	25154	17041	3706

Table 3: Selection 1.  $\Delta\phi_{(Z,jet)} = 180^\circ \pm 15^\circ$ . LUCCELL algorithm.

$P_{tCUT}^{clust}$	30	20	15	10	5
$P_t^{jet}$	47.326	46.854	46.677	46.732	47.016
$P_t^{Jet} - P_t^{jet}$	0.144	0.133	0.128	0.118	0.095
$P_{t(\nu)}^{Jet}$	0.145	0.134	0.129	0.119	0.096
$R_{event}^{\nu \in Jet}$	0.028	0.027	0.026	0.025	0.023
$P_{t(\mu)}^{Jet}$	0.049	0.048	0.043	0.040	0.034
$R_{event}^{\mu \in Jet}$	0.010	0.010	0.009	0.009	0.010
$P_t^{miss}$	5.007	4.902	4.791	4.600	4.255
$P_{t\nu \in Jet}^{miss}$	9.104	8.871	8.666	8.140	7.124
$Nevent_{(c)}$	2961	2488	1921	1086	195
$Nevent_{(b)}$	2282	1811	1335	642	64
30sub/all	0.72	0.71	0.70	0.69	0.67
$R_{qc}^{jet}$	0.66	0.66	0.66	0.66	0.65
Entries	36434	32748	28104	18599	3948

$$70 < P_t^Z < 85 \text{ GeV}/c$$

Table 4: Selection 1.  $\Delta\phi_{(Z,jet)} = 180^\circ \pm 15^\circ$ . UA1 algorithm.

$P_{tCUT}^{clust}$	30	20	15	10	5
$P_t^{jet}$	71.393	72.833	73.509	74.073	74.192
$P_t^{Jet} - P_t^{jet}$	0.339	0.326	0.319	0.270	0.271
$P_{t(\nu)}^{Jet}$	0.341	0.328	0.321	0.271	0.272
$R_{event}^{\nu \in Jet}$	0.039	0.037	0.036	0.031	0.027
$P_{t(\mu)}^{Jet}$	0.147	0.144	0.141	0.124	0.126
$R_{event}^{\mu \in Jet}$	0.019	0.018	0.018	0.016	0.016
$P_t^{miss}$	5.489	5.324	5.230	5.056	4.662
$P_{t\nu \in Jet}^{miss}$	14.357	14.273	14.484	14.504	15.842
$Nevent_{(c)}$	1478	1025	710	396	62
$Nevent_{(b)}$	1173	787	528	263	35
30sub/all	0.81	0.80	0.79	0.77	0.74
$R_{qc}^{jet}$	0.65	0.65	0.65	0.65	0.65
Entries	21649	17169	13309	8132	1628

Table 5: Selection 1.  $\Delta\phi_{(Z,jet)} = 180^\circ \pm 15^\circ$ . UA2 algorithm.

$P_{tCUT}^{clust}$	30	20	15	10	5
$P_t^{jet}$	71.065	72.035	72.483	72.896	72.976
$P_t^{Jet} - P_t^{jet}$	0.329	0.319	0.316	0.274	0.319
$P_{t(\nu)}^{Jet}$	0.331	0.322	0.318	0.276	0.320
$R_{event}^{\nu \in Jet}$	0.039	0.037	0.036	0.031	0.030
$P_{t(\mu)}^{Jet}$	0.147	0.144	0.141	0.124	0.138
$R_{event}^{\mu \in Jet}$	0.019	0.018	0.018	0.017	0.018
$P_t^{miss}$	5.465	5.308	5.216	4.999	4.577
$P_{t\nu \in Jet}^{miss}$	13.783	13.586	13.684	13.688	15.203
$Nevent_{(c)}$	1557	1114	787	440	67
$Nevent_{(b)}$	1349	924	624	324	40
30sub/all	0.79	0.78	0.77	0.75	0.71
$R_{qc}^{jet}$	0.58	0.58	0.58	0.58	0.57
Entries	22238	17993	14199	8656	1719

Table 6: Selection 1.  $\Delta\phi_{(Z,jet)} = 180^\circ \pm 15^\circ$ . LUCCELL algorithm.

$P_{tCUT}^{clust}$	30	20	15	10	5
$P_t^{jet}$	71.054	72.235	72.910	73.608	73.869
$P_t^{Jet} - P_t^{jet}$	0.334	0.328	0.318	0.264	0.258
$P_{t(\nu)}^{Jet}$	0.336	0.330	0.319	0.265	0.258
$R_{event}^{\nu \in Jet}$	0.038	0.037	0.035	0.031	0.026
$P_{t(\mu)}^{Jet}$	0.151	0.150	0.148	0.126	0.129
$R_{event}^{\mu \in Jet}$	0.019	0.018	0.018	0.017	0.018
$P_t^{miss}$	5.480	5.336	5.229	5.040	4.615
$P_{t\nu \in Jet}^{miss}$	14.412	14.301	14.423	14.095	15.959
$Nevent_{(c)}$	1488	1057	735	401	64
$Nevent_{(b)}$	1166	812	547	270	34
30sub/all	0.81	0.80	0.79	0.78	0.75
$R_{qc}^{jet}$	0.66	0.66	0.66	0.65	0.64
Entries	22439	18123	14046	8434	1600

$$100 < P_t^Z < 120 \text{ GeV}/c$$

Table 7: Selection 1.  $\Delta\phi_{(Z,jet)} = 180^\circ \pm 15^\circ$ . UA1 algorithm.

$P_{tCUT}^{clust}$	30	20	15	10	5
$P_t^{jet}$	105.311	106.781	107.596	108.186	108.211
$P_t^{Jet} - P_t^{jet}$	0.579	0.536	0.503	0.464	0.306
$P_{t(\nu)}^{Jet}$	0.582	0.538	0.505	0.465	0.308
$R_{event}^{\nu \in Jet}$	0.043	0.040	0.038	0.035	0.027
$P_{t(\mu)}^{Jet}$	0.256	0.236	0.229	0.248	0.190
$R_{event}^{\mu \in Jet}$	0.021	0.021	0.020	0.019	0.017
$P_t^{miss}$	6.021	5.773	5.565	5.410	4.998
$P_{t\nu \in Jet}^{miss}$	21.291	20.555	19.968	19.964	20.603
$Nevent_{(c)}$	1101	837	611	348	71
$Nevent_{(b)}$	804	584	418	214	27
30sub/all	0.84	0.83	0.82	0.81	0.78
$R_{qc}^{jet}$	0.65	0.65	0.65	0.65	0.65
Entries	26365	19658	14669	8491	1690

Table 8: Selection 1.  $\Delta\phi_{(Z,jet)} = 180^\circ \pm 15^\circ$ . UA2 algorithm.

$P_{tCUT}^{clust}$	30	20	15	10	5
$P_t^{jet}$	105.053	106.086	106.624	107.032	107.226
$P_t^{Jet} - P_t^{jet}$	0.584	0.536	0.499	0.458	0.300
$P_{t(\nu)}^{Jet}$	0.587	0.539	0.502	0.461	0.302
$R_{event}^{\nu \in Jet}$	0.045	0.041	0.038	0.036	0.028
$P_{t(\mu)}^{Jet}$	0.258	0.236	0.229	0.218	0.209
$R_{event}^{\mu \in Jet}$	0.022	0.022	0.021	0.018	0.017
$P_t^{miss}$	5.998	5.781	5.578	5.430	5.000
$P_{t\nu \in Jet}^{miss}$	20.530	19.980	19.456	19.427	18.699
$Nevent_{(c)}$	1136	881	652	372	76
$Nevent_{(b)}$	881	658	478	250	31
30sub/all	0.83	0.82	0.81	0.80	0.76
$R_{qc}^{jet}$	0.59	0.60	0.59	0.59	0.59
Entries	28311	21607	16358	9541	1845

Table 9: Selection 1.  $\Delta\phi_{(Z,jet)} = 180^\circ \pm 15^\circ$ . LUCCELL algorithm.

$P_{tCUT}^{clust}$	30	20	15	10	5
$P_t^{jet}$	104.919	106.238	107.024	107.700	108.019
$P_t^{Jet} - P_t^{jet}$	0.579	0.539	0.511	0.468	0.318
$P_{t(\nu)}^{Jet}$	0.581	0.541	0.514	0.470	0.319
$R_{event}^{\nu \in Jet}$	0.043	0.040	0.038	0.035	0.026
$P_{t(\mu)}^{Jet}$	0.264	0.247	0.244	0.222	0.188
$R_{event}^{\mu \in Jet}$	0.022	0.022	0.021	0.019	0.018
$P_t^{miss}$	6.014	5.787	5.602	5.424	4.991
$P_{t\nu \in Jet}^{miss}$	21.514	20.833	20.528	20.390	21.456
$Nevent_{(c)}$	1131	878	641	354	71
$Nevent_{(b)}$	818	612	438	219	25
30sub/all	0.84	0.83	0.82	0.82	0.80
$R_{qc}^{jet}$	0.66	0.66	0.66	0.65	0.64
Entries	26920	20362	15184	8643	1636

$$150 < P_t^Z < 200 \text{ GeV}/c$$

Table 10: Selection 1.  $\Delta\phi_{(Z,jet)} = 180^\circ \pm 15^\circ$ . UA1 algorithm.

$P_{tCUT}^{clust}$	30	20	15	10	5
$P_t^{jet}$	166.611	167.904	168.504	168.711	169.574
$P_t^{Jet} - P_t^{jet}$	0.808	0.763	0.732	0.652	0.548
$P_{t(\nu)}^{Jet}$	0.811	0.766	0.734	0.655	0.551
$R_{event}^{\nu \in Jet}$	0.043	0.041	0.041	0.038	0.034
$P_{t(\mu)}^{Jet}$	0.368	0.357	0.348	0.302	0.261
$R_{event}^{\mu \in Jet}$	0.021	0.021	0.021	0.020	0.019
$P_t^{miss}$	6.647	6.468	6.306	6.086	5.462
$P_{t\nu \in Jet}^{miss}$	29.802	29.934	29.081	28.699	22.469
$Nevent_{(c)}$	629	429	306	173	29
$Nevent_{(b)}$	459	305	201	97	14
30sub/all	0.85	0.84	0.83	0.81	0.77
$R_{qc}^{jet}$	0.66	0.66	0.66	0.66	0.65
Entries	27148	19298	14089	8022	1517

Table 11: Selection 1.  $\Delta\phi_{(Z,jet)} = 180^\circ \pm 15^\circ$ . UA2 algorithm.

$P_{tCUT}^{clust}$	30	20	15	10	5
$P_t^{jet}$	166.410	167.275	167.612	167.794	168.717
$P_t^{Jet} - P_t^{jet}$	0.797	0.736	0.722	0.648	0.486
$P_{t(\nu)}^{Jet}$	0.801	0.740	0.725	0.652	0.490
$R_{event}^{\nu \in Jet}$	0.044	0.041	0.041	0.037	0.035
$P_{t(\mu)}^{Jet}$	0.377	0.352	0.344	0.322	0.237
$R_{event}^{\mu \in Jet}$	0.023	0.022	0.022	0.021	0.020
$P_t^{miss}$	6.616	6.385	6.250	6.042	5.382
$P_{t\nu \in Jet}^{miss}$	28.727	28.831	28.168	28.360	20.770
$Nevent_{(c)}$	698	476	348	193	33
$Nevent_{(b)}$	545	364	247	119	15
30sub/all	0.84	0.83	0.82	0.80	0.76
$R_{qc}^{jet}$	0.62	0.62	0.62	0.62	0.63
Entries	30379	22130	16501	9520	1731

Table 12: Selection 1.  $\Delta\phi_{(Z,jet)} = 180^\circ \pm 15^\circ$ . LUCCELL algorithm.

$P_{tCUT}^{clust}$	30	20	15	10	5
$P_t^{jet}$	166.046	167.273	167.865	168.298	169.319
$P_t^{Jet} - P_t^{jet}$	0.800	0.739	0.714	0.629	0.594
$P_{t(\nu)}^{Jet}$	0.803	0.742	0.716	0.631	0.596
$R_{event}^{\nu \in Jet}$	0.043	0.040	0.040	0.036	0.036
$P_{t(\mu)}^{Jet}$	0.396	0.361	0.352	0.326	0.297
$R_{event}^{\mu \in Jet}$	0.022	0.021	0.021	0.019	0.018
$P_t^{miss}$	6.644	6.446	6.292	6.072	5.555
$P_{t\nu \in Jet}^{miss}$	29.840	30.057	29.270	29.107	22.946
$Nevent_{(c)}$	626	434	313	169	28
$Nevent_{(b)}$	457	304	200	91	13
30sub/all	0.85	0.84	0.83	0.82	0.79
$R_{qc}^{jet}$	0.66	0.66	0.65	0.65	0.64
Entries	27334	19833	14494	8069	1430

## Appendix 2

$45 < P_t^Z < 55 \text{ GeV}/c$

Table 1: Selection 1.  $\Delta\phi_{(Z,jet)} = 180^\circ \pm 180^\circ$ . UA1 algorithm.

$P_{tCUT}^{clust}$	30	20	15	10	5
Nevent*	44812	33355	25413	15342	3246
$P_t^{56}$	19.6	15.0	12.4	9.9	7.4
$\Delta\phi$	13.8	9.8	7.9	6.0	4.2
$P_t^{out}$	15.3	11.9	10.0	7.9	5.6
$P_t^{\eta>5}$	5.1	4.9	4.9	4.8	4.3
$(P_t^Z - P_t^{part})/P_t^Z$	0.0487	0.0315	0.0189	0.0113	0.0026
$(P_t^J - P_t^{part})/P_t^J$	0.0140	-0.0016	-0.0069	-0.0032	-0.0057
$(P_t^Z - P_t^J)/P_t^Z$	0.0243	0.0262	0.0200	0.0109	0.0064
$P_t(O+\eta>5)/P_t^Z$	-0.0300	-0.0005	0.0031	0.0011	0.0014
$1 - \cos(\Delta\phi)$	0.0543	0.0267	0.0170	0.0098	0.0050
$\sigma(Db[Z, J])**$	0.2140	0.1814	0.1591	0.1304	0.1010
Entries	18857	14036	10694	6456	1366

Table 2: Selection 1.  $\Delta\phi_{(Z,jet)} = 180^\circ \pm 180^\circ$ . UA2 algorithm.

$P_{tCUT}^{clust}$	30	20	15	10	5
Nevent	43198	32713	25458	15489	3189
$P_t^{56}$	19.3	14.8	12.4	10.0	7.6
$\Delta\phi$	13.3	9.6	7.7	5.9	4.1
$P_t^{out}$	15.0	11.8	10.0	8.0	5.8
$P_t^{\eta>5}$	5.0	4.9	4.9	4.8	4.4
$(P_t^Z - P_t^{part})/P_t^Z$	0.0399	0.0239	0.0153	0.0119	0.0080
$(P_t^J - P_t^{part})/P_t^J$	-0.0048	-0.0257	-0.0333	-0.0295	-0.0259
$(P_t^Z - P_t^J)/P_t^Z$	0.0330	0.0405	0.0405	0.0357	0.0302
$P_t(O+\eta>5)/P_t^Z$	-0.0175	0.0152	0.0241	0.0263	0.0254
$1 - \cos(\Delta\phi)$	0.0505	0.0253	0.0165	0.0094	0.0048
$\sigma(Db[Z, J])$	0.2088	0.1773	0.1563	0.1305	0.1009
Entries	18178	13766	10713	6518	1342

Table 3: Selection 1.  $\Delta\phi_{(Z,jet)} = 180^\circ \pm 180^\circ$ . LUCCELL algorithm.

$P_{tCUT}^{clust}$	30	20	15	10	5
Nevent	48402	36720	27923	16411	3296
$P_t^{56}$	19.4	15.2	12.6	10.0	7.3
$\Delta\phi$	13.6	10.0	8.0	6.1	4.3
$P_t^{out}$	15.2	12.2	10.2	8.0	5.7
$P_t^{\eta>5}$	5.0	4.9	4.9	4.8	4.4
$(P_t^Z - P_t^{part})/P_t^Z$	0.0552	0.0378	0.0250	0.0142	0.0009
$(P_t^J - P_t^{part})/P_t^J$	0.0043	-0.0120	-0.0170	-0.0123	-0.0119
$(P_t^Z - P_t^J)/P_t^Z$	0.0413	0.0420	0.0355	0.0223	0.0105
$P_t(O+\eta>5)/P_t^Z$	-0.0108	0.0143	0.0182	0.0122	0.0047
$1 - \cos(\Delta\phi)$	0.0521	0.0278	0.0173	0.0102	0.0058
$\sigma(Db[Z, J])$	0.2121	0.1842	0.1626	0.1337	0.1031
Entries	20368	15452	11750	6906	1387

\*Number of events (Nevent) is given in this and in the following tables for integrated luminosity  $L_{int} = 10 \text{ fb}^{-1}$ \*\*  $Db[Z, J] \equiv (P_t^Z - P_t^J)/P_t^Z$

Table 4: Selection 1.  $\Delta\phi_{(Z,jet)} = 180^\circ \pm 15^\circ$ . UA1 algorithm.

$P_{tCUT}^{clust}$	30	20	15	10	5
Nevent	29624	26022	21782	14320	3189
$P_t56$	14.5	12.5	11.0	9.3	7.2
$\Delta\phi$	6.1	5.9	5.6	4.9	3.9
$P_t^{out}$	10.5	9.6	8.7	7.4	5.5
$P_t^{\eta>5}$	4.9	4.8	4.7	4.6	4.2
$(P_t^Z - P_t^{part})/P_t^Z$	0.0156	0.0156	0.0107	0.0078	0.0004
$(P_t^J - P_t^{part})/P_t^J$	0.0015	-0.0047	-0.0062	-0.0033	-0.0054
$(P_t^Z - P_t^J)/P_t^Z$	0.0051	0.0140	0.0120	0.0077	0.0039
$P_t(O+\eta>5)/P_t^Z$	-0.0033	0.0060	0.0047	0.0019	0.0001
$1 - \cos(\Delta\phi)$	0.0084	0.0080	0.0073	0.0058	0.0039
$\sigma(Db[Z, J])$	0.2025	0.1745	0.1543	0.1282	0.0992
Entries	12466	10950	9166	6026	1342

Table 5: Selection 1.  $\Delta\phi_{(Z,jet)} = 180^\circ \pm 15^\circ$ . UA2 algorithm.

$P_{tCUT}^{clust}$	30	20	15	10	5
Nevent	29089	25734	21915	14491	3144
$P_t56$	14.3	12.4	11.0	9.4	7.4
$\Delta\phi$	6.0	5.9	5.5	4.9	3.9
$P_t^{out}$	10.4	9.5	8.7	7.5	5.8
$P_t^{\eta>5}$	4.9	4.8	4.7	4.6	4.3
$(P_t^Z - P_t^{part})/P_t^Z$	0.0087	0.0093	0.0081	0.0093	0.0064
$(P_t^J - P_t^{part})/P_t^J$	-0.0203	-0.0292	-0.0324	-0.0293	-0.0262
$(P_t^Z - P_t^J)/P_t^Z$	0.0187	0.0302	0.0335	0.0332	0.0289
$P_t(O+\eta>5)/P_t^Z$	0.0105	0.0225	0.0264	0.0275	0.0252
$1 - \cos(\Delta\phi)$	0.0082	0.0078	0.0071	0.0057	0.0038
$\sigma(Db[Z, J])$	0.1972	0.1704	0.1513	0.1286	0.0998
Entries	12241	10829	9222	6098	1323

Table 6: Selection 1.  $\Delta\phi_{(Z,jet)} = 180^\circ \pm 15^\circ$ . LUCCELL algorithm.

$P_{tCUT}^{clust}$	30	20	15	10	5
Nevent	32153	28405	23849	15294	3237
$P_t56$	14.5	12.6	11.2	9.3	7.0
$\Delta\phi$	6.2	6.0	5.7	5.0	4.0
$P_t^{out}$	10.6	9.7	8.9	7.5	5.6
$P_t^{\eta>5}$	4.9	4.8	4.8	4.6	4.2
$(P_t^Z - P_t^{part})/P_t^Z$	0.0213	0.0206	0.0164	0.0103	-0.0013
$(P_t^J - P_t^{part})/P_t^J$	-0.0081	-0.0145	-0.0161	-0.0120	-0.0118
$(P_t^Z - P_t^J)/P_t^Z$	0.0207	0.0281	0.0268	0.0184	0.0082
$P_t(O+\eta>5)/P_t^Z$	0.0122	0.0200	0.0195	0.0124	0.0043
$1 - \cos(\Delta\phi)$	0.0085	0.0081	0.0074	0.0060	0.0039
$\sigma(Db[Z, J])$	0.2017	0.1768	0.1578	0.1312	0.1009
Entries	13530	11953	10036	6436	1362

Table 7: Selection 1.  $\Delta\phi_{(Z,jet)} = 180^\circ \pm 10^\circ$ . UA1 algorithm.

$P_{tCUT}^{clust}$	30	20	15	10	5
Nevent	23075	20713	17892	12512	2985
$P_t^{56}$	13.0	11.3	10.1	8.6	6.8
$\Delta\phi$	4.3	4.3	4.2	3.9	3.4
$P_t^{out}$	9.4	8.6	7.9	6.9	5.3
$P_t^{\eta>5}$	4.8	4.8	4.7	4.5	4.1
$(P_t^Z - P_t^{part})/P_t^Z$	0.0079	0.0091	0.0069	0.0048	-0.0024
$(P_t^J - P_t^{part})/P_t^J$	-0.0009	-0.0053	-0.0051	-0.0027	-0.0061
$(P_t^Z - P_t^J)/P_t^Z$	0.0011	0.0085	0.0070	0.0044	0.0018
$P_t(O+\eta>5)/P_t^Z$	-0.0030	0.0045	0.0032	0.0009	-0.0009
$1 - \cos(\Delta\phi)$	0.0041	0.0040	0.0038	0.0034	0.0026
$\sigma(Db[Z, J])$	0.1944	0.1691	0.1496	0.1255	0.0980
Entries	9710	8716	7529	5265	1256

Table 8: Selection 1.  $\Delta\phi_{(Z,jet)} = 180^\circ \pm 10^\circ$ . UA2 algorithm.

$P_{tCUT}^{clust}$	30	20	15	10	5
Nevent	22965	20713	18196	12780	2966
$P_t^{56}$	13.0	11.3	10.1	8.8	7.1
$\Delta\phi$	4.3	4.3	4.2	3.9	3.4
$P_t^{out}$	9.3	8.6	8.0	7.1	5.6
$P_t^{\eta>5}$	4.8	4.8	4.7	4.6	4.2
$(P_t^Z - P_t^{part})/P_t^Z$	0.0050	0.0069	0.0070	0.0063	0.0046
$(P_t^J - P_t^{part})/P_t^J$	-0.0226	-0.0294	-0.0308	-0.0296	-0.0260
$(P_t^Z - P_t^J)/P_t^Z$	0.0183	0.0285	0.0309	0.0307	0.0271
$P_t(O+\eta>5)/P_t^Z$	0.0142	0.0245	0.0271	0.0273	0.0245
$1 - \cos(\Delta\phi)$	0.0041	0.0040	0.0038	0.0035	0.0026
$\sigma(Db[Z, J])$	0.1895	0.1643	0.1468	0.1258	0.0983
Entries	9664	8716	7657	5378	1248

Table 9: Selection 1.  $\Delta\phi_{(Z,jet)} = 180^\circ \pm 10^\circ$ . LUCCELL algorithm.

$P_{tCUT}^{clust}$	30	20	15	10	5
Nevent	25028	22564	19532	13332	3035
$P_t^{56}$	13.1	11.5	10.3	8.7	6.7
$\Delta\phi$	4.4	4.3	4.2	4.0	3.4
$P_t^{out}$	9.5	8.8	8.1	7.0	5.4
$P_t^{\eta>5}$	4.8	4.8	4.7	4.5	4.1
$(P_t^Z - P_t^{part})/P_t^Z$	0.0140	0.0147	0.0129	0.0070	-0.0035
$(P_t^J - P_t^{part})/P_t^J$	-0.0102	-0.0141	-0.0144	-0.0118	-0.0115
$(P_t^Z - P_t^J)/P_t^Z$	0.0166	0.0225	0.0220	0.0151	0.0058
$P_t(O+\eta>5)/P_t^Z$	0.0125	0.0185	0.0181	0.0116	0.0032
$1 - \cos(\Delta\phi)$	0.0042	0.0041	0.0039	0.0035	0.0027
$\sigma(Db[Z, J])$	0.1944	0.1721	0.1535	0.1282	0.0997
Entries	10532	9495	8219	5610	1277

Table 10: Selection 1.  $\Delta\phi_{(Z,jet)} = 180^\circ \pm 5^\circ$ . UA1 algorithm.

$P_{tCUT}^{clust}$	30	20	15	10	5
Nevent	14078	12852	11364	8477	2246
$P_t56$	11.6	10.1	9.1	7.8	6.2
$\Delta\phi$	2.4	2.4	2.3	2.3	2.2
$P_t^{out}$	8.4	7.7	7.1	6.2	4.9
$P_t^{\eta>5}$	4.8	4.7	4.6	4.4	4.0
$(P_t^Z - P_t^{part})/P_t^Z$	0.0082	0.0090	0.0074	0.0038	-0.0029
$(P_t^J - P_t^{part})/P_t^J$	0.0001	-0.0035	-0.0028	-0.0025	-0.0065
$(P_t^Z - P_t^J)/P_t^Z$	0.0013	0.0070	0.0055	0.0031	0.0013
$P_t(O+\eta>5)/P_t^Z$	0.0001	0.0059	0.0044	0.0020	0.0003
$1 - \cos(\Delta\phi)$	0.0012	0.0012	0.0012	0.0011	0.0010
$\sigma(Db[Z, J])$	0.1847	0.1611	0.1432	0.1203	0.0938
Entries	5924	5408	4782	3567	945

Table 11: Selection 1.  $\Delta\phi_{(Z,jet)} = 180^\circ \pm 5^\circ$ . UA2 algorithm.

$P_{tCUT}^{clust}$	30	20	15	10	5
Nevent	13961	12775	11511	8607	2243
$P_t56$	11.5	10.0	9.1	8.0	6.5
$\Delta\phi$	2.4	2.4	2.3	2.3	2.2
$P_t^{out}$	8.4	7.6	7.1	6.3	5.2
$P_t^{\eta>5}$	4.8	4.7	4.6	4.5	4.0
$(P_t^Z - P_t^{part})/P_t^Z$	0.0033	0.0048	0.0060	0.0046	0.0032
$(P_t^J - P_t^{part})/P_t^J$	-0.0242	-0.0301	-0.0307	-0.0300	-0.0271
$(P_t^Z - P_t^J)/P_t^Z$	0.0186	0.0275	0.0300	0.0292	0.0264
$P_t(O+\eta>5)/P_t^Z$	0.0174	0.0263	0.0289	0.0281	0.0254
$1 - \cos(\Delta\phi)$	0.0012	0.0012	0.0011	0.0011	0.0010
$\sigma(Db[Z, J])$	0.1832	0.1583	0.1414	0.1216	0.0936
Entries	5875	5376	4844	3622	944

Table 12: Selection 1.  $\Delta\phi_{(Z,jet)} = 180^\circ \pm 5^\circ$ . LUCCELL algorithm.

$P_{tCUT}^{clust}$	30	20	15	10	5
Nevent	15114	13840	12286	8930	2272
$P_t56$	11.7	10.3	9.2	7.8	6.1
$\Delta\phi$	2.4	2.4	2.4	2.3	2.2
$P_t^{out}$	8.5	7.8	7.2	6.3	5.0
$P_t^{\eta>5}$	4.7	4.7	4.6	4.5	4.0
$(P_t^Z - P_t^{part})/P_t^Z$	0.0121	0.0124	0.0111	0.0053	-0.0032
$(P_t^J - P_t^{part})/P_t^J$	-0.0097	-0.0129	-0.0138	-0.0119	-0.0127
$(P_t^Z - P_t^J)/P_t^Z$	0.0146	0.0194	0.0197	0.0135	0.0070
$P_t(O+\eta>5)/P_t^Z$	0.0134	0.0183	0.0185	0.0123	0.0060
$1 - \cos(\Delta\phi)$	0.0012	0.0012	0.0012	0.0011	0.0011
$\sigma(Db[Z, J])$	0.1849	0.1639	0.1470	0.1225	0.0959
Entries	6360	5824	5170	3758	956

Table 13: Selection 2.  $\Delta\phi_{(Z,jet)} = 180^\circ \pm 15^\circ$ ,  $\epsilon^{jet} < 9\%$ . UA1 algorithm.

$P_{tCUT}^{clust}$	30	20	15	10	5
Nevent	23186	20758	17956	12419	3011
$P_t^{56}$	13.8	11.9	10.6	9.0	7.1
$\Delta\phi$	5.9	5.8	5.5	4.8	3.9
$P_t^{out}$	10.2	9.2	8.5	7.2	5.5
$P_t^{\eta>\delta}$	4.9	4.8	4.8	4.6	4.2
$(P_t^Z - P_t^{part})/P_t^Z$	-0.0088	-0.0057	-0.0060	-0.0023	-0.0023
$(P_t^J - P_t^{part})/P_t^J$	0.0136	0.0048	-0.0002	-0.0004	-0.0042
$(P_t^Z - P_t^J)/P_t^Z$	-0.0299	-0.0153	-0.0098	-0.0048	0.0000
$P_t(O+\eta>5)/P_t^Z$	-0.0379	-0.0229	-0.0168	-0.0105	-0.0037
$1 - \cos(\Delta\phi)$	0.0080	0.0076	0.0070	0.0057	0.0038
$\sigma(Db[Z, J])$	0.1986	0.1682	0.1487	0.1246	0.0984
Entries	9757	8735	7556	5226	1267

 Table 14: Selection 2.  $\Delta\phi_{(Z,jet)} = 180^\circ \pm 15^\circ$ ,  $\epsilon^{jet} < 6\%$ . UA2 algorithm.

$P_{tCUT}^{clust}$	30	20	15	10	5
Nevent	12671	11321	9895	6946	1811
$P_t^{56}$	13.6	11.5	10.2	8.7	6.8
$\Delta\phi$	5.8	5.6	5.3	4.7	3.7
$P_t^{out}$	10.2	9.2	8.3	7.1	5.5
$P_t^{\eta>\delta}$	4.9	4.8	4.8	4.6	4.3
$(P_t^Z - P_t^{part})/P_t^Z$	-0.0467	-0.0385	-0.0314	-0.0213	-0.0175
$(P_t^J - P_t^{part})/P_t^J$	-0.0118	-0.0229	-0.0272	-0.0290	-0.0341
$(P_t^Z - P_t^J)/P_t^Z$	-0.0421	-0.0206	-0.0083	0.0042	0.0103
$P_t(O+\eta>5)/P_t^Z$	-0.0497	-0.0278	-0.0149	-0.0010	0.0068
$1 - \cos(\Delta\phi)$	0.0077	0.0072	0.0066	0.0053	0.0035
$\sigma(Db[Z, J])$	0.2024	0.1694	0.1494	0.1252	0.0992
Entries	5332	4764	4164	2923	762

 Table 15: Selection 2.  $\Delta\phi_{(Z,jet)} = 180^\circ \pm 15^\circ$ ,  $\epsilon^{jet} < 9\%$ . LUCCELL algorithm.

$P_{tCUT}^{clust}$	30	20	15	10	5
Nevent	24510	22048	19047	13027	3068
$P_t^{56}$	13.6	11.9	10.5	9.0	7.0
$\Delta\phi$	6.0	5.8	5.5	4.9	3.9
$P_t^{out}$	10.1	9.3	8.5	7.3	5.5
$P_t^{\eta>\delta}$	4.9	4.8	4.8	4.6	4.2
$(P_t^Z - P_t^{part})/P_t^Z$	-0.0089	-0.0054	-0.0055	-0.0026	-0.0039
$(P_t^J - P_t^{part})/P_t^J$	0.0019	-0.0058	-0.0104	-0.0089	-0.0098
$(P_t^Z - P_t^J)/P_t^Z$	-0.0179	-0.0049	0.0003	0.0029	0.0038
$P_t(O+\eta>5)/P_t^Z$	-0.0259	-0.0125	-0.0067	-0.0029	0.0000
$1 - \cos(\Delta\phi)$	0.0081	0.0077	0.0071	0.0057	0.0039
$\sigma(Db[Z, J])$	0.1979	0.1705	0.1510	0.1263	0.0993
Entries	10314	9278	8015	5482	1291

Table 16: Selection 3.  $\Delta\phi_{(Z,jet)} = 180^\circ \pm 15^\circ$ ,  $e^{jet} < 9\%$ . UA1 algorithm.

$P_{tCUT}^{clust}$	30	20	15	10	5
Nevent	17640	15872	13835	9541	2224
$P_t^{56}$	13.4	11.6	10.3	8.8	7.0
$\Delta\phi$	5.8	5.6	5.4	4.7	3.8
$P_t^{out}$	10.0	9.0	8.3	7.1	5.4
$P_t^{\eta>\delta}$	4.9	4.8	4.7	4.6	4.3
$(P_t^Z - P_t^{part})/P_t^Z$	-0.0221	-0.0171	-0.0153	-0.0083	-0.0059
$(P_t^J - P_t^{part})/P_t^J$	0.0132	0.0046	-0.0006	-0.0007	-0.0061
$(P_t^Z - P_t^J)/P_t^Z$	-0.0422	-0.0261	-0.0182	-0.0102	-0.0016
$P_t(O+\eta>5)/P_t^Z$	-0.0498	-0.0334	-0.0249	-0.0155	-0.0051
$1 - \cos(\Delta\phi)$	0.0076	0.0073	0.0067	0.0054	0.0037
$\sigma(Db[Z, J])$	0.1948	0.1646	0.1460	0.1225	0.0971
Entries	7423	6679	5822	4015	936

 Table 17: Selection 3.  $\Delta\phi_{(Z,jet)} = 180^\circ \pm 15^\circ$ ,  $e^{jet} < 6\%$ . UA2 algorithm.

$P_{tCUT}^{clust}$	30	20	15	10	5
Nevent	17640	15872	13835	9541	2224
$P_t^{56}$	13.4	11.6	10.3	8.8	7.0
$\Delta\phi$	5.8	5.7	5.4	4.8	3.9
$P_t^{out}$	10.0	9.1	8.4	7.2	5.6
$P_t^{\eta>\delta}$	4.9	4.8	4.7	4.6	4.3
$(P_t^Z - P_t^{part})/P_t^Z$	-0.0221	-0.0171	-0.0153	-0.0083	-0.0059
$(P_t^J - P_t^{part})/P_t^J$	-0.0174	-0.0266	-0.0319	-0.0320	-0.0339
$(P_t^Z - P_t^J)/P_t^Z$	-0.0124	0.0037	0.0115	0.0166	0.0217
$P_t(O+\eta>5)/P_t^Z$	-0.0200	-0.0036	0.0048	0.0113	0.0181
$1 - \cos(\Delta\phi)$	0.0077	0.0073	0.0068	0.0054	0.0038
$\sigma(Db[Z, J])$	0.1958	0.1658	0.1475	0.1243	0.0992
Entries	7423	6679	5822	4015	936

 Table 18: Selection 3.  $\Delta\phi_{(Z,jet)} = 180^\circ \pm 15^\circ$ ,  $e^{jet} < 9\%$ . LUCCELL algorithm.

$P_{tCUT}^{clust}$	30	20	15	10	5
Nevent	17640	15872	13835	9541	2224
$P_t^{56}$	13.4	11.6	10.3	8.8	7.0
$\Delta\phi$	5.8	5.7	5.4	4.8	3.8
$P_t^{out}$	10.0	9.1	8.4	7.2	5.5
$P_t^{\eta>\delta}$	4.9	4.8	4.7	4.6	4.3
$(P_t^Z - P_t^{part})/P_t^Z$	-0.0221	-0.0171	-0.0153	-0.0083	-0.0059
$(P_t^J - P_t^{part})/P_t^J$	0.0065	-0.0024	-0.0076	-0.0070	-0.0096
$(P_t^Z - P_t^J)/P_t^Z$	-0.0355	-0.0194	-0.0116	-0.0041	0.0019
$P_t(O+\eta>5)/P_t^Z$	-0.0431	-0.0268	-0.0183	-0.0095	-0.0016
$1 - \cos(\Delta\phi)$	0.0077	0.0074	0.0068	0.0055	0.0037
$\sigma(Db[Z, J])$	0.1950	0.1653	0.1469	0.1237	0.0975
Entries	7423	6679	5822	4015	936

Table 19: Selection 3.  $\Delta\phi_{(Z,jet)} = 180^\circ \pm 15^\circ$ ,  $\epsilon^{jet} < 9\%$ . UA1 algorithm.

$P_t^{clust}$ $P_t^{CUT}$	30	20	15	10	5
Nevent	22010	19805	17153	11818	2795
$P_t^{56}$	13.5	11.8	10.4	8.9	7.0
$\Delta\phi$	5.9	5.7	5.4	4.8	3.9
$P_t^{out}$	10.1	9.2	8.4	7.2	5.5
$P_t^{\eta>5}$	4.9	4.8	4.8	4.6	4.2
$(P_t^Z - P_t^{part})/P_t^Z$	-0.0125	-0.0089	-0.0086	-0.0040	-0.0044
$(P_t^J - P_t^{part})/P_t^J$	0.0107	0.0028	-0.0018	-0.0017	-0.0055
$(P_t^Z - P_t^J)/P_t^Z$	-0.0302	-0.0165	-0.0108	-0.0052	-0.0009
$P_t(O+\eta>5)/P_t^Z$	-0.0383	-0.0243	-0.0179	-0.0111	-0.0045
$1 - \cos(\Delta\phi)$	0.0079	0.0075	0.0069	0.0056	0.0038
$\sigma(Db[Z, J])$	0.1971	0.1683	0.1488	0.1246	0.0986
Entries	9262	8334	7218	4973	1176

Table 20: Selection 3.  $\Delta\phi_{(Z,jet)} = 180^\circ \pm 15^\circ$ ,  $\epsilon^{jet} < 9\%$ . LUCCELL algorithm.

$P_t^{clust}$ $P_t^{CUT}$	30	20	15	10	5
Nevent	22010	19805	17153	11818	2795
$P_t^{56}$	13.5	11.8	10.4	8.9	7.0
$\Delta\phi$	5.9	5.8	5.5	4.9	3.9
$P_t^{out}$	10.1	9.2	8.5	7.3	5.5
$P_t^{\eta>5}$	4.9	4.8	4.8	4.6	4.2
$(P_t^Z - P_t^{part})/P_t^Z$	-0.0125	-0.0089	-0.0086	-0.0040	-0.0044
$(P_t^J - P_t^{part})/P_t^J$	0.0041	-0.0040	-0.0087	-0.0078	-0.0089
$(P_t^Z - P_t^J)/P_t^Z$	-0.0237	-0.0099	-0.0042	0.0005	0.0024
$P_t(O+\eta>5)/P_t^Z$	-0.0318	-0.0178	-0.0114	-0.0054	-0.0012
$1 - \cos(\Delta\phi)$	0.0080	0.0076	0.0070	0.0057	0.0038
$\sigma(Db[Z, J])$	0.1971	0.1689	0.1495	0.1257	0.0993
Entries	9262	8334	7218	4973	1176

## Appendix 3

$$70 < P_t^Z < 85 \text{ GeV}/c$$

Table 1: Selection 1.  $\Delta\phi_{(Z,jet)} = 180^\circ \pm 180^\circ$ . UA1 algorithm.

$P_{tCUT}^{clust}$	30	20	15	10	5
Nevent*	17258	12124	8956	5313	1058
$P_t^{56}$	21.0	16.0	13.3	10.7	8.0
$\Delta\phi$	9.0	6.4	5.1	3.9	2.8
$P_t^{out}$	17.3	12.8	10.3	8.0	5.7
$P_t^{\eta>5}$	5.4	5.3	5.2	5.1	4.7
$(P_t^Z - P_t^{part})/P_t^Z$	0.0508	0.0227	0.0137	0.0090	0.0049
$(P_t^J - P_t^{part})/P_t^J$	-0.0273	-0.0163	-0.0100	-0.0037	-0.0068
$(P_t^Z - P_t^J)/P_t^Z$	0.0648	0.0316	0.0186	0.0092	0.0081
$P_t(O+\eta>5)/P_t^Z$	0.0365	0.0158	0.0072	0.0015	0.0022
$1 - \cos(\Delta\phi)$	0.0236	0.0113	0.0071	0.0040	0.0023
$\sigma(Db[Z, J])**$	0.1915	0.1478	0.1219	0.0968	0.0801
Entries	26667	18734	13839	8209	1635

Table 2: Selection 1.  $\Delta\phi_{(Z,jet)} = 180^\circ \pm 180^\circ$ . UA2 algorithm.

$P_{tCUT}^{clust}$	30	20	15	10	5
Nevent	17564	12705	9563	5664	1120
$P_t^{56}$	20.9	16.2	13.6	11.0	8.5
$\Delta\phi$	8.8	6.3	5.1	3.9	2.9
$P_t^{out}$	16.9	12.7	10.5	8.1	5.8
$P_t^{\eta>5}$	5.4	5.3	5.2	5.0	4.7
$(P_t^Z - P_t^{part})/P_t^Z$	0.0489	0.0243	0.0161	0.0128	0.0103
$(P_t^J - P_t^{part})/P_t^J$	-0.0309	-0.0258	-0.0226	-0.0165	-0.0182
$(P_t^Z - P_t^J)/P_t^Z$	0.0670	0.0421	0.0325	0.0252	0.0240
$P_t(O+\eta>5)/P_t^Z$	0.0401	0.0265	0.0212	0.0174	0.0174
$1 - \cos(\Delta\phi)$	0.0224	0.0112	0.0071	0.0041	0.0024
$\sigma(Db[Z, J])$	0.1856	0.1450	0.1207	0.0962	0.0792
Entries	27139	19631	14776	8752	1730

Table 3: Selection 1.  $\Delta\phi_{(Z,jet)} = 180^\circ \pm 180^\circ$ . LUCCELL algorithm.

$P_{tCUT}^{clust}$	30	20	15	10	5
Nevent	17643	12828	9459	5512	1041
$P_t^{56}$	20.5	16.1	13.3	10.5	7.6
$\Delta\phi$	8.7	6.4	5.1	3.9	2.8
$P_t^{out}$	16.9	12.9	10.5	8.1	5.7
$P_t^{\eta>5}$	5.4	5.3	5.2	5.1	4.7
$(P_t^Z - P_t^{part})/P_t^Z$	0.0492	0.0249	0.0143	0.0079	0.0012
$(P_t^J - P_t^{part})/P_t^J$	-0.0302	-0.0227	-0.0180	-0.0108	-0.0143
$(P_t^Z - P_t^J)/P_t^Z$	0.0673	0.0400	0.0267	0.0152	0.0121
$P_t(O+\eta>5)/P_t^Z$	0.0404	0.0239	0.0152	0.0075	0.0063
$1 - \cos(\Delta\phi)$	0.0223	0.0116	0.0072	0.0041	0.0024
$\sigma(Db[Z, J])$	0.1865	0.1489	0.1232	0.0974	0.0803
Entries	27262	19821	14615	8517	1608

\*Number of events (Nevent) is given in this and in the following tables for integrated luminosity  $L_{int} = 10 \text{ fb}^{-1}$ \*\*  $Db[Z, J] \equiv (P_t^Z - P_t^J)/P_t^Z$

Table 4: Selection 1.  $\Delta\phi_{(Z,jet)} = 180^\circ \pm 15^\circ$ . UA1 algorithm.

$P_t^{clust}$ $P_t^{CUT}$	30	20	15	10	5
Nevent	14012	11112	8613	5263	1054
$P_t^{56}$	17.5	14.6	12.7	10.5	7.9
$\Delta\phi$	5.6	5.1	4.5	3.8	2.7
$P_t^{out}$	13.7	11.5	9.8	7.9	5.7
$P_t^{\eta>\delta}$	5.2	5.1	5.1	5.0	4.6
$(P_t^Z - P_t^{part})/P_t^Z$	0.0320	0.0171	0.0113	0.0083	0.0042
$(P_t^J - P_t^{part})/P_t^J$	-0.0243	-0.0148	-0.0094	-0.0037	-0.0068
$(P_t^Z - P_t^J)/P_t^Z$	0.0447	0.0252	0.0158	0.0085	0.0074
$P_t(O+\eta>5)/P_t^Z$	0.0330	0.0147	0.0066	0.0014	0.0018
$1 - \cos(\Delta\phi)$	0.0072	0.0061	0.0050	0.0035	0.0020
$\sigma(Db[Z, J])$	0.1783	0.1420	0.1191	0.0958	0.0787
Entries	21651	17170	13309	8132	1628

Table 5: Selection 1.  $\Delta\phi_{(Z,jet)} = 180^\circ \pm 15^\circ$ . UA2 algorithm.

$P_t^{clust}$ $P_t^{CUT}$	30	20	15	10	5
Nevent	14394	11646	9190	5603	1113
$P_t^{56}$	17.7	14.9	13.0	10.8	8.4
$\Delta\phi$	5.5	5.0	4.5	3.7	2.8
$P_t^{out}$	13.5	11.5	9.9	8.0	5.8
$P_t^{\eta>\delta}$	5.2	5.1	5.1	4.9	4.5
$(P_t^Z - P_t^{part})/P_t^Z$	0.0316	0.0189	0.0139	0.0120	0.0094
$(P_t^J - P_t^{part})/P_t^J$	-0.0287	-0.0246	-0.0219	-0.0165	-0.0180
$(P_t^Z - P_t^J)/P_t^Z$	0.0494	0.0361	0.0299	0.0244	0.0229
$P_t(O+\eta>5)/P_t^Z$	0.0379	0.0257	0.0207	0.0173	0.0167
$1 - \cos(\Delta\phi)$	0.0071	0.0061	0.0050	0.0035	0.0020
$\sigma(Db[Z, J])$	0.1729	0.1391	0.1182	0.0950	0.0772
Entries	22241	17995	14200	8657	1720

Table 6: Selection 1.  $\Delta\phi_{(Z,jet)} = 180^\circ \pm 15^\circ$ . LUCCELL algorithm.

$P_t^{clust}$ $P_t^{CUT}$	30	20	15	10	5
Nevent	14523	11730	9090	5458	1035
$P_t^{56}$	17.4	14.7	12.7	10.3	7.5
$\Delta\phi$	5.6	5.1	4.6	3.8	2.7
$P_t^{out}$	13.6	11.6	10.0	8.0	5.7
$P_t^{\eta>\delta}$	5.2	5.2	5.1	5.0	4.6
$(P_t^Z - P_t^{part})/P_t^Z$	0.0322	0.0185	0.0115	0.0072	0.0003
$(P_t^J - P_t^{part})/P_t^J$	-0.0273	-0.0214	-0.0175	-0.0108	-0.0142
$(P_t^Z - P_t^J)/P_t^Z$	0.0491	0.0330	0.0237	0.0145	0.0112
$P_t(O+\eta>5)/P_t^Z$	0.0375	0.0224	0.0144	0.0074	0.0057
$1 - \cos(\Delta\phi)$	0.0072	0.0062	0.0051	0.0036	0.0020
$\sigma(Db[Z, J])$	0.1744	0.1426	0.1204	0.0965	0.0786
Entries	22441	18124	14046	8434	1600

Table 7: Selection 1.  $\Delta\phi_{(Z,jet)} = 180^\circ \pm 10^\circ$ . UA1 algorithm.

$P_{tCUT}^{clust}$	30	20	15	10	5
Nevent	11553	9597	7794	5014	1039
$P_t^{56}$	16.0	13.5	11.9	10.1	7.8
$\Delta\phi$	4.1	3.9	3.7	3.3	2.6
$P_t^{out}$	12.2	10.4	9.1	7.6	5.7
$P_t^{\eta>5}$	5.2	5.1	5.0	4.9	4.6
$(P_t^Z - P_t^{part})/P_t^Z$	0.0267	0.0141	0.0091	0.0076	0.0047
$(P_t^J - P_t^{part})/P_t^J$	-0.0222	-0.0137	-0.0089	-0.0037	-0.0066
$(P_t^Z - P_t^J)/P_t^Z$	0.0384	0.0214	0.0133	0.0079	0.0077
$P_t(O+\eta>5)/P_t^Z$	0.0303	0.0137	0.0061	0.0017	0.0024
$1 - \cos(\Delta\phi)$	0.0037	0.0035	0.0032	0.0026	0.0017
$\sigma(Db[Z, J])$	0.1721	0.1382	0.1163	0.0944	0.0778
Entries	17852	14829	12043	7748	1606

Table 8: Selection 1.  $\Delta\phi_{(Z,jet)} = 180^\circ \pm 10^\circ$ . UA2 algorithm.

$P_{tCUT}^{clust}$	30	20	15	10	5
Nevent	11917	10088	8332	5350	1099
$P_t^{56}$	16.1	13.8	12.2	10.5	8.3
$\Delta\phi$	4.1	3.9	3.7	3.4	2.6
$P_t^{out}$	12.0	10.4	9.2	7.7	5.8
$P_t^{\eta>5}$	5.1	5.1	5.0	4.9	4.5
$(P_t^Z - P_t^{part})/P_t^Z$	0.0266	0.0162	0.0122	0.0111	0.0093
$(P_t^J - P_t^{part})/P_t^J$	-0.0275	-0.0238	-0.0209	-0.0166	-0.0181
$(P_t^Z - P_t^J)/P_t^Z$	0.0441	0.0328	0.0276	0.0237	0.0230
$P_t(O+\eta>5)/P_t^Z$	0.0362	0.0252	0.0203	0.0175	0.0170
$1 - \cos(\Delta\phi)$	0.0037	0.0035	0.0032	0.0026	0.0018
$\sigma(Db[Z, J])$	0.1655	0.1347	0.1152	0.0938	0.0763
Entries	18413	15588	12874	8267	1698

Table 9: Selection 1.  $\Delta\phi_{(Z,jet)} = 180^\circ \pm 10^\circ$ . LUCCELL algorithm.

$P_{tCUT}^{clust}$	30	20	15	10	5
Nevent	11986	10121	8209	5192	1021
$P_t^{56}$	15.9	13.6	11.9	9.9	7.4
$\Delta\phi$	4.1	4.0	3.8	3.4	2.6
$P_t^{out}$	12.2	10.5	9.2	7.7	5.7
$P_t^{\eta>5}$	5.2	5.1	5.0	4.9	4.5
$(P_t^Z - P_t^{part})/P_t^Z$	0.0270	0.0158	0.0093	0.0063	0.0006
$(P_t^J - P_t^{part})/P_t^J$	-0.0250	-0.0198	-0.0161	-0.0104	-0.0142
$(P_t^Z - P_t^J)/P_t^Z$	0.0427	0.0291	0.0206	0.0134	0.0114
$P_t(O+\eta>5)/P_t^Z$	0.0347	0.0214	0.0134	0.0073	0.0062
$1 - \cos(\Delta\phi)$	0.0038	0.0035	0.0032	0.0027	0.0017
$\sigma(Db[Z, J])$	0.1684	0.1391	0.1174	0.0948	0.0771
Entries	18520	15639	12684	8023	1577

Table 10: Selection 1.  $\Delta\phi_{(Z,jet)} = 180^\circ \pm 5^\circ$ . UA1 algorithm.

$P_{tCUT}^{clust}$	30	20	15	10	5
Nevent	7410	6408	5471	3787	899
$P_t^{56}$	14.1	12.0	10.8	9.1	7.2
$\Delta\phi$	2.3	2.3	2.3	2.2	2.0
$P_t^{out}$	10.5	8.9	7.9	6.7	5.3
$P_t^{\eta>5}$	5.0	5.0	4.9	4.8	4.3
$(P_t^Z - P_t^{part})/P_t^Z$	0.0221	0.0115	0.0081	0.0061	0.0031
$(P_t^J - P_t^{part})/P_t^J$	-0.0171	-0.0091	-0.0054	-0.0018	-0.0053
$(P_t^Z - P_t^J)/P_t^Z$	0.0302	0.0152	0.0093	0.0047	0.0051
$P_t(O+\eta>5)/P_t^Z$	0.0252	0.0103	0.0044	0.0006	0.0010
$1 - \cos(\Delta\phi)$	0.0011	0.0011	0.0011	0.0010	0.0009
$\sigma(Db[Z, J])$	0.1597	0.1294	0.1112	0.0905	0.0728
Entries	11449	9901	8454	5851	1389

Table 11: Selection 1.  $\Delta\phi_{(Z,jet)} = 180^\circ \pm 5^\circ$ . UA2 algorithm.

$P_{tCUT}^{clust}$	30	20	15	10	5
Nevent	7657	6737	5821	4029	942
$P_t^{56}$	14.1	12.2	11.1	9.5	7.7
$\Delta\phi$	2.3	2.3	2.3	2.2	2.0
$P_t^{out}$	10.3	8.9	8.0	6.9	5.4
$P_t^{\eta>5}$	5.0	4.9	4.9	4.7	4.2
$(P_t^Z - P_t^{part})/P_t^Z$	0.0217	0.0127	0.0109	0.0096	0.0087
$(P_t^J - P_t^{part})/P_t^J$	-0.0242	-0.0205	-0.0181	-0.0153	-0.0162
$(P_t^Z - P_t^J)/P_t^Z$	0.0372	0.0270	0.0240	0.0214	0.0209
$P_t(O+\eta>5)/P_t^Z$	0.0320	0.0219	0.0188	0.0172	0.0163
$1 - \cos(\Delta\phi)$	0.0011	0.0011	0.0011	0.0010	0.0009
$\sigma(Db[Z, J])$	0.1538	0.1270	0.1105	0.0897	0.0733
Entries	11831	10409	8994	6225	1456

Table 12: Selection 1.  $\Delta\phi_{(Z,jet)} = 180^\circ \pm 5^\circ$ . LUCCELL algorithm.

$P_{tCUT}^{clust}$	30	20	15	10	5
Nevent	7648	6700	5713	3892	876
$P_t^{56}$	14.0	12.1	10.7	8.9	6.7
$\Delta\phi$	2.3	2.3	2.3	2.2	1.9
$P_t^{out}$	10.4	9.0	8.1	6.8	5.3
$P_t^{\eta>5}$	5.0	5.0	4.9	4.7	4.3
$(P_t^Z - P_t^{part})/P_t^Z$	0.0231	0.0134	0.0083	0.0045	-0.0027
$(P_t^J - P_t^{part})/P_t^J$	-0.0196	-0.0154	-0.0129	-0.0089	-0.0142
$(P_t^Z - P_t^J)/P_t^Z$	0.0349	0.0232	0.0167	0.0101	0.0084
$P_t(O+\eta>5)/P_t^Z$	0.0300	0.0184	0.0118	0.0060	0.0045
$1 - \cos(\Delta\phi)$	0.0011	0.0011	0.0011	0.0010	0.0008
$\sigma(Db[Z, J])$	0.1566	0.1310	0.1127	0.0911	0.0723
Entries	11818	10353	8827	6014	1354

Table 13: Selection 2.  $\Delta\phi_{(Z,jet)} = 180^\circ \pm 15^\circ$ ,  $\epsilon^{jet} < 5\%$ . UA1 algorithm.

$P_{tCUT}^{clust}$	30	20	15	10	5
Nevent	7623	6466	5291	3473	818
$P_t^{56}$	15.8	13.6	11.9	9.9	7.5
$\Delta\phi$	5.3	4.9	4.4	3.7	2.7
$P_t^{out}$	12.4	10.7	9.4	7.7	5.7
$P_t^{\eta>\delta}$	5.1	5.1	5.0	4.9	4.5
$(P_t^Z - P_t^{part})/P_t^Z$	-0.0125	-0.0126	-0.0107	-0.0069	-0.0052
$(P_t^J - P_t^{part})/P_t^J$	-0.0016	-0.0031	-0.0028	-0.0021	-0.0052
$(P_t^Z - P_t^J)/P_t^Z$	-0.0146	-0.0125	-0.0105	-0.0070	-0.0018
$P_t(O+\eta>5)/P_t^Z$	-0.0246	-0.0214	-0.0181	-0.0129	-0.0058
$1 - \cos(\Delta\phi)$	0.0067	0.0058	0.0047	0.0034	0.0020
$\sigma(Db[Z, J])$	0.1534	0.1263	0.1085	0.0891	0.0686
Entries	11778	9991	8175	5367	1264

Table 14: Selection 2.  $\Delta\phi_{(Z,jet)} = 180^\circ \pm 15^\circ$ ,  $\epsilon^{jet} < 4\%$ . UA2 algorithm.

$P_{tCUT}^{clust}$	30	20	15	10	5
Nevent	4198	3593	2975	1975	485
$P_t^{56}$	15.5	13.3	11.7	9.7	7.4
$\Delta\phi$	5.2	4.8	4.3	3.6	2.7
$P_t^{out}$	12.2	10.6	9.3	7.7	5.6
$P_t^{\eta>\delta}$	5.1	5.0	5.0	4.9	4.4
$(P_t^Z - P_t^{part})/P_t^Z$	-0.0294	-0.0261	-0.0215	-0.0146	-0.0095
$(P_t^J - P_t^{part})/P_t^J$	-0.0205	-0.0220	-0.0213	-0.0192	-0.0214
$(P_t^Z - P_t^J)/P_t^Z$	-0.0127	-0.0075	-0.0030	0.0025	0.0097
$P_t(O+\eta>5)/P_t^Z$	-0.0227	-0.0163	-0.0108	-0.0031	0.0059
$1 - \cos(\Delta\phi)$	0.0065	0.0056	0.0046	0.0032	0.0019
$\sigma(Db[Z, J])$	0.1509	0.1260	0.1089	0.0896	0.0695
Entries	6487	5552	4597	3052	749

Table 15: Selection 2.  $\Delta\phi_{(Z,jet)} = 180^\circ \pm 15^\circ$ ,  $\epsilon^{jet} < 5\%$ . LUCCELL algorithm.

$P_{tCUT}^{clust}$	30	20	15	10	5
Nevent	7835	6688	5471	3569	814
$P_t^{56}$	15.6	13.5	11.8	9.8	7.3
$\Delta\phi$	5.3	4.9	4.4	3.7	2.7
$P_t^{out}$	12.3	10.8	9.4	7.7	5.6
$P_t^{\eta>\delta}$	5.1	5.1	5.0	4.9	4.5
$(P_t^Z - P_t^{part})/P_t^Z$	-0.0130	-0.0131	-0.0115	-0.0084	-0.0066
$(P_t^J - P_t^{part})/P_t^J$	-0.0080	-0.0087	-0.0085	-0.0076	-0.0106
$(P_t^Z - P_t^J)/P_t^Z$	-0.0088	-0.0075	-0.0056	-0.0030	0.0022
$P_t(O+\eta>5)/P_t^Z$	-0.0189	-0.0165	-0.0133	-0.0090	-0.0019
$1 - \cos(\Delta\phi)$	0.0067	0.0058	0.0048	0.0035	0.0020
$\sigma(Db[Z, J])$	0.1523	0.1269	0.1092	0.0894	0.0692
Entries	12107	10334	8454	5515	1258

Table 16: Selection 3.  $\Delta\phi_{(Z,jet)} = 180^\circ \pm 15^\circ$ ,  $\epsilon^{jet} < 5\%$ . UA1 algorithm.

$P_{tCUT}^{clust}$	30	20	15	10	5
Nevent	4945	4250	3496	2275	539
$P_t56$	15.4	13.4	11.8	9.7	7.3
$\Delta\phi$	5.1	4.8	4.3	3.6	2.7
$P_t^{out}$	12.2	10.7	9.4	7.7	5.6
$P_t^{\eta>\delta}$	5.0	5.0	5.0	4.9	4.4
$(P_t^Z - P_t^{part})/P_t^Z$	-0.0233	-0.0209	-0.0182	-0.0126	-0.0081
$(P_t^J - P_t^{part})/P_t^J$	-0.0019	-0.0041	-0.0032	-0.0031	-0.0065
$(P_t^Z - P_t^J)/P_t^Z$	-0.0247	-0.0197	-0.0174	-0.0116	-0.0033
$P_t(O+\eta>5)/P_t^Z$	-0.0344	-0.0285	-0.0250	-0.0175	-0.0073
$1 - \cos(\Delta\phi)$	0.0064	0.0056	0.0046	0.0033	0.0020
$\sigma(Db[Z, J])$	0.1487	0.1257	0.1078	0.0889	0.0684
Entries	7641	6567	5402	3515	833

 Table 17: Selection 3.  $\Delta\phi_{(Z,jet)} = 180^\circ \pm 15^\circ$ ,  $\epsilon^{jet} < 5\%$ . UA2 algorithm.

$P_{tCUT}^{clust}$	30	20	15	10	5
Nevent	4945	4250	3496	2275	539
$P_t56$	15.4	13.4	11.8	9.7	7.3
$\Delta\phi$	5.2	4.8	4.3	3.6	2.7
$P_t^{out}$	12.1	10.6	9.3	7.7	5.7
$P_t^{\eta>\delta}$	5.0	5.0	5.0	4.9	4.4
$(P_t^Z - P_t^{part})/P_t^Z$	-0.0233	-0.0209	-0.0182	-0.0126	-0.0081
$(P_t^J - P_t^{part})/P_t^J$	-0.0201	-0.0220	-0.0207	-0.0204	-0.0228
$(P_t^Z - P_t^J)/P_t^Z$	-0.0070	-0.0022	-0.0002	0.0053	0.0126
$P_t(O+\eta>5)/P_t^Z$	-0.0167	-0.0111	-0.0079	-0.0007	0.0085
$1 - \cos(\Delta\phi)$	0.0064	0.0056	0.0046	0.0033	0.0020
$\sigma(Db[Z, J])$	0.1492	0.1259	0.1081	0.0897	0.0688
Entries	7641	6567	5402	3515	833

 Table 18: Selection 3.  $\Delta\phi_{(Z,jet)} = 180^\circ \pm 15^\circ$ ,  $\epsilon^{jet} < 5\%$ . LUCCELL algorithm.

$P_{tCUT}^{clust}$	30	20	15	10	5
Nevent	4945	4250	3496	2275	539
$P_t56$	15.4	13.4	11.8	9.7	7.3
$\Delta\phi$	5.2	4.8	4.3	3.6	2.7
$P_t^{out}$	12.2	10.7	9.4	7.7	5.6
$P_t^{\eta>\delta}$	5.0	5.0	5.0	4.9	4.4
$(P_t^Z - P_t^{part})/P_t^Z$	-0.0233	-0.0209	-0.0182	-0.0126	-0.0081
$(P_t^J - P_t^{part})/P_t^J$	-0.0063	-0.0080	-0.0072	-0.0065	-0.0089
$(P_t^Z - P_t^J)/P_t^Z$	-0.0205	-0.0159	-0.0135	-0.0082	-0.0009
$P_t(O+\eta>5)/P_t^Z$	-0.0302	-0.0247	-0.0212	-0.0142	-0.0050
$1 - \cos(\Delta\phi)$	0.0064	0.0056	0.0046	0.0033	0.0020
$\sigma(Db[Z, J])$	0.1494	0.1263	0.1085	0.0894	0.0682
Entries	7641	6567	5402	3515	833

## Appendix 4

$100 < P_t^Z < 120 \text{ GeV}/c$

Table 1: Selection 1.  $\Delta\phi_{(Z,jet)} = 180^\circ \pm 180^\circ$ . UA1 algorithm.

$P_{tCUT}^{clust}$	30	20	15	10	5
Nevent*	9840	6949	5114	2944	586
$P_t^{56}$	21.9	17.0	14.4	11.7	8.6
$\Delta\phi$	6.0	4.4	3.6	2.8	2.1
$P_t^{out}$	17.4	13.0	10.6	8.0	5.6
$P_t^{\eta>5}$	5.8	5.6	5.5	5.4	5.1
$(P_t^Z - P_t^{part})/P_t^Z$	0.0322	0.0183	0.0129	0.0104	0.0052
$(P_t^J - P_t^{part})/P_t^J$	-0.0166	-0.0082	-0.0035	0.0007	-0.0014
$(P_t^Z - P_t^J)/P_t^Z$	0.0400	0.0208	0.0121	0.0061	0.0040
$P_t(O+\eta>5)/P_t^Z$	0.0244	0.0107	0.0040	-0.0002	-0.0001
$1 - \cos(\Delta\phi)$	0.0102	0.0052	0.0034	0.0020	0.0013
$\sigma(Db[Z, J])**$	0.1442	0.1093	0.0920	0.0751	0.0602
Entries	28431	20078	14777	8505	1694

Table 2: Selection 1.  $\Delta\phi_{(Z,jet)} = 180^\circ \pm 180^\circ$ . UA2 algorithm.

$P_{tCUT}^{clust}$	30	20	15	10	5
Nevent	10518	7623	5697	3306	640
$P_t^{56}$	22.2	17.6	15.1	12.5	9.5
$\Delta\phi$	5.9	4.3	3.6	2.8	2.1
$P_t^{out}$	17.0	12.9	10.6	8.2	5.8
$P_t^{\eta>5}$	5.8	5.6	5.5	5.4	5.0
$(P_t^Z - P_t^{part})/P_t^Z$	0.0341	0.0225	0.0181	0.0162	0.0121
$(P_t^J - P_t^{part})/P_t^J$	-0.0164	-0.0110	-0.0081	-0.0049	-0.0043
$(P_t^Z - P_t^J)/P_t^Z$	0.0422	0.0275	0.0214	0.0169	0.0141
$P_t(O+\eta>5)/P_t^Z$	0.0269	0.0174	0.0135	0.0107	0.0100
$1 - \cos(\Delta\phi)$	0.0098	0.0051	0.0034	0.0020	0.0013
$\sigma(Db[Z, J])$	0.1394	0.1076	0.0913	0.0759	0.0596
Entries	30391	22026	16462	9553	1848

Table 3: Selection 1.  $\Delta\phi_{(Z,jet)} = 180^\circ \pm 180^\circ$ . LUCCELL algorithm.

$P_{tCUT}^{clust}$	30	20	15	10	5
Nevent	9967	7202	5295	2996	568
$P_t^{56}$	21.4	17.0	14.3	11.4	8.1
$\Delta\phi$	5.8	4.4	3.6	2.8	2.1
$P_t^{out}$	17.0	13.1	10.7	8.1	5.6
$P_t^{\eta>5}$	5.8	5.7	5.5	5.4	5.1
$(P_t^Z - P_t^{part})/P_t^Z$	0.0311	0.0185	0.0120	0.0083	0.0008
$(P_t^J - P_t^{part})/P_t^J$	-0.0195	-0.0132	-0.0099	-0.0059	-0.0072
$(P_t^Z - P_t^J)/P_t^Z$	0.0424	0.0259	0.0172	0.0101	0.0053
$P_t(O+\eta>5)/P_t^Z$	0.0275	0.0156	0.0090	0.0038	0.0012
$1 - \cos(\Delta\phi)$	0.0095	0.0053	0.0035	0.0021	0.0013
$\sigma(Db[Z, J])$	0.1399	0.1101	0.0933	0.0767	0.0609
Entries	28798	20809	15300	8658	1640

\*Number of events (Nevent) is given in this and in the following tables for integrated luminosity  $L_{int} = 10 \text{ fb}^{-1}$ \*\*  $Db[Z, J] \equiv (P_t^Z - P_t^J)/P_t^Z$

Table 4: Selection 1.  $\Delta\phi_{(Z,jet)} = 180^\circ \pm 15^\circ$ . UA1 algorithm.

$P_{tCUT}^{clust}$	30	20	15	10	5
Nevent	9125	6803	5077	2939	585
$P_t56$	20.3	16.6	14.2	11.6	8.5
$\Delta\phi$	4.9	4.1	3.5	2.7	2.0
$P_t^{out}$	15.7	12.5	10.5	8.0	5.6
$P_t^{\eta>5}$	5.7	5.6	5.4	5.4	5.0
$(P_t^Z - P_t^{part})/P_t^Z$	0.0266	0.0170	0.0123	0.0103	0.0048
$(P_t^J - P_t^{part})/P_t^J$	-0.0150	-0.0080	-0.0036	0.0007	-0.0014
$(P_t^Z - P_t^J)/P_t^Z$	0.0336	0.0195	0.0115	0.0060	0.0036
$P_t(O+\eta>5)/P_t^Z$	0.0225	0.0104	0.0038	-0.0002	-0.0003
$1 - \cos(\Delta\phi)$	0.0058	0.0042	0.0031	0.0019	0.0011
$\sigma(Db[Z, J])$	0.1382	0.1080	0.0916	0.0750	0.0596
Entries	26365	19658	14669	8491	1690

Table 5: Selection 1.  $\Delta\phi_{(Z,jet)} = 180^\circ \pm 15^\circ$ . UA2 algorithm.

$P_{tCUT}^{clust}$	30	20	15	10	5
Nevent	9798	7478	5661	3302	639
$P_t56$	20.6	17.3	14.9	12.5	9.5
$\Delta\phi$	4.8	4.1	3.5	2.7	2.0
$P_t^{out}$	15.4	12.5	10.5	8.2	5.8
$P_t^{\eta>5}$	5.7	5.6	5.4	5.4	5.0
$(P_t^Z - P_t^{part})/P_t^Z$	0.0286	0.0215	0.0177	0.0162	0.0119
$(P_t^J - P_t^{part})/P_t^J$	-0.0152	-0.0106	-0.0080	-0.0049	-0.0042
$(P_t^Z - P_t^J)/P_t^Z$	0.0362	0.0262	0.0209	0.0168	0.0139
$P_t(O+\eta>5)/P_t^Z$	0.0251	0.0171	0.0133	0.0107	0.0100
$1 - \cos(\Delta\phi)$	0.0057	0.0042	0.0031	0.0020	0.0011
$\sigma(Db[Z, J])$	0.1337	0.1064	0.0907	0.0758	0.0593
Entries	28311	21607	16358	9541	1845

Table 6: Selection 1.  $\Delta\phi_{(Z,jet)} = 180^\circ \pm 15^\circ$ . LUCCELL algorithm.

$P_{tCUT}^{clust}$	30	20	15	10	5
Nevent	9317	7047	5255	2991	566
$P_t56$	20.0	16.6	14.1	11.4	8.0
$\Delta\phi$	4.8	4.1	3.5	2.7	2.0
$P_t^{out}$	15.5	12.7	10.6	8.1	5.6
$P_t^{\eta>5}$	5.7	5.6	5.5	5.4	5.0
$(P_t^Z - P_t^{part})/P_t^Z$	0.0265	0.0172	0.0115	0.0082	0.0005
$(P_t^J - P_t^{part})/P_t^J$	-0.0181	-0.0128	-0.0097	-0.0058	-0.0072
$(P_t^Z - P_t^J)/P_t^Z$	0.0370	0.0244	0.0166	0.0100	0.0050
$P_t(O+\eta>5)/P_t^Z$	0.0260	0.0152	0.0087	0.0038	0.0010
$1 - \cos(\Delta\phi)$	0.0057	0.0043	0.0032	0.0020	0.0011
$\sigma(Db[Z, J])$	0.1349	0.1087	0.0927	0.0766	0.0604
Entries	26920	20362	15184	8643	1636

Table 7: Selection 1.  $\Delta\phi_{(Z,jet)} = 180^\circ \pm 10^\circ$ . UA1 algorithm.

$P_{tCUT}^{clust}$	30	20	15	10	5
Nevent	7979	6323	4882	2897	581
$P_t56$	18.7	15.7	13.7	11.4	8.4
$\Delta\phi$	3.8	3.5	3.1	2.6	2.0
$P_t^{out}$	14.0	11.7	10.0	7.9	5.6
$P_t^{\eta>5}$	5.6	5.5	5.4	5.3	4.9
$(P_t^Z - P_t^{part})/P_t^Z$	0.0233	0.0155	0.0114	0.0098	0.0049
$(P_t^J - P_t^{part})/P_t^J$	-0.0126	-0.0072	-0.0032	0.0007	-0.0014
$(P_t^Z - P_t^J)/P_t^Z$	0.0288	0.0175	0.0103	0.0055	0.0037
$P_t(O+\eta>5)/P_t^Z$	0.0204	0.0099	0.0034	-0.0004	-0.0001
$1 - \cos(\Delta\phi)$	0.0033	0.0029	0.0024	0.0017	0.0010
$\sigma(Db[Z, J])$	0.1332	0.1061	0.0901	0.0742	0.0591
Entries	23056	18271	14105	8371	1679

Table 8: Selection 1.  $\Delta\phi_{(Z,jet)} = 180^\circ \pm 10^\circ$ . UA2 algorithm.

$P_{tCUT}^{clust}$	30	20	15	10	5
Nevent	8590	6952	5449	3256	634
$P_t56$	19.1	16.4	14.5	12.3	9.3
$\Delta\phi$	3.8	3.5	3.1	2.6	2.0
$P_t^{out}$	13.8	11.7	10.1	8.1	5.8
$P_t^{\eta>5}$	5.6	5.5	5.4	5.3	4.8
$(P_t^Z - P_t^{part})/P_t^Z$	0.0250	0.0199	0.0165	0.0157	0.0116
$(P_t^J - P_t^{part})/P_t^J$	-0.0140	-0.0101	-0.0080	-0.0050	-0.0042
$(P_t^Z - P_t^J)/P_t^Z$	0.0319	0.0243	0.0198	0.0164	0.0135
$P_t(O+\eta>5)/P_t^Z$	0.0235	0.0168	0.0129	0.0106	0.0097
$1 - \cos(\Delta\phi)$	0.0033	0.0028	0.0024	0.0017	0.0010
$\sigma(Db[Z, J])$	0.1290	0.1044	0.0894	0.0749	0.0574
Entries	24819	20086	15744	9407	1832

Table 9: Selection 1.  $\Delta\phi_{(Z,jet)} = 180^\circ \pm 10^\circ$ . LUCCELL algorithm.

$P_{tCUT}^{clust}$	30	20	15	10	5
Nevent	8188	6546	5051	2951	563
$P_t56$	18.5	15.7	13.6	11.2	7.9
$\Delta\phi$	3.8	3.5	3.2	2.6	2.0
$P_t^{out}$	14.0	11.8	10.1	8.0	5.6
$P_t^{\eta>5}$	5.6	5.5	5.4	5.3	4.9
$(P_t^Z - P_t^{part})/P_t^Z$	0.0229	0.0155	0.0103	0.0079	0.0007
$(P_t^J - P_t^{part})/P_t^J$	-0.0163	-0.0123	-0.0096	-0.0058	-0.0072
$(P_t^Z - P_t^J)/P_t^Z$	0.0324	0.0224	0.0152	0.0096	0.0052
$P_t(O+\eta>5)/P_t^Z$	0.0240	0.0148	0.0082	0.0037	0.0012
$1 - \cos(\Delta\phi)$	0.0033	0.0029	0.0024	0.0017	0.0010
$\sigma(Db[Z, J])$	0.1308	0.1069	0.0915	0.0760	0.0601
Entries	23659	18915	14593	8528	1628

Table 10: Selection 1.  $\Delta\phi_{(Z,jet)} = 180^\circ \pm 5^\circ$ . UA1 algorithm.

$P_t^{clust}$ $P_t^{CUT}$	30	20	15	10	5
Nevent	5491	4657	3850	2514	546
$P_t^{56}$	16.4	14.0	12.4	10.6	8.0
$\Delta\phi$	2.2	2.2	2.1	2.0	1.7
$P_t^{out}$	11.7	9.9	8.7	7.3	5.4
$P_t^{\eta>5}$	5.5	5.3	5.2	5.1	4.7
$(P_t^Z - P_t^{part})/P_t^Z$	0.0203	0.0141	0.0108	0.0090	0.0055
$(P_t^J - P_t^{part})/P_t^J$	-0.0090	-0.0049	-0.0017	0.0007	-0.0005
$(P_t^Z - P_t^J)/P_t^Z$	0.0229	0.0141	0.0086	0.0047	0.0038
$P_t(O+\eta>5)/P_t^Z$	0.0172	0.0087	0.0035	-0.0001	0.0005
$1 - \cos(\Delta\phi)$	0.0011	0.0010	0.0010	0.0009	0.0007
$\sigma(Db[Z, J])$	0.1248	0.1018	0.0869	0.0724	0.0561
Entries	15866	13457	11125	7263	1579

Table 11: Selection 1.  $\Delta\phi_{(Z,jet)} = 180^\circ \pm 5^\circ$ . UA2 algorithm.

$P_t^{clust}$ $P_t^{CUT}$	30	20	15	10	5
Nevent	5935	5124	4285	2822	597
$P_t^{56}$	16.7	14.7	13.2	11.5	9.0
$\Delta\phi$	2.2	2.2	2.1	2.0	1.7
$P_t^{out}$	11.5	9.9	8.8	7.4	5.6
$P_t^{\eta>5}$	5.4	5.3	5.2	5.1	4.6
$(P_t^Z - P_t^{part})/P_t^Z$	0.0224	0.0185	0.0162	0.0150	0.0127
$(P_t^J - P_t^{part})/P_t^J$	-0.0108	-0.0080	-0.0060	-0.0044	-0.0029
$(P_t^Z - P_t^J)/P_t^Z$	0.0271	0.0215	0.0180	0.0155	0.0137
$P_t(O+\eta>5)/P_t^Z$	0.0213	0.0162	0.0131	0.0110	0.0104
$1 - \cos(\Delta\phi)$	0.0011	0.0010	0.0010	0.0009	0.0007
$\sigma(Db[Z, J])$	0.1205	0.0999	0.0856	0.0723	0.0545
Entries	17150	14806	12380	8153	1726

Table 12: Selection 1.  $\Delta\phi_{(Z,jet)} = 180^\circ \pm 5^\circ$ . LUCCELL algorithm.

$P_t^{clust}$ $P_t^{CUT}$	30	20	15	10	5
Nevent	5621	4788	3958	2556	531
$P_t^{56}$	16.2	13.9	12.2	10.3	7.5
$\Delta\phi$	2.2	2.2	2.1	2.0	1.7
$P_t^{out}$	11.6	10.0	8.8	7.3	5.4
$P_t^{\eta>5}$	5.5	5.4	5.2	5.1	4.7
$(P_t^Z - P_t^{part})/P_t^Z$	0.0195	0.0137	0.0094	0.0067	0.0013
$(P_t^J - P_t^{part})/P_t^J$	-0.0136	-0.0101	-0.0082	-0.0059	-0.0061
$(P_t^Z - P_t^J)/P_t^Z$	0.0268	0.0187	0.0132	0.0086	0.0051
$P_t(O+\eta>5)/P_t^Z$	0.0211	0.0134	0.0081	0.0037	0.0018
$1 - \cos(\Delta\phi)$	0.0011	0.0010	0.0010	0.0009	0.0007
$\sigma(Db[Z, J])$	0.1228	0.1023	0.0880	0.0738	0.0565
Entries	16241	13834	11437	7385	1534

Table 13: Selection 2.  $\Delta\phi_{(Z,jet)} = 180^\circ \pm 15^\circ$ ,  $e^{jet} < 4\%$ . UA1 algorithm.

$P_{tCUT}^{clust}$	30	20	15	10	5
Nevent	5597	4453	3499	2187	493
$P_t 56$	18.3	15.2	13.1	10.8	8.0
$\Delta\phi$	4.6	3.9	3.3	2.7	2.0
$P_t^{out}$	14.2	11.7	9.9	7.8	5.5
$P_t^{\eta>\delta}$	5.5	5.4	5.3	5.2	5.0
$(P_t^Z - P_t^{part})/P_t^Z$	-0.0041	-0.0034	-0.0037	-0.0009	-0.0021
$(P_t^J - P_t^{part})/P_t^J$	-0.0037	-0.0026	-0.0017	0.0001	-0.0044
$(P_t^Z - P_t^J)/P_t^Z$	-0.0038	-0.0035	-0.0045	-0.0029	0.0000
$P_t(O+\eta>5)/P_t^Z$	-0.0130	-0.0109	-0.0105	-0.0076	-0.0037
$1 - \cos(\Delta\phi)$	0.0053	0.0039	0.0029	0.0019	0.0011
$\sigma(Db[Z, J])$	0.1206	0.0963	0.0822	0.0668	0.0575
Entries	16173	12867	10110	6319	1424

 Table 14: Selection 2.  $\Delta\phi_{(Z,jet)} = 180^\circ \pm 15^\circ$ ,  $e^{jet} < 4\%$ . UA2 algorithm.

$P_{tCUT}^{clust}$	30	20	15	10	5
Nevent	5859	4677	3664	2290	502
$P_t 56$	18.3	15.3	13.2	11.0	8.3
$\Delta\phi$	4.6	3.9	3.3	2.7	2.0
$P_t^{out}$	14.2	11.7	10.0	7.9	5.6
$P_t^{\eta>\delta}$	5.5	5.4	5.3	5.2	4.9
$(P_t^Z - P_t^{part})/P_t^Z$	-0.0053	-0.0035	-0.0032	0.0000	0.0001
$(P_t^J - P_t^{part})/P_t^J$	-0.0155	-0.0143	-0.0131	-0.0110	-0.0126
$(P_t^Z - P_t^J)/P_t^Z$	0.0067	0.0079	0.0074	0.0090	0.0108
$P_t(O+\eta>5)/P_t^Z$	-0.0024	0.0006	0.0016	0.0044	0.0073
$1 - \cos(\Delta\phi)$	0.0053	0.0039	0.0029	0.0019	0.0012
$\sigma(Db[Z, J])$	0.1181	0.0959	0.0817	0.0672	0.0567
Entries	16928	13513	10586	6617	1450

 Table 15: Selection 2.  $\Delta\phi_{(Z,jet)} = 180^\circ \pm 15^\circ$ ,  $e^{jet} < 4\%$ . LUCCELL algorithm.

$P_{tCUT}^{clust}$	30	20	15	10	5
Nevent	5639	4525	3554	2205	493
$P_t 56$	17.9	15.0	12.9	10.5	7.8
$\Delta\phi$	4.6	3.9	3.3	2.7	2.0
$P_t^{out}$	14.1	11.7	10.0	7.8	5.5
$P_t^{\eta>\delta}$	5.5	5.4	5.3	5.2	4.9
$(P_t^Z - P_t^{part})/P_t^Z$	-0.0046	-0.0045	-0.0051	-0.0029	-0.0040
$(P_t^J - P_t^{part})/P_t^J$	-0.0083	-0.0072	-0.0065	-0.0043	-0.0073
$(P_t^Z - P_t^J)/P_t^Z$	0.0004	-0.0001	-0.0011	-0.0005	0.0010
$P_t(O+\eta>5)/P_t^Z$	-0.0088	-0.0075	-0.0072	-0.0053	-0.0026
$1 - \cos(\Delta\phi)$	0.0052	0.0039	0.0029	0.0019	0.0011
$\sigma(Db[Z, J])$	0.1189	0.0966	0.0830	0.0672	0.0572
Entries	16292	13074	10268	6371	1425

Table 16: Selection 3.  $\Delta\phi_{(Z,jet)} = 180^\circ \pm 15^\circ$ ,  $\epsilon^{jet} < 4\%$ . UA1 algorithm.

$P_{tCUT}^{clust}$	30	20	15	10	5
Nevent	4686	3785	2962	1846	400
$P_t^{56}$	17.8	15.0	12.8	10.5	7.7
$\Delta\phi$	4.5	3.9	3.3	2.7	2.0
$P_t^{out}$	13.9	11.7	9.9	7.8	5.5
$P_t^{\eta>\delta}$	5.5	5.4	5.3	5.2	4.9
$(P_t^Z - P_t^{part})/P_t^Z$	-0.0074	-0.0067	-0.0066	-0.0034	-0.0058
$(P_t^J - P_t^{part})/P_t^J$	-0.0048	-0.0042	-0.0034	-0.0023	-0.0061
$(P_t^Z - P_t^J)/P_t^Z$	-0.0058	-0.0052	-0.0055	-0.0031	-0.0015
$P_t(O+\eta>5)/P_t^Z$	-0.0149	-0.0125	-0.0115	-0.0079	-0.0049
$1 - \cos(\Delta\phi)$	0.0051	0.0038	0.0028	0.0019	0.0012
$\sigma(Db[Z, J])$	0.1169	0.0960	0.0815	0.0669	0.0553
Entries	13541	10935	8559	5333	1157

 Table 17: Selection 3.  $\Delta\phi_{(Z,jet)} = 180^\circ \pm 15^\circ$ ,  $\epsilon^{jet} < 4\%$ . UA2 algorithm.

$P_{tCUT}^{clust}$	30	20	15	10	5
Nevent	4686	3785	2962	1846	400
$P_t^{56}$	17.8	15.0	12.8	10.5	7.7
$\Delta\phi$	4.5	3.9	3.3	2.7	2.0
$P_t^{out}$	13.9	11.7	9.9	7.8	5.6
$P_t^{\eta>\delta}$	5.5	5.4	5.3	5.2	4.9
$(P_t^Z - P_t^{part})/P_t^Z$	-0.0074	-0.0067	-0.0066	-0.0034	-0.0058
$(P_t^J - P_t^{part})/P_t^J$	-0.0176	-0.0169	-0.0160	-0.0147	-0.0169
$(P_t^Z - P_t^J)/P_t^Z$	0.0065	0.0071	0.0067	0.0090	0.0090
$P_t(O+\eta>5)/P_t^Z$	-0.0026	-0.0003	0.0008	0.0042	0.0056
$1 - \cos(\Delta\phi)$	0.0051	0.0039	0.0029	0.0019	0.0012
$\sigma(Db[Z, J])$	0.1171	0.0963	0.0820	0.0673	0.0555
Entries	13541	10935	8559	5333	1157

 Table 18: Selection 3.  $\Delta\phi_{(Z,jet)} = 180^\circ \pm 15^\circ$ ,  $\epsilon^{jet} < 4\%$ . LUCCELL algorithm.

$P_{tCUT}^{clust}$	30	20	15	10	5
Nevent	4686	3785	2962	1846	400
$P_t^{56}$	17.8	15.0	12.8	10.5	7.7
$\Delta\phi$	4.5	3.9	3.3	2.7	2.0
$P_t^{out}$	14.0	11.7	9.9	7.8	5.5
$P_t^{\eta>\delta}$	5.5	5.4	5.3	5.2	4.9
$(P_t^Z - P_t^{part})/P_t^Z$	-0.0074	-0.0067	-0.0066	-0.0034	-0.0058
$(P_t^J - P_t^{part})/P_t^J$	-0.0082	-0.0073	-0.0062	-0.0047	-0.0077
$(P_t^Z - P_t^J)/P_t^Z$	-0.0025	-0.0021	-0.0027	-0.0007	0.0000
$P_t(O+\eta>5)/P_t^Z$	-0.0116	-0.0095	-0.0087	-0.0056	-0.0034
$1 - \cos(\Delta\phi)$	0.0051	0.0038	0.0029	0.0019	0.0012
$\sigma(Db[Z, J])$	0.1174	0.0964	0.0819	0.0672	0.0556
Entries	13541	10935	8559	5333	1157

## Appendix 5

$150 < P_t^Z < 200 \text{ GeV}/c$

Table 1: Selection 1.  $\Delta\phi_{(Z,jet)} = 180^\circ \pm 180^\circ$ . UA1 algorithm.

$P_{tCUT}^{clust}$	30	20	15	10	5
Nevent*	4103	2886	2104	1198	227
$P_t^{56}$	23.4	18.6	15.8	13.0	10.0
$\Delta\phi$	3.9	2.9	2.4	1.9	1.4
$P_t^{out}$	17.6	13.2	10.8	8.4	6.0
$P_t^{\eta>5}$	6.4	6.3	6.2	6.0	5.5
$(P_t^Z - P_t^{part})/P_t^Z$	0.0186	0.0133	0.0112	0.0104	0.0067
$(P_t^J - P_t^{part})/P_t^J$	-0.0081	-0.0036	-0.0009	0.0012	0.0018
$(P_t^Z - P_t^J)/P_t^Z$	0.0214	0.0126	0.0085	0.0061	0.0028
$P_t(O+\eta>5)/P_t^Z$	0.0123	0.0058	0.0027	0.0014	-0.0011
$1 - \cos(\Delta\phi)$	0.0042	0.0024	0.0015	0.0009	0.0006
$\sigma(Db[Z, J])**$	0.0990	0.0791	0.0684	0.0586	0.0465
Entries	27490	19335	14096	8024	1518

Table 2: Selection 1.  $\Delta\phi_{(Z,jet)} = 180^\circ \pm 180^\circ$ . UA2 algorithm.

$P_{tCUT}^{clust}$	30	20	15	10	5
Nevent	4585	3309	2464	1421	259
$P_t^{56}$	24.2	19.7	17.1	14.3	11.3
$\Delta\phi$	3.8	2.9	2.4	1.9	1.4
$P_t^{out}$	17.1	13.1	10.8	8.5	6.0
$P_t^{\eta>5}$	6.4	6.2	6.2	6.0	5.4
$(P_t^Z - P_t^{part})/P_t^Z$	0.0234	0.0186	0.0173	0.0156	0.0110
$(P_t^J - P_t^{part})/P_t^J$	-0.0048	-0.0023	-0.0004	0.0004	0.0013
$(P_t^Z - P_t^J)/P_t^Z$	0.0231	0.0168	0.0142	0.0121	0.0082
$P_t(O+\eta>5)/P_t^Z$	0.0142	0.0101	0.0085	0.0074	0.0048
$1 - \cos(\Delta\phi)$	0.0040	0.0023	0.0015	0.0009	0.0006
$\sigma(Db[Z, J])$	0.0959	0.0772	0.0675	0.0580	0.0439
Entries	30719	22169	16509	9522	1732

Table 3: Selection 1.  $\Delta\phi_{(Z,jet)} = 180^\circ \pm 180^\circ$ . LUCCELL algorithm.

$P_{tCUT}^{clust}$	30	20	15	10	5
Nevent	4123	2966	2165	1205	214
$P_t^{56}$	22.8	18.4	15.6	12.5	9.4
$\Delta\phi$	3.8	2.9	2.4	1.9	1.4
$P_t^{out}$	17.3	13.4	11.0	8.5	6.0
$P_t^{\eta>5}$	6.4	6.3	6.2	6.0	5.6
$(P_t^Z - P_t^{part})/P_t^Z$	0.0180	0.0125	0.0103	0.0081	0.0039
$(P_t^J - P_t^{part})/P_t^J$	-0.0115	-0.0078	-0.0055	-0.0036	-0.0029
$(P_t^Z - P_t^J)/P_t^Z$	0.0242	0.0161	0.0121	0.0087	0.0042
$P_t(O+\eta>5)/P_t^Z$	0.0153	0.0093	0.0064	0.0040	0.0001
$1 - \cos(\Delta\phi)$	0.0040	0.0024	0.0015	0.0009	0.0006
$\sigma(Db[Z, J])$	0.0974	0.0792	0.0691	0.0585	0.0478
Entries	27621	19870	14502	8071	1431

\*Number of events (Nevent) is given in this and in the following tables for integrated luminosity  $L_{int} = 10 \text{ fb}^{-1}$ \*\*  $Db[Z, J] \equiv (P_t^Z - P_t^J)/P_t^Z$

Table 4: Selection 1.  $\Delta\phi_{(Z,jet)} = 180^\circ \pm 15^\circ$ . UA1 algorithm.

$P_{tCUT}^{clust}$	30	20	15	10	5
Nevent	4052	2880	2103	1197	226
$P_{t56}$	22.9	18.5	15.8	13.0	10.0
$\Delta\phi$	3.7	2.9	2.4	1.9	1.4
$P_t^{out}$	17.1	13.2	10.8	8.4	6.0
$P_t^{\eta>5}$	6.3	6.3	6.2	6.0	5.4
$(P_t^Z - P_t^{part})/P_t^Z$	0.0178	0.0131	0.0111	0.0104	0.0067
$(P_t^J - P_t^{part})/P_t^J$	-0.0078	-0.0036	-0.0009	0.0012	0.0018
$(P_t^Z - P_t^J)/P_t^Z$	0.0204	0.0124	0.0085	0.0061	0.0028
$P_t(O+\eta>5)/P_t^Z$	0.0120	0.0057	0.0027	0.0014	-0.0010
$1 - \cos(\Delta\phi)$	0.0036	0.0022	0.0015	0.0009	0.0005
$\sigma(Db[Z, J])$	0.0976	0.0787	0.0683	0.0586	0.0465
Entries	27148	19298	14089	8022	1517

Table 5: Selection 1.  $\Delta\phi_{(Z,jet)} = 180^\circ \pm 10^\circ$ . UA2 algorithm.

$P_{tCUT}^{clust}$	30	20	15	10	5
Nevent	4534	3303	2463	1421	258
$P_{t56}$	23.8	19.6	17.1	14.3	11.2
$\Delta\phi$	3.6	2.9	2.4	1.9	1.4
$P_t^{out}$	16.7	13.1	10.8	8.5	6.0
$P_t^{\eta>5}$	6.3	6.2	6.1	6.0	5.4
$(P_t^Z - P_t^{part})/P_t^Z$	0.0227	0.0185	0.0173	0.0156	0.0110
$(P_t^J - P_t^{part})/P_t^J$	-0.0044	-0.0023	-0.0005	0.0004	0.0013
$(P_t^Z - P_t^J)/P_t^Z$	0.0222	0.0166	0.0142	0.0121	0.0083
$P_t(O+\eta>5)/P_t^Z$	0.0140	0.0101	0.0085	0.0074	0.0048
$1 - \cos(\Delta\phi)$	0.0035	0.0022	0.0015	0.0009	0.0005
$\sigma(Db[Z, J])$	0.0946	0.0769	0.0674	0.0580	0.0439
Entries	30379	22130	16501	9520	1731

Table 6: Selection 1.  $\Delta\phi_{(Z,jet)} = 180^\circ \pm 15^\circ$ . LUCCELL algorithm.

$P_{tCUT}^{clust}$	30	20	15	10	5
Nevent	4080	2960	2163	1204	213
$P_{t56}$	22.5	18.3	15.6	12.5	9.4
$\Delta\phi$	3.6	2.9	2.4	1.9	1.4
$P_t^{out}$	16.9	13.3	11.0	8.5	6.0
$P_t^{\eta>5}$	6.3	6.3	6.2	6.0	5.5
$(P_t^Z - P_t^{part})/P_t^Z$	0.0175	0.0123	0.0102	0.0081	0.0039
$(P_t^J - P_t^{part})/P_t^J$	-0.0110	-0.0078	-0.0055	-0.0036	-0.0029
$(P_t^Z - P_t^J)/P_t^Z$	0.0233	0.0159	0.0121	0.0087	0.0043
$P_t(O+\eta>5)/P_t^Z$	0.0152	0.0093	0.0064	0.0041	0.0002
$1 - \cos(\Delta\phi)$	0.0035	0.0022	0.0015	0.0009	0.0005
$\sigma(Db[Z, J])$	0.0963	0.0788	0.0689	0.0585	0.0478
Entries	27334	19833	14494	8069	1430

Table 7: Selection 1.  $\Delta\phi_{(Z,jet)} = 180^\circ \pm 10^\circ$ . UA1 algorithm.

$P_{tCUT}^{clust}$	30	20	15	10	5
Nevent	3842	2831	2091	1195	226
$P_t^{56}$	21.9	18.2	15.7	12.9	10.0
$\Delta\phi$	3.2	2.7	2.3	1.9	1.4
$P_t^{out}$	16.0	12.8	10.7	8.4	6.0
$P_t^{\eta>5}$	6.3	6.2	6.2	6.0	5.4
$(P_t^Z - P_t^{part})/P_t^Z$	0.0165	0.0127	0.0110	0.0103	0.0068
$(P_t^J - P_t^{part})/P_t^J$	-0.0074	-0.0034	-0.0008	0.0014	0.0019
$(P_t^Z - P_t^J)/P_t^Z$	0.0188	0.0119	0.0083	0.0060	0.0028
$P_t(O+\eta>5)/P_t^Z$	0.0114	0.0056	0.0026	0.0013	-0.0010
$1 - \cos(\Delta\phi)$	0.0026	0.0019	0.0014	0.0009	0.0005
$\sigma(Db[Z, J])$	0.0959	0.0782	0.0680	0.0583	0.0465
Entries	25739	18965	14012	8009	1515

 Table 8: Selection 1.  $\Delta\phi_{(Z,jet)} = 180^\circ \pm 10^\circ$ . UA2 algorithm.

$P_{tCUT}^{clust}$	30	20	15	10	5
Nevent	4308	3245	2449	1418	258
$P_t^{56}$	22.8	19.3	17.0	14.2	11.2
$\Delta\phi$	3.2	2.7	2.3	1.9	1.4
$P_t^{out}$	15.7	12.7	10.7	8.5	6.1
$P_t^{\eta>5}$	6.3	6.2	6.1	5.9	5.3
$(P_t^Z - P_t^{part})/P_t^Z$	0.0214	0.0180	0.0171	0.0156	0.0111
$(P_t^J - P_t^{part})/P_t^J$	-0.0042	-0.0021	-0.0004	0.0005	0.0013
$(P_t^Z - P_t^J)/P_t^Z$	0.0207	0.0160	0.0139	0.0119	0.0083
$P_t(O+\eta>5)/P_t^Z$	0.0136	0.0099	0.0084	0.0073	0.0049
$1 - \cos(\Delta\phi)$	0.0025	0.0019	0.0014	0.0009	0.0005
$\sigma(Db[Z, J])$	0.0930	0.0763	0.0670	0.0577	0.0439
Entries	28861	21739	16409	9500	1727

 Table 9: Selection 1.  $\Delta\phi_{(Z,jet)} = 180^\circ \pm 10^\circ$ . LUCCELL algorithm.

$P_{tCUT}^{clust}$	30	20	15	10	5
Nevent	3884	2907	2152	1202	213
$P_t^{56}$	21.5	17.9	15.5	12.5	9.4
$\Delta\phi$	3.2	2.8	2.4	1.9	1.4
$P_t^{out}$	15.9	12.9	10.9	8.5	6.0
$P_t^{\eta>5}$	6.3	6.2	6.1	6.0	5.5
$(P_t^Z - P_t^{part})/P_t^Z$	0.0161	0.0117	0.0100	0.0080	0.0039
$(P_t^J - P_t^{part})/P_t^J$	-0.0109	-0.0077	-0.0055	-0.0036	-0.0029
$(P_t^Z - P_t^J)/P_t^Z$	0.0220	0.0153	0.0119	0.0086	0.0043
$P_t(O+\eta>5)/P_t^Z$	0.0148	0.0091	0.0063	0.0040	0.0002
$1 - \cos(\Delta\phi)$	0.0025	0.0019	0.0014	0.0009	0.0005
$\sigma(Db[Z, J])$	0.0948	0.0783	0.0687	0.0584	0.0478
Entries	26020	19473	14415	8056	1428

Table 10: Selection 1.  $\Delta\phi_{(Z,jet)} = 180^\circ \pm 5^\circ$ . UA1 algorithm.

$P_{tCUT}^{clust}$	30	20	15	10	5
Nevent	2937	2388	1884	1143	223
$P_t56$	19.3	16.6	14.7	12.5	9.8
$\Delta\phi$	2.1	2.0	1.9	1.7	1.3
$P_t^{out}$	13.2	11.2	9.8	8.1	6.0
$P_t^{\eta>5}$	6.2	6.1	6.0	5.8	5.2
$(P_t^Z - P_t^{part})/P_t^Z$	0.0148	0.0118	0.0102	0.0098	0.0064
$(P_t^J - P_t^{part})/P_t^J$	-0.0052	-0.0021	-0.0004	0.0012	0.0020
$(P_t^Z - P_t^J)/P_t^Z$	0.0152	0.0101	0.0072	0.0056	0.0023
$P_t(O+\eta>5)/P_t^Z$	0.0096	0.0049	0.0022	0.0012	-0.0012
$1 - \cos(\Delta\phi)$	0.0010	0.0009	0.0008	0.0007	0.0004
$\sigma(Db[Z, J])$	0.0909	0.0754	0.0665	0.0577	0.0448
Entries	19676	15996	12622	7657	1495

 Table 11: Selection 1.  $\Delta\phi_{(Z,jet)} = 180^\circ \pm 5^\circ$ . UA2 algorithm.

$P_{tCUT}^{clust}$	30	20	15	10	5
Nevent	3317	2740	2204	1357	254
$P_t56$	20.3	17.7	16.1	13.8	11.1
$\Delta\phi$	2.1	2.0	1.9	1.7	1.3
$P_t^{out}$	13.0	11.1	9.8	8.2	6.0
$P_t^{\eta>5}$	6.1	6.0	6.0	5.8	5.1
$(P_t^Z - P_t^{part})/P_t^Z$	0.0196	0.0172	0.0165	0.0153	0.0113
$(P_t^J - P_t^{part})/P_t^J$	-0.0026	-0.0008	0.0006	0.0009	0.0022
$(P_t^Z - P_t^J)/P_t^Z$	0.0177	0.0141	0.0126	0.0115	0.0080
$P_t(O+\eta>5)/P_t^Z$	0.0123	0.0092	0.0078	0.0072	0.0049
$1 - \cos(\Delta\phi)$	0.0009	0.0009	0.0008	0.0007	0.0004
$\sigma(Db[Z, J])$	0.0883	0.0735	0.0652	0.0566	0.0416
Entries	22222	18359	14764	9089	1705

 Table 12: Selection 1.  $\Delta\phi_{(Z,jet)} = 180^\circ \pm 5^\circ$ . UA2 algorithm.

$P_{tCUT}^{clust}$	30	20	15	10	5
Nevent	2984	2443	1931	1149	210
$P_t56$	19.0	16.3	14.5	12.1	9.2
$\Delta\phi$	2.1	2.0	1.9	1.7	1.3
$P_t^{out}$	13.2	11.3	9.9	8.2	6.0
$P_t^{\eta>5}$	6.2	6.1	6.0	5.8	5.3
$(P_t^Z - P_t^{part})/P_t^Z$	0.0141	0.0106	0.0093	0.0076	0.0040
$(P_t^J - P_t^{part})/P_t^J$	-0.0091	-0.0065	-0.0049	-0.0036	-0.0025
$(P_t^Z - P_t^J)/P_t^Z$	0.0185	0.0133	0.0107	0.0082	0.0041
$P_t(O+\eta>5)/P_t^Z$	0.0130	0.0083	0.0057	0.0039	0.0002
$1 - \cos(\Delta\phi)$	0.0010	0.0009	0.0008	0.0007	0.0004
$\sigma(Db[Z, J])$	0.0902	0.0754	0.0672	0.0576	0.0467
Entries	19995	16364	12936	7700	1409

Table 13: Selection 2.  $\Delta\phi_{(Z,jet)} = 180^\circ \pm 15^\circ$ ,  $e^{jet} < 3\%$ . UA1 algorithm.

$P_{tCUT}^{clust}$	30	20	15	10	5
Nevent	3193	2403	1835	1093	217
$P_t^{56}$	21.4	17.5	15.0	12.3	9.6
$\Delta\phi$	3.5	2.8	2.3	1.9	1.4
$P_t^{out}$	16.0	12.6	10.5	8.3	5.9
$P_t^{\eta>\delta}$	6.1	6.1	6.0	5.9	5.3
$(P_t^Z - P_t^{part})/P_t^Z$	0.0049	0.0051	0.0052	0.0058	0.0044
$(P_t^J - P_t^{part})/P_t^J$	-0.0015	-0.0006	0.0000	0.0005	0.0028
$(P_t^Z - P_t^J)/P_t^Z$	0.0035	0.0029	0.0028	0.0032	0.0009
$P_t(O+\eta>5)/P_t^Z$	-0.0035	-0.0028	-0.0021	-0.0009	-0.0020
$1 - \cos(\Delta\phi)$	0.0033	0.0021	0.0014	0.0009	0.0005
$\sigma(Db[Z, J])$	0.0870	0.0714	0.0625	0.0539	0.0390
Entries	21392	16101	12291	7321	1457

Table 14: Selection 2.  $\Delta\phi_{(Z,jet)} = 180^\circ \pm 15^\circ$ ,  $e^{jet} < 3\%$ . UA2 algorithm.

$P_{tCUT}^{clust}$	30	20	15	10	5
Nevent	3458	2605	2000	1198	229
$P_t^{56}$	21.4	17.6	15.2	12.5	9.8
$\Delta\phi$	3.5	2.8	2.3	1.9	1.4
$P_t^{out}$	15.9	12.6	10.5	8.4	6.0
$P_t^{\eta>\delta}$	6.1	6.1	6.0	5.9	5.4
$(P_t^Z - P_t^{part})/P_t^Z$	0.0055	0.0053	0.0059	0.0064	0.0046
$(P_t^J - P_t^{part})/P_t^J$	-0.0089	-0.0082	-0.0071	-0.0066	-0.0046
$(P_t^Z - P_t^J)/P_t^Z$	0.0111	0.0103	0.0102	0.0105	0.0080
$P_t(O+\eta>5)/P_t^Z$	0.0040	0.0046	0.0052	0.0062	0.0046
$1 - \cos(\Delta\phi)$	0.0033	0.0021	0.0014	0.0009	0.0006
$\sigma(Db[Z, J])$	0.0869	0.0721	0.0633	0.0548	0.0428
Entries	23169	17455	13397	8023	1537

Table 15: Selection 2.  $\Delta\phi_{(Z,jet)} = 180^\circ \pm 15^\circ$ ,  $e^{jet} < 3\%$ . LUCCELL algorithm.

$P_{tCUT}^{clust}$	30	20	15	10	5
Nevent	3184	2429	1851	1095	209
$P_t^{56}$	20.9	17.3	14.8	12.1	9.3
$\Delta\phi$	3.5	2.8	2.4	1.9	1.4
$P_t^{out}$	15.8	12.7	10.6	8.4	6.0
$P_t^{\eta>\delta}$	6.1	6.1	6.0	5.9	5.4
$(P_t^Z - P_t^{part})/P_t^Z$	0.0040	0.0039	0.0041	0.0049	0.0033
$(P_t^J - P_t^{part})/P_t^J$	-0.0056	-0.0047	-0.0037	-0.0023	-0.0004
$(P_t^Z - P_t^J)/P_t^Z$	0.0068	0.0059	0.0053	0.0052	0.0027
$P_t(O+\eta>5)/P_t^Z$	0.0000	0.0002	0.0004	0.0012	-0.0007
$1 - \cos(\Delta\phi)$	0.0032	0.0021	0.0014	0.0009	0.0005
$\sigma(Db[Z, J])$	0.0863	0.0720	0.0631	0.0536	0.0410
Entries	21330	16275	12399	7339	1400

Table 16: Selection 3.  $\Delta\phi_{(Z,jet)} = 180^\circ \pm 15^\circ$ ,  $\epsilon^{jet} < 3\%$ . UA1 algorithm.

$P_{tCUT}^{clust}$	30	20	15	10	5
Nevent	2770	2119	1616	957	179
$P_t56$	20.6	17.1	14.6	11.9	9.3
$\Delta\phi$	3.4	2.8	2.3	1.9	1.4
$P_t^{out}$	15.6	12.5	10.5	8.3	6.0
$P_t^{\eta>\delta}$	6.1	6.1	6.0	5.9	5.4
$(P_t^Z - P_t^{part})/P_t^Z$	0.0024	0.0027	0.0031	0.0038	0.0029
$(P_t^J - P_t^{part})/P_t^J$	-0.0032	-0.0028	-0.0018	-0.0011	0.0007
$(P_t^Z - P_t^J)/P_t^Z$	0.0027	0.0026	0.0024	0.0028	0.0013
$P_t(O+\eta>5)/P_t^Z$	-0.0042	-0.0031	-0.0025	-0.0012	-0.0021
$1 - \cos(\Delta\phi)$	0.0032	0.0021	0.0014	0.0009	0.0005
$\sigma(Db[Z, J])$	0.0848	0.0712	0.0626	0.0536	0.0406
Entries	18559	14199	10824	6409	1200

Table 17: Selection 3.  $\Delta\phi_{(Z,jet)} = 180^\circ \pm 15^\circ$ ,  $\epsilon^{jet} < 3\%$ . UA2 algorithm.

$P_{tCUT}^{clust}$	30	20	15	10	5
Nevent	2770	2119	1616	957	179
$P_t56$	20.6	17.1	14.6	11.9	9.3
$\Delta\phi$	3.4	2.8	2.3	1.9	1.4
$P_t^{out}$	15.6	12.5	10.5	8.4	6.1
$P_t^{\eta>\delta}$	6.1	6.1	6.0	5.9	5.4
$(P_t^Z - P_t^{part})/P_t^Z$	0.0024	0.0027	0.0031	0.0038	0.0029
$(P_t^J - P_t^{part})/P_t^J$	-0.0110	-0.0104	-0.0094	-0.0086	-0.0059
$(P_t^Z - P_t^J)/P_t^Z$	0.0101	0.0100	0.0098	0.0102	0.0078
$P_t(O+\eta>5)/P_t^Z$	0.0033	0.0043	0.0048	0.0061	0.0044
$1 - \cos(\Delta\phi)$	0.0032	0.0021	0.0014	0.0009	0.0005
$\sigma(Db[Z, J])$	0.0851	0.0714	0.0628	0.0538	0.0408
Entries	18559	14199	10824	6409	1200

Table 18: Selection 3.  $\Delta\phi_{(Z,jet)} = 180^\circ \pm 15^\circ$ ,  $\epsilon^{jet} < 3\%$ . LUCCELL algorithm.

$P_{tCUT}^{clust}$	30	20	15	10	5
Nevent	2770	2119	1616	957	179
$P_t56$	20.6	17.1	14.6	11.9	9.3
$\Delta\phi$	3.5	2.8	2.3	1.9	1.4
$P_t^{out}$	15.7	12.6	10.5	8.4	6.0
$P_t^{\eta>\delta}$	6.1	6.1	6.0	5.9	5.4
$(P_t^Z - P_t^{part})/P_t^Z$	0.0024	0.0027	0.0031	0.0038	0.0029
$(P_t^J - P_t^{part})/P_t^J$	-0.0061	-0.0052	-0.0040	-0.0031	-0.0006
$(P_t^Z - P_t^J)/P_t^Z$	0.0055	0.0050	0.0047	0.0048	0.0027
$P_t(O+\eta>5)/P_t^Z$	-0.0014	-0.0007	-0.0003	0.0007	-0.0007
$1 - \cos(\Delta\phi)$	0.0032	0.0021	0.0014	0.0009	0.0005
$\sigma(Db[Z, J])$	0.0853	0.0714	0.0628	0.0539	0.0408
Entries	18559	14199	10824	6409	1200

## Appendix 6

$$P_t^Z = 40 \text{ GeV}/c$$

Table 1: Number of events per  $L_{int} = 10 \text{ fb}^{-1}$ 

$P_{t \max}^{clust}$ (GeV/c)	$P_{t \max}^{out}$ (GeV/c)					
	5	10	15	20	30	1000
5	20400	37400	40600	41000	41000	41000
10	62000	142500	178700	187900	189600	189600
15	75400	186700	257900	286600	297500	298400
20	79600	201700	289100	334400	359800	363600
30	81900	210300	308400	366800	415100	429900

Table 2:  $S/B$ 

$P_{t \max}^{clust}$ (GeV/c)	$P_{t \max}^{out}$ (GeV/c)					
	5	10	15	20	30	1000
5	$1.8 \pm 0.2$	$1.9 \pm 0.2$	$1.9 \pm 0.2$	$1.9 \pm 0.2$	$1.9 \pm 0.2$	$1.9 \pm 0.2$
10	$1.9 \pm 0.1$	$2.0 \pm 0.1$	$2.0 \pm 0.1$	$2.0 \pm 0.1$	$2.0 \pm 0.1$	$2.0 \pm 0.1$
15	$1.9 \pm 0.1$	$1.9 \pm 0.1$	$1.9 \pm 0.1$	$2.0 \pm 0.1$	$2.1 \pm 0.1$	$2.1 \pm 0.1$
20	$1.9 \pm 0.1$	$2.0 \pm 0.1$	$2.0 \pm 0.1$	$2.1 \pm 0.1$	$2.2 \pm 0.1$	$2.2 \pm 0.1$
30	$1.9 \pm 0.1$	$2.0 \pm 0.1$	$2.0 \pm 0.1$	$2.1 \pm 0.1$	$2.3 \pm 0.1$	$2.4 \pm 0.1$

Table 3:  $\langle F \rangle$ ,  $F = (P_t^Z - P_t^{jet})/P_t^Z$ 

$P_{t \max}^{clust}$ (GeV/c)	$P_{t \max}^{out}$ (GeV/c)					
	5	10	15	20	30	1000
5	0.009	0.015	0.017	0.017	0.017	0.017
10	0.008	0.014	0.019	0.019	0.020	0.020
15	0.008	0.016	0.024	0.027	0.030	0.031
20	0.009	0.017	0.027	0.032	0.037	0.039
30	0.009	0.018	0.028	0.035	0.044	0.050

Table 4:  $\sigma(F)$ ,  $F = (P_t^Z - P_t^{jet})/P_t^Z$ 

$P_{t \max}^{clust}$ (GeV/c)	$P_{t \max}^{out}$ (GeV/c)					
	5	10	15	20	30	1000
5	0.066	0.082	0.089	0.090	0.090	0.090
10	0.077	0.095	0.107	0.111	0.113	0.113
15	0.079	0.097	0.115	0.124	0.132	0.133
20	0.079	0.098	0.117	0.132	0.145	0.151
30	0.079	0.099	0.119	0.136	0.160	0.175

$$P_t^Z = 70 \text{ GeV}/c$$

Table 5: Number of events per  $L_{int} = 10 \text{ fb}^{-1}$

$P_{t \max}^{clust}$ (GeV/c)	$P_{t \max}^{out}$ (GeV/c)					
	5	10	15	20	30	1000
5	3500	6700	7300	7400	7400	7400
10	11100	26600	34400	36900	37600	37600
15	13700	35400	51000	59300	63600	64000
20	14500	38400	58000	71200	81400	83400
30	14900	40400	62500	80000	100000	108500

Table 6:  $S/B$

$P_{t \max}^{clust}$ (GeV/c)	$P_{t \max}^{out}$ (GeV/c)					
	5	10	15	20	30	1000
5	18.1± 4.7	19.3± 3.7	20.5± 3.9	19.3± 3.5	18.5± 3.3	17.6± 3.1
10	24.5± 4.0	27.2± 3.0	28.6± 2.8	28.4± 2.7	27.3± 2.5	26.9± 2.5
15	25.9± 3.9	27.0± 2.6	28.0± 2.2	28.8± 2.2	28.6± 2.1	28.3± 2.0
20	24.4± 3.5	27.7± 2.5	28.8± 2.2	28.4± 1.9	28.5± 1.8	28.5± 1.8
30	24.7± 3.5	28.3± 2.6	28.8± 2.1	28.0± 1.8	28.6± 1.6	28.1± 1.5

Table 7:  $\langle F \rangle$ ,  $F = (P_t^Z - P_t^{jet})/P_t^Z$

$P_{t \max}^{clust}$ (GeV/c)	$P_{t \max}^{out}$ (GeV/c)					
	5	10	15	20	30	1000
5	0.004	0.007	0.009	0.009	0.009	0.010
10	0.005	0.007	0.010	0.011	0.013	0.013
15	0.006	0.009	0.013	0.015	0.019	0.019
20	0.007	0.010	0.015	0.018	0.026	0.028
30	0.007	0.010	0.015	0.020	0.033	0.041

Table 8:  $\sigma(F)$ ,  $F = (P_t^Z - P_t^{jet})/P_t^Z$

$P_{t \max}^{clust}$ (GeV/c)	$P_{t \max}^{out}$ (GeV/c)					
	5	10	15	20	30	1000
5	0.056	0.059	0.063	0.063	0.064	0.065
10	0.055	0.063	0.071	0.076	0.079	0.079
15	0.056	0.067	0.078	0.086	0.095	0.096
20	0.058	0.068	0.081	0.092	0.106	0.110
30	0.059	0.069	0.082	0.095	0.118	0.130

$$P_t^Z = 100 \text{ GeV}/c$$

Table 9: Number of events per  $L_{int} = 10 \text{ fb}^{-1}$

$P_{t \max}^{clust}$ (GeV/c)	$P_{t \max}^{out}$ (GeV/c)					
	5	10	15	20	30	1000
5	1160	2200	2430	2450	2460	2470
10	3740	8920	11700	12610	12890	12910
15	4610	12060	17560	20520	22330	22530
20	4910	13170	20160	24980	29350	30370
30	5090	13890	21780	28160	36630	40710

Table 10:  $S/B$

$P_{t \max}^{clust}$ (GeV/c)	$P_{t \max}^{out}$ (GeV/c)					
	5	10	15	20	30	1000
5	217± 94	305± 114	335± 124	269± 89	225± 69	192± 55
10	997± 512	2346±1190	2016± 833	1613± 578	1100± 324	943± 258
15	—	6091±4308	4318±2160	3283±1337	2143± 682	1548± 419
20	1247± 633	—	9457±6563	2929±1035	1684± 423	1509± 355
30	1201± 590	—	4543±2128	1801± 477	1338± 273	1236± 233

Table 11:  $\langle F \rangle$ ,  $F = (P_t^Z - P_t^{jet})/P_t^Z$

$P_{t \max}^{clust}$ (GeV/c)	$P_{t \max}^{out}$ (GeV/c)					
	5	10	15	20	30	1000
5	0.006	0.006	0.007	0.007	0.007	0.007
10	0.006	0.007	0.008	0.008	0.009	0.009
15	0.006	0.007	0.010	0.011	0.013	0.013
20	0.006	0.008	0.010	0.013	0.017	0.019
30	0.006	0.008	0.011	0.014	0.022	0.028

Table 12:  $\sigma(F)$ ,  $F = (P_t^Z - P_t^{jet})/P_t^Z$

$P_{t \max}^{clust}$ (GeV/c)	$P_{t \max}^{out}$ (GeV/c)					
	5	10	15	20	30	1000
5	0.040	0.046	0.048	0.049	0.049	0.050
10	0.042	0.049	0.055	0.058	0.060	0.061
15	0.044	0.051	0.060	0.066	0.073	0.074
20	0.044	0.052	0.062	0.070	0.082	0.087
30	0.044	0.052	0.063	0.072	0.091	0.105